ELSEVIER

Progress in Nuclear Magnetic Resonance Spectroscopy
27 (1995) 555–633

PROGRESS IN NUCLEAR
MAGNETIC RESONANCE
SPECTROSCOPY

^{13}C Nuclear Magnetic Relaxation and Local Dynamics of Synthetic Polymers in Dilute Solution and in the Bulk State

Photis Dais*, Apostolos Spyros

University of Crete, Department of Chemistry, 71409 Iraklion, Crete, Greece

Received 19 September 1994

Contents

* Corresponding author.

SSDI 0079-6565(95)01014-9

1. Introduction

Important mechanical properties of synthetic polymers depend on molecular structure and molecular motion [1]. For instance, mechanical properties such as toughness or impact strength of glassy polymers are often linked with the local structure and the type, amplitude and time-scale of molecular motions of these polymeric materials.

NMR spectroscopy offers the potential to probe motion at a molecular level, and provides the basic connectivity between primary structure and motion and the observed mechanical properties. In particular, ^{13}C relaxation experiments can probe motion at several carbon sites in a repeat unit simultaneously, thus providing a detailed insight into molecular motion at a repeat-unit level. Although investigation of the dynamic properties of a polymer in the solid is perhaps of greater practical significance, relaxation studies using high resolution NMR of dilute solutions are not without considerable value [2–4]. Dilute solution studies provide valuable information on the importance of intramolecular barriers to rates and energetics of motional processes. In certain cases this information can be linked with bulk properties such as glass transition, dynamic mechanical or dielectric maxima, impact resistance, etc. [5–7]. Nevertheless, polymer dynamics can be studied by high resolution NMR spectroscopy even for bulk macromolecules. The relaxation parameters can be measured with conventional NMR spectrometers under proton decoupling, if the samples are in the rubbery state or include rubbery material as a non-crystalline content in semi-crystalline polymers [7–12]. At temperatures above T_g, molecular motions in amorphous polymers are sufficiently rapid to reduce significantly the effects of the ^{13}C–^{1}H dipolar interactions.

Polymer motions fall into two general categories: (1) local motions, and (2) long-range collective motions. These types of motion, differing in time-scale and activation energy, are manifested in a polymer chain regardless of its physical state, i.e. liquid, amorphous, or crystalline. Local motions of polymers in dilute solutions can be segmental reorientation via conformational transitions of the crankshaft-type, or trans–gauche isomerism occurring at a frequency of the order of 10^9 Hz, anisotropic internal rotations of pendent groups such as methyl or phenyl internal motions, or multiple internal rotations (free or restricted) in hydrocarbon side-chains at frequencies 10^9–10^{10} Hz, and small-scale librational motions with amplitudes of 30–60° and frequencies of 10^{11}–10^{12} Hz. These motions are strongly dependent on the local conformational details. Segmental motions are almost independent of molecular weight, but they retain some dependence on the excluded volume and hydrodynamic interactions. As the frequency decreases, the spatial range of motion increases, and in the frequency range below 10^9 Hz, low frequency modes of motions are manifested from reptation at 10^2 Hz to overall molecular tumbling at 10^5–10^7 Hz. These collective motions are strongly dependent on molecular weight and they are dominated by excluded volume and hydrodynamic interaction effects in solution.

In dilute solutions, intramolecular potential barriers are the main source of constraints to local motions, whereas in solid polymers, local motions are hindered by both intra- and inter-molecular barriers owing to strong interchain interactions. As a result, segmental motion becomes more restricted and anisotropic rotations become more important. Thus, backbone and side-group motions, or motions of different components of a polymer can be better differentiated in solution than in a solid. Another advantage of studying polymer dynamics in dilute solutions is that interchain interactions are unimportant, thus allowing the elucidation of the nature of intramolecular constraints and the hydrodynamic interactions with the solvent. NMR anisotropic interactions are averaged out in solution and relaxation methods provide the best means of probing motions and critically testing theoretical models that describe polymer chain dynamics.

For a survey of earlier works (before 1979) on dynamics of synthetic polymers in dilute solutions, the reader is referred to the excellent review of Heatley [3]. Schaefer [2] and Heatley [4] have reviewed some aspects of nuclear magnetic relaxation and dynamic modeling of synthetic and natural macromolecules.

The main objective of the present article is to present and critically discuss more recent theoretical and experimental developments in the study of local chain motions in solution and in the bulk state. This review comprises five sections. In Section 2, a short description of the principles underlying ^{13}C nuclear magnetic relaxation theory will be given. In Section 3, the theoretical approaches used to

interpret quantitatively the experimental relaxation data will be discussed. Section 4 will give an overview of the experimental results and their quantitative interpretation. A short discussion and some general remarks are given in Section 5.

2. Basic relaxation theory

Relaxation theory of nuclear spin-systems is well documented in several books [13–15] and review articles [16–19]. Therefore, the theory presented in this section is limited to a summary of the basic concepts crucial for understanding the material in the following sections.

^{13}C nuclear magnetic relaxation of polymers in dilute solutions and in the bulk state is dominated by dipole–dipole (DD) interactions between a ^{13}C nucleus and the directly bonded proton(s). At low magnetic fields the DD relaxation mechanism is also important for quaternary saturated nuclei interacting with neighboring but more distant protons [20]. Since the efficiency of DD relaxation diminishes with the sixth power of the distance between the ^{13}C and ^{1}H nuclei, the relaxation contribution of non-bonded protons to a protonated carbon, CH_N (N = number of protons) is very small ($<3\%$) compared to that from the directly attached proton(s), which make(s) the most significant contribution to the relaxation of the carbon in question. On the basis of this estimate, relaxation with protons on the same chain that are far removed along the contour length, but temporarily nearby in space, is also likely to be negligible [21, 22]. Dipolar interactions with protons on neighboring polymer chains is also unimportant. The relaxation parameters are known [3, 23] to be independent of polymer concentration below about 15% (w/v). All these contributions to spin-relaxation from non-bonded protons have been ignored in most applications.

For non-protonated ^{13}C nuclei, especially unsaturated nuclei, at high magnetic fields (>50 MHz), contribution from the chemical shift anisotropy (CSA) mechanism may be significant.

2.1 ^{13}C NMR relaxation parameters

For the case of the heteronuclear ^{13}C–^{1}H dipole–dipole interactions where the spin ^{13}C is observed and the spin ^{1}H is irradiated, the spin–lattice or longitudinal relaxation time (T_1), the spin–spin or transverse relaxation time (T_2), and the Nuclear Overhauser Enhancement (NOE) of a ^{13}C nucleus in a CH_N group are given (in SI units) by [13, 18]

$$\frac{1}{T_1^{DD}} = \frac{K}{20}\left[J_0(\omega_H - \omega_C) + 3J_1(\omega_C) + 6J_2(\omega_H + \omega_C)\right] \tag{1}$$

$$\frac{1}{T_2^{DD}} = \frac{K}{40}\left[4J(0) + J_0(\omega_H - \omega_C) + 3J_1(\omega_C) + 6J_1(\omega_H) + 6J_2(\omega_H + \omega_C)\right] \tag{2}$$

$$NOE^{DD} = 1 + \frac{\gamma_H}{\gamma_C}\left[\frac{6J_2(\omega_H + \omega_C) - J_0(\omega_H - \omega_C)}{J_0(\omega_H - \omega_C) + 3J_1(\omega_C) + 6J_2(\omega_H + \omega_C)}\right] \tag{3}$$

and

$$K = N\left(\frac{\mu_0 \gamma_H \gamma_C \hbar}{4\pi r_{CH}^3}\right)^2 \tag{4}$$

where γ_H, γ_C are the gyromagnetic ratios of proton and carbon nuclei respectively, ω_H, ω_C are their Larmor frequencies, μ_0 is the vacuum magnetic permeability ($4\pi \times 10^{-7}$ H m^{-1}), $\hbar = h/2\pi$ where h is the Planck constant, N is the number of directly bonded protons, and r_{CH} is the C–H internuclear distance. $J_m(\omega)$ is the spectral density function related to the time-correlation function (TCF), $G_m(t)$

$$J_m(\omega_m) = 2\mathrm{Re}\left[\int_0^\infty G_m(t) e^{-i\omega t} dt\right] \tag{5}$$

with Re indicating the real part of the complex Fourier transform of Eq. (5).

If the chemical shift tensor is axially symmetric, the relaxation parameters, T_1^{CSA} and T_2^{CSA}, for the CSA mechanism are given by

$$\frac{1}{T_1^{CSA}} = (2/15)\omega_C^2 \Delta\sigma^2 J_1(\omega_C) \tag{6}$$

$$\frac{1}{T_2^{CSA}} = (1/45)\omega_C^2 \Delta\sigma^2 [4J(0) + 3J_1(\omega_C)] \tag{7}$$

where

$$\Delta\sigma = \sigma_{33} - \tfrac{1}{2}(\sigma_{11} + \sigma_{22}) \tag{8}$$

From the above equations, it is evident that the relaxation parameters of the CSA contribution depend on the frequency through the spectral density, but also are directly proportional to ω_C^2. Also, T_1^{CSA} and T_2^{CSA} depend on the diagonal components, σ_{ii}, of the CSA tensor $\Delta\sigma$. If both mechanisms of relaxation of ^{13}C exists, then T_1 and T_2 and NOE may be written as

$$\frac{1}{T_i^{obs}} = \frac{1}{T_i^{DD}} + \frac{1}{T_i^{CSA}} \quad (i = 1, 2) \tag{9}$$

$$NOE^{CSA} = 1 + \left[\frac{(NOE^{DD} - 1)}{\frac{1}{T_1^{DD}}\left(\frac{1}{T_1^{DD}} + \frac{1}{T_1^{CSA}}\right)} \right] \tag{10}$$

Given Eqs. (1)–(10), the problem is to evaluate the time correlation function (TCF) and the spectral density function in Eq. (5).

2.2 Time-correlation function (TCF) and spectral density function

The fluctuating Hamiltonian describing DD and CSA interactions may be written as the product of two spherical tensors [13]

$$H = \sum_m (-1)^m F_m A_{-m} \tag{11}$$

where A_m is a function of spin operators and F_m are the familiar orientation factors or second-rank spherical harmonics. For both DD and CSA mechanisms the time dependence, because of random molecular motions, is contained entirely in the orientation factor. The average behavior of F_m is expressed by a TCF

$$G_m(t) = \langle F_m(\Omega, 0) F_m(\Omega, t) \rangle \tag{12}$$

In the case of DD interactions $G_m(t)$ is given by

$$G_m(t) = 8\pi^2 \langle D^*_{m0}(\Omega, 0) D_{m0}(\Omega, t) \rangle_{eq} \tag{13}$$

The TCF in Eq. (13) has been written in terms of the normalized Wigner rotation matrix [24], D_{ml}, with $\Omega = (\alpha_{LF}, \beta_{LF}, \gamma_{LF})$ the Euler angles which transform F_m from the laboratory frame, L, to a coordinate frame, F, with one axis along the internuclear ^{13}C–^1H vector. The asterisk indicates the complex conjugate, and $\langle\ \rangle_{eq}$ denotes an equilibrium average. For isotropic motion, the TCF in Eqs. (12) and (13) is independent of m.

The TCF for the CSA interaction from which the corresponding spectral density function can be calculated through Eq. (4) is given by Eq. (12) with [13]

$$F_m(t) = D_{m0}(\Omega, t) + (\eta/\sqrt{6})[D_{m(2)}(\Omega, t) + D_{m(-2)}(\Omega, t)] \tag{14}$$

Here, the Euler angles define the instantaneous orientation of the principal axes of the CSA tensor with respect to the external coordinate system. η is the asymmetry parameter defined by [13]

$$\eta = \frac{\sigma_{11} - \sigma_{22}}{\sigma_{33}} \tag{15}$$

Note that $\eta = 0$, when the CSA tensor is cylindrically symmetric.

The form of the TCF in Eqs. (12) and (13) depends on the motional model chosen. Although polymer motion is often neither isotropic nor diffusional, it is helpful in understanding some important general properties of ^{13}C NMR relaxation to gain an insight into the form of the $G_m(t)$ and $J_m(\omega)$ functions for the simple case of isotropic rotational diffusion. It is convenient to introduce the reduced TCF [13]

$$G(t) = G_m(t)/G_m(0) \tag{16}$$

which is assumed to be the same for all m, and can be represented by the exponential form

$$G(t) = (1/5)\mathrm{e}^{-t/\tau_c} \tag{17}$$

The Fourier transform of $G(t)$ gives the reduced spectral density, $J(\omega)$

$$J(\omega) = \frac{2\tau_c}{1 + \omega^2\tau_c^2} \tag{18}$$

where τ_c is the molecular correlation time. Eq. (18) may be substituted into Eqs. (1)–(3) for the DD relaxation to express the relaxation parameters in terms of the molecular correlation time and frequency. As τ_c (i.e. temperature) varies, T_1^{DD} passes through a minimum when $\omega^2\tau_c^2 \approx 1$, whereas T_2^{DD} decreases monotonically as τ_c increases. In the extreme narrowing limit ($\omega^2\tau_c^2 \ll 1$), T_1^{DD} and T_2^{DD} are equal and independent of frequency. In the opposite extreme (long τ_c, slow motions) where $\omega^2\tau_c^2 > 1$, T_1^{DD} and T_2^{DD} become frequency-dependent and $T_2^{DD} < T_1^{DD}$. The NOE^{DD} (Eq. (3)) varies with τ_c. For the most common situation of a ^{13}C–^{1}H pair, the limits are 2.988 for $\omega^2\tau_c^2 \ll 1$ and 1.15 for $\omega^2\tau_c^2 > 1$. Fig. 1 illustrates the behavior of T_1^{DD}, T_2^{DD} and NOE^{DD} for the isotropic case. Although T_1^{DD} is the easiest relaxation parameter to measure accurately, a given T_1^{DD} value corresponds to two possible values of τ_c. The correct one can be selected by measuring additional data such as T_2^{DD}, NOE^{DD}, or the temperature dependence of T_1^{DD}.

Internal motional freedom is incorporated in the TCF in terms of Wigner rotation matrices which transform successively the orientation of an internuclear ^{13}C–^{1}H vector from the Nth internal frame to the laboratory frame [23, 25] i.e.

$$\begin{aligned} G_m(t) = \sum_{aa'}\sum_{bb'}\sum_{mm'}\sum_{nn'} & \langle D^*_{ma}(\Omega_{LD}, 0) D_{ma'}(\Omega_{LD}, t)\rangle \\ & \times \langle D^*_{ab}(\Omega_{D1}, 0) D_{a'b'}(\Omega_{D1}, t)\rangle \ldots \times \langle D^*_{mn}(\Omega_{N-1N}, 0) D_{m'n'}(\Omega_{N-1N}, t)\rangle \\ & \times \langle D^*_{n0}(\Omega_{NF}, 0) D_{n'0}(\Omega_{NF}, t)\rangle \end{aligned} \tag{19}$$

A similar expression exists for the CSA contribution, but the last ensemble average contains the $D_{n,2}$ and $D_{n,-2}$ components (cf. Eqs. (13) and (14)). The first ensemble average in Eq. (19) represents the orientation of an axis system, the D frame, which is embedded in the polymer. For isotropic motion, the first ensemble average becomes [23, 25]

$$\sum_{aa'}\langle D^*_{ma}(\Omega_{LD}, 0) D_{ma'}(\Omega_{LD}, t)\rangle = \delta_{aa'}(1/5)\mathrm{e}^{-6D_0 t} \tag{20}$$

where D_0 is the isotropic rotational diffusion constant related to the molecular correlation time by $D_0 = 1/6\tau_c$. Note that Eq. (20) is similar to Eq. (17). The overall motion can also be modeled as anisotropic motion of an ellipsoid (or cylinder) [23, 25–27]. Also, the ensemble average of Eq. (20) can be expressed in terms of motional parameters that describe segmental motion of a polymer chain

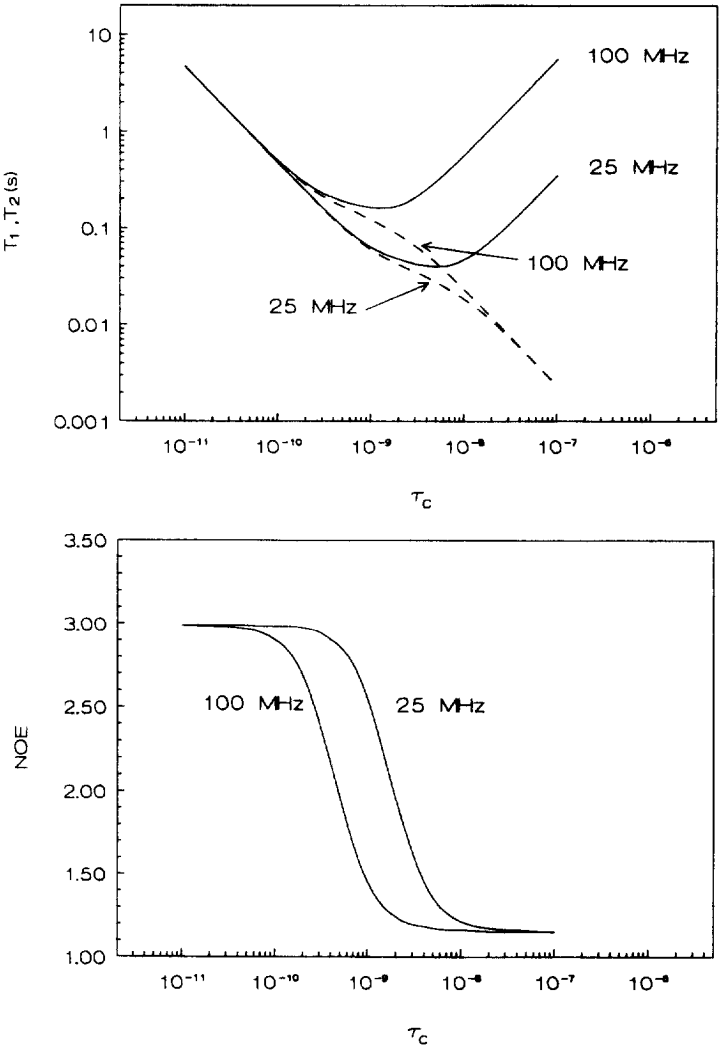

Fig. 1. ^{13}C Relaxation parameters, T_1 (solid curves), T_2 (dashed curves), and NOE as a function of correlation time τ_c and radiofrequency.

[26, 27]. The remaining ensemble averages in Eq. (19) describing internal rotational diffusion can be evaluated for free diffusion [23, 25–29], restricted diffusion [25, 26, 30, 31], i.e. restricting internal rotation to occur within a specific angular region ($< 360°$), and for jumps through the full 360° range or part of it in two or three discrete configurations [25, 32–34]. As we shall see in the following sections, the aforementioned models for internal motions are very useful in describing the motion of side-chains attached to the polymer backbone. It should be noted that the formulation of Eq. (19) assumes that internal rotations are all independent. However, this assumption may be less satisfactory for longer side-chains where hydrodynamic effects induce concerted type of motions involving partial rotations about several bonds so that only local displacements occur. The problem can be partially solved by restricting the amplitude of rotational diffusion about certain bonds [25]. A more realistic description is to consider a model in which the side-chain can jump among configurations which are restricted to lie on a tetrahedral lattice [25].

2.3 Cross-correlation effects

When various internuclear vectors reorient as a unit such as in methyl or methylene groups, cross-correlation interaction terms describe the average correlation between the orientation of one internuclear vector at a given moment and the orientation of a different internuclear vector at a later time. For various reasons, cross-correlation effects have been generally neglected from consideration of interpretation of relaxation data. The effect is often assumed to be small or non-existent. Several theoretical advances, however, have shown [35,36] that cross-correlation interactions may be more prevalent than anticipated, especially for proton relaxation, and that useful information may be derived from an explicit consideration of cross-correlation spectral densities.

The influence of multi-spin dipolar cross-correlation effects on ^{13}C relaxation has been investigated by London and Avitabile [29] in the context of the theory of multiple internal rotations. Cross-correlation effects have been calculated for the NOE values of carbon nuclei in a methylene chain attached to a heavy anchor for several values of the diffusion constant, D_i, describing internal rotations about successive C–C bonds, while varying the diffusion constant, D_0, for the overall motion of the system assumed to be isotropic. It is found [29] that the effect of cross-correlations on the NOE^{DD} values is relatively small, except in the region of NOE^{DD} where the isotropic diffusion constant satisfies the condition $6D_0 \approx \omega_c$. In this region the effect depends on the rotational diffusion constant D_i, being insignificant for $D_i = 10^9\ s^{-1}$ and somewhat more important for $D_i = 10^{10}$ and $10^{11}\ s^{-1}$. The longitudinal relaxation time is also most markedly non-exponential in the region where $6D_0 \approx \omega_c$. As D_0 increases or decreases beyond this value the relaxation becomes more nearly exponential. Cross-correlation effects attenuate rapidly toward the free end of the chain, where the influence of the overall anisotropic motion becomes unimportant.

Calculated cross-correlation spectral densities from ^{13}C relaxation data obtained without proton irradiation have been used to describe the dynamics of poly(methylene oxide) [37] in phenol solution and *cis*-1,4 poly(butadiene) [38] in the solid state and in CD_2Cl_2 solution. In the limit of extreme narrowing, the dipolar relaxation of a $^{13}CH_2$ group is completely described by four frequency-independent spectral densities. Two of them are autocorrelation terms related to the CH or HH′ intramolecular vectors ($J_{CHCH'}$ and $J_{HH'HH'}$) and the other two are cross-correlation terms relating one CH vector to the other ($J_{CHCH'}$) or to the HH′ vector ($J_{CHHH'}$). These spectral densities can be evaluated by fitting the relaxation data obtained from four different experiments involving four different initial perturbations of the coupled $^{13}CH_2$ spin system to the theoretical expressions generated by Werbelow and Grant [35]. Since the four TCFs obtainable from inverse Fourier transform of the dipolar spectral densities are not easily interpretable (especially the cross-correlation functions), the observed spectral densities have been expressed in terms of four autocorrelated Cartesian spectral densities with four correlation times [39], $\tau_{xx}, \tau_{yy}, \tau_{zz}$, and τ_{xy}. This model-independent transformation appears to be very useful, removing the difficulty of interpreting cross-correlation functions and presenting the results in the Cartesian axis system common to most statistical mechanical treatments of chain dynamics.

2.4 Strategies in describing polymer dynamics in solution by ^{13}C magnetic relaxation

The TCF which embodies all the information about mechanisms and rates of motions occurring in a polymer chain can be obtained, in principle, by an inverse Fourier transform of the experimentally obtained spectral density, i.e.

$$G_m(t) = 2\mathrm{Re}\left[\int_0^{\infty} J_m(\omega)e^{i\omega t}\,dt\right] \tag{21}$$

Unfortunately, magnetic relaxation measurements at one magnetic field respond to values of $J(\omega)$ at a very limited number of frequencies. For the ^{13}C–^{1}H dipolar pair the relaxation parameters, T_1^{DD}, T_2^{DD}, and NOE^{DD} involve spectral densities at sum and difference frequencies, $\omega_{I;} + \omega_C$ and

$\omega_H - \omega_C$, as well as individual resonance frequencies ω_H and ω_C (Eqs. (1)–(3)). Also, T_2^{DD} involves the zero-frequency spectral density (Eq. (2)). Both $\omega_H + \omega_C$ and $\omega_H - \omega_C$ are in the same radio-frequency region as the resonance frequencies $\omega_H$and ω_C. One solution to the problem would be to perform variable frequency experiments over a wide frequency range as in dielectric and viscoelastic relaxation experiments. However, this methodology is neither practical nor economical. Notwithstanding this, by measuring several relaxation parameters at different resonance frequencies, $J(\omega)$ can be sampled discretely at a number of frequencies and will give some insight into the form of the TCF. Commercial spectrometers are now available which in combination will cover the frequency range 20–125 MHz or more for the carbon nucleus. It is preferable to study the same nucleus by varying field and frequency together. An alternative methodology [3,4] is to study different nuclei resonating at different frequencies in the same field, e.g. ^1H at 200 MHz and ^{13}C at 50 MHz. However, ^1H relaxation measurements have the disadvantage of involving a large number of individual interactions in a typical polymer.

Although for a two-proton spin system the relaxation equations are not very difficult to handle [3,4], multi-spin systems require a formal density matrix treatment [19]. Even for the simpler two-spin system care should be taken in a relaxation experiment to avoid cross-relaxation and cross-correlation effects in the evolution of the longitudinal magnetization [40]. Problems associated with non-exponential decay of magnetization and cross-correlation effects may be avoided by confining the measurements to those of initial relaxation rates [40,41]. Another disadvantage in measuring proton relaxation rates is the spin-diffusion phenomenon manifested in polymer systems in solution [42]. For slow motions ($\omega^2\tau_c^2 > 1$) all proton spins relax at the same rate because rapid spin diffusion maintains a uniform temperature, and hence segmental details are lost [40,42]. This situation may be remedied by using selective relaxation experiments [40,41]. Despite the difficulties inherent in the multi-spin relaxation experiments, Heatley and co-workers [3,4,43,44] have investigated coupled relaxation between backbone protons in typical vinyl polymers. These authors, by performing non-selective and selective relaxation experiments, were able to obtain relaxation times and NOEs and interpret these experimental data by using dynamic models.

It is advisable to include the transverse relaxation time, T_2 in the measured relaxation parameters for polymer systems in solution or in the bulk. Although T_2 is difficult to measure accurately, it fills an important complementary role to T_1. T_2 depends on $J(0)$ (see Eq. (2)), that is on the total area under the correlation function, whereas T_1 involves components in the resonance frequency region. In other words, T_2 is more sensitive to low-frequency motions, while T_1 samples high-frequency motions.

Since the spectral density function is normally tested only at a few frequencies, and hence the TCF cannot be obtained from experiments, it is customary to develop theoretical TCFs (models) for a quantitative interpretation of the experimental relaxation data. The formulation of a theoretical model relating the TCF to the local structural complexity of the chain is not an easy task. As a result of steric constraints and concerted motions, the dynamics of the polymer main-chain and any possible side-chains is extremely complicated. Therefore, it is not expected that a detailed picture of polymer motions could be constructed from a few experimentally accessible parameters. However, despite these enormous difficulties some relevant progress has been made recently, resulting in well-founded theoretical procedures.

Another problem that may be encountered in applying dynamic models to the relaxation data is the possibility that the resulting physical picture of the motions may not be unique. This means that the relaxation data may not uniquely define a particular dynamic model, and several models are able to reproduce the experimental relaxation parameters. Indeed, as we shall see in Sections 3.4 and 4.0, this phenomenon is the rule and not the exception.

The problem of discriminating among models has been confronted by many investigators by conducting variable temperature relaxation measurements at several magnetic fields. A suitable model should reproduce the experimental relaxation data corresponding to the minimum in the curve of the longitudinal relaxation time versus the reciprocal of temperature, $1/T$ (K). A further test of model relevancy is the capability of a particular model to predict some independent relaxation data not previously used for adjusting the model parameters, provided that these data exhibit, also, a good sensitivity to the experimental conditions of temperature and frequency [45,46]. According

to this procedure, the model parameters obtained by fitting the T_1 data are used to calculate the NOE values, which should be compared with the experimental ones. It has been found [45,46] that NOE values can provide direct experimental evidence whenever a large dispersion of the C–H vector motional frequencies occurs in a polymer system, and they provide a much more discriminating physical quantity than T_1 for testing model applicability.

Another important aspect of relaxation measurements and dynamic modeling refers to experiments at high magnetic fields (corresponding to resonance at >50 MHz for the ^{13}C nucleus). Since the relaxation parameters for the CSA mechanism (Eqs. (6)–(10)) depend on ω_C^2, such measurements facilitate the unraveling of the contribution of this mechanism to the relaxation of unsaturated carbon nuclei in the polymer system.

3. Theoretical considerations of dynamic modeling

3.1 Modes of motion of a polymer molecule

A macromolecule comprises a large number of monomer units, so that any attempt to characterize its motion in terms of a coordinate system located at each atom becomes an almost impossible task. Therefore, such a methodology to define possible modes of motion is equally intractable. However, it is possible to consider a number of simplifying assumptions and to divide possible modes into a number of groups, each of them having particular motional characteristics exhibited by the polymer system. As mentioned in the introductory section, motions in a polymer chain can be divided into two general classes differing in time-scale: (1) local chain motions, and (2) collective motions. To the first class belong the localized motions of short segments of the polymer backbone, the so-called chain segmental motion. The moving unit consists of a very small number of monomer residues, and the characteristics of the motion depend on the nature and the environment of the segment rather than on the molecular weight of the whole chain. The movement can range from a simple torsional libration inside a potential well to motions between potential energy minima separated by intramolecular potential barriers. ^{13}C relaxation studies which probe such motions, particularly in dilute solutions, provide an excellent measure of chain flexibility.

Rotational motions of groups substituted on a polymer chain, e.g. methyl, phenyl, naphthyl, and pyridyl moieties, are considered as the most localized motions in a polymer system. Single internal rotations may be extended to include multiple internal rotations of side-chains attached to the polymer backbone by chemical bonds. Internal rotations of side-chains are usually restricted in amplitude due to constraints imposed by neighboring side-chains and the backbone chains, as well as by hydrodynamic interactions.

The longest-scale motions are those which involve large sections of the chain, or even the whole macromolecule, moving in a cooperative fashion. For stiff chains, which are unable to undergo conformational changes, the main chain carbon nuclei are relaxed by such long-range motional modes. However, random-coil flexible polymer chains are characterized by a large number of conformational changes or molecular distortions, the relaxation being controlled by small-scale segmental motions, which are much faster than the motion of the chain as a whole (overall molecular motion). Members of this class include synthetic polymers and natural molecules such as polysaccharides and polypeptides in conditions where the "rigid" conformation is disrupted.

Unlike dilute polymer solutions, the lateral displacement of chains in concentrated polymer solutions or for polymers in the amorphous state is hindered by topological constraints due to the entanglement of many neighboring chains. Although the interchain interactions are transient because of translational diffusion, they generate very low frequency motions such as chain fluctuations, reptation, or material displacement along the chain axis which are described in terms of the slow evolution of a fictitious tube occupied by a chain immersed in the polymer or solvent matrix. These very slow collective motions, which have a dramatic effect on the mechanical relaxation times, are not manifested in the relaxation time-scale of the present NMR experiments. These types of motion are excluded from the present article, which will emphasize intramolecular motions.

Kimmich et al. [47] have recently published a comprehensive review dealing with the tube concept of concentrated polymer solutions and bulk polymers, as well as with the appropriate NMR experiments which are sensitive to these very slow motions.

3.2 The nature of chain segmental motion

Early investigations [3] of polymer dynamics have shown that the measured T_1 and T_2 values are independent of molecular weight above a fairly low critical value of 1000–10,000, depending on chemical structure of the synthetic polymers. These observations led to the conclusion that for sufficiently large molecules in dilute solutions, relaxation of the backbone carbons is controlled by segmental motions unaffected by chain length. However, at these early stages the nature of segmental motion remained rather unclear. Although several models [48–53] were developed to interpret the experimental relaxation data in terms of segmental motions, they treated these high-frequency relaxation modes in a generalized and abstract way. Segmental motions were described as cooperative motions involving a few monomer units.

The correlation length (the size) of the mobile segments depends on the polymer structure and the hydrodynamic friction exerted by the solvent [4]. The time-scale of the reorientation of this chain segment is described by a correlation time. Initially, this localized mode of motion was generally viewed as one in which the movement of any one segment was independent of the motion of any other segment in the chain, i.e. an incoherent mode of motion with presumably very weak coupling between effective segments. However, subsequent theoretical results showed [54] that the assumption of weak intersegment coupling is unjustified, and that the choice of an appropriate strong coupling model can also predict modes of motions with these characteristics.

Another point of interest concerning segmental motion is that different relaxation techniques probe different length-scales for the mobile chain segment [55]. For instance, motions of relatively short segments are probed by NMR, whereas dielectric relaxation [56–58] and fluorescence anisotropy [59] probe larger scale motions. The length-scale of motional units is estimated to be approximately 7–10 times larger in the latter relaxation methods than in NMR. Although the description of chain segmental motion as a contribution from mobile segments of various sizes appears to be correct, the lack of a concrete definition of these motional units does not allow the elucidation of the mechanism of segmental motion, and the importance of constraints imposed by chain connectivity. Several experimental findings [60–64] and theoretical calculations [65–72] have shown the importance of specific conformational transitions available in a polymer chain in order to achieve a proper understanding of relaxation in polymers. The fact that local chain motions result from conformational transitions of the backbone bonds from one isomeric state to another is now well established [73–91].

Three principal factors determine the rate of a conformational transition: (1) the internal resistance associated with the intramolecular potential barrier to conformational transitions, (2) the external resistance of the medium, i.e. hydrodynamic forces exerted by the surroundings hindering the segmental motion, and (3) constraints imposed by chain connectivity. The first factor favors those transitions requiring rotation about the least number of bonds. The second factor favors transitions requiring the least displaced volume of the medium. Chain connectivity, which distinguishes the dynamic behavior of small molecules from macromolecules, is related to the motion of the tails of the chain and the resistance imposed by the tails on the mobile segment.

On these principles, it was suggested [65] that segmental motions occur in the form of "crankshaft" transitions, i.e. those consisting of the motion of a segment involving a few monomer units by rotation about two collinear bonds. Fig. 2 illustrates the crankshaft motion considered by Schatzki [92] as the origin of high frequency motions in polymers. In this type of motion the polymer tails attached to the segment remain undisturbed in the initial and final states. Another type of crankshaft motion is the three-bond motion [71, 73, 78] depicted in Fig. 3. This motion is considered to occur in a hypothetical cyclohexane ring, where the bonds occupy half of the cyclohexane ring in the initial state and flip to the other half of the ring by a concerted motion in such a way that leaves the tails in the same position as they were initially. Although crankshaft-type motion is a useful concept to

describe localized motions in a polymer chain, it seemingly calls for high activation energies because several bonds must be in the activated state almost simultaneously. Moreover, this localized mode of motion neglects completely the effect of chain connectivity. The argument that the tails are completely stationary, while collinear bonds are rotated, could lead to an energetically unfavorable distortion of the bonds adjacent to the transforming bonds. What is observed experimentally [93–95] and theoretically [79, 82, 85, 88] are activation energies for segmental motions of about one barrier height.

Helfand [66] has investigated the kinetics of conformational transitions based on a multidimensional extension of Kramers' reaction rate theory [96], and classified them according to changes in orientation induced in the attached tails. Type 1* motion is illustrated in Fig. 3 for a three-bond motion where P and Q denote the polymer tails, and t and g stand for trans and gauche conformations, respectively. Type 1* motion is actually a crankshaft motion. Owing to the simultaneous orientational change of the moving bonds, the motion involves several barrier crossings. For example an average of two barrier crossings is considered for a three-bond motion. Type 2* motions are those conformational processes that lead to a relative translation of P and Q tails. They correspond to transitions PgttQ → PttgQ (Fig. 4) and PtttQ → PgtgQ. The third type of motion,

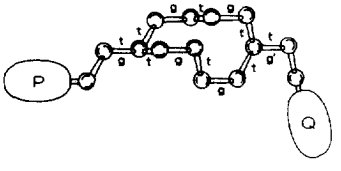

Pg(tgtgt)g'Q ⇌ Pt(tgtgt)tQ

Fig. 2. The Schatzki crankshaft conformational transition; five-bond motion about two collinear bonds. P and Q denote the polymer tails, t and g(g') represent trans and gauche conformations, respectively.

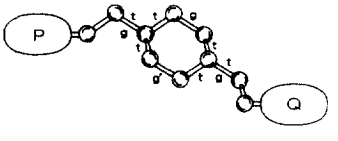

PttgttQ ⇌ Pgtg'tgQ

Fig. 3. A type 1* transition. P and Q denote the polymer tails, t and g(g') represent trans and gauche conformations, respectively.

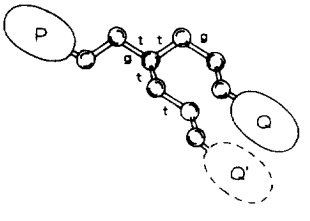

PgttQ ⇌ PttgQ'

Fig. 4. A type 2* transition. P and Q denote the polymer tails, t and g represent trans and gauche conformations, respectively.

type 3* motion, is related to the single bond t → g transition in which the tails suffer reorientation. Although type 1* motion is energetically less favorable than type 2* and 3* transitions, the latter motions are expected to be much slower than the former because of the strong viscous drag on the bulky tails. However, subsequent Brownian dynamics simulation [79, 80, 84] and kinetic analysis [82, 83] on a polyethylene chain embedded in a continuum showed that this is not necessarily the case. It is found that the tails do not behave as rigid bodies, but instead the rotation of a bond is accompanied by distortion of neighboring degrees of freedom along the chain, which makes the mode totally localized. The distortion diminishes with distance from the motional center, and favors the softest modes, namely, bond angle torsions in order to decrease the total energy of the system as rapidly as possible. Such a motion is very often associated with an appropriate motion of the second neighbor bond, which allows the motion of the first bond to be accommodated without involving a wide swing of the tails. Then other distortions can be invoked to eliminate asymptotically the translation. Counter-rotation of the second-neighbor bond is likely to occur when the first-neighbor bond of the rotating bond is trans, so that both single and pair transitions, e.g. gtt → ttg are observed. The activation energy of this process is one barrier crossing because cooperative pair transitions occur successively rather than simultaneously. Frequently, the induced counter-rotation of the second-neighbor bond is dissipated before being brought all the way to the point of its own transition. Then the second neighbor falls back to its initial state, and a single transition is observed overall. Helfand and co-workers [80, 84] have reported that ≈ 29% of all polyethylene transitions are cooperative at 330 K. Among these ≈ 14% are gauche migration (gtt → ttg) and ≈ 10% are gauche pair transitions (ttt → gtg). The remaining transitions are single-bond transitions which account for the two-thirds of the total number of transitions in the polyethylene chain. Nevertheless, these unfavourable single-bond transitions are damped by the fluctuations of the internal rotation angles of neighboring bonds, as well as by distortions of the harder degrees of freedom such as bond angles and bond lengths. Molecular dynamics analysis of transitions between rotational isomers in linear polyethylene chains has shown [97] that at very short times (< 1 ps) along the molecular dynamics trajectories, correlations between second-neighbor bonds dominate the rotational isomeric transitions over isolated transitions or larger scale cooperative transitions. However, the dominance of second-neighbor correlations decreases as the time-scale of the analysis increases.

Recently, Brownian dynamics computer simulations have been performed by Adolf and Ediger [86, 98] in an attempt to examine cooperativity in polyethylene and poly(isoprene) chains, and to compare the local dynamics between these two polymers. Their analysis showed that for cooperative transition pairs, the probability that the second-neighbor torsion in polyethylene undergoes a given angular change is only slightly different from that for the group of all transitions, i.e. cooperative transition pairs plus isolated transitions. Moreover, distortions of neighboring degrees of freedom (torsional angles and bond angles) along the simulated polyethylene chain were found to be very similar for both the subset of cooperative transition pairs and the group of all transitions. Thus, cooperative transition pairs and isolated transitions are not so very different as was previously thought. The motion which occurs in connection with a conformational transition in polyethylene is almost independent of whether a second transition occurs cooperatively with the first. The displacement of the second-neighbor torsional angle can be viewed as a continuous process rather than a two-stage process. Nevertheless, second-neighbor torsions are the most important mechanism in localizing conformational transitions in polyethylene, as suggested by Helfand and co-workers [66, 79, 80, 84, 85]. This effect is not observed in polyisoprene [86]. The torsional coupling is strong for first neighbors, but much less important for second neighbors. The different behavior of polyisoprene and polyethylene chains in terms of cooperativity has been attributed [86, 98] to the different structures and potentials of these two polymers. This important finding indicates that the simple picture of torsional cooperativity in polyethylene cannot be directly applied to po lyisoprene or other polymer systems of different structures.

In view of the above discussion and the notion that cooperative transition pairs and isolated transitions have the same activation energy of about one barrier crossing, it can be concluded that chain connectivity may not play a dramatic role in segmental motion. Indeed, in a series of papers on local dynamics, Bahar and co-workers [87, 88, 91] have established in a rigorous manner that the

resistance imposed by the tails on the mobile segment is not strong enough to have a major influence on conformational transitions provided that compensating fluctuations of the various degrees of freedom of the chain are spread out over a large distance along the chain, as described by Helfand and Ediger.

An important feature of segmental motion is the size or the length-scale over which conformational transitions are localized. Early motional models [48,49,51] describing polymer dynamics in terms of a distribution of correlation times include an adjustable parameter defining the width of the distribution. This parameter is related to the number of degrees of freedom involved in the backbone segmental motion, and hence it is suggested to be a semi-quantitative measure of the extent of cooperativity. Other models, [56,78] which describe segmental motion in terms of conformational transitions of the crankshaft type, confine the conformational coupling to a finite chain segment of length [78] $2m - 1$, m being the number of bonds involved in cooperative motions, or between a lower and an upper wavelength limit for conformational transitions [56]. The lower wavelength limit is set by the size of the smallest displaceable segment (up to a repeat unit), and the upper limit is set by the length of the whole chain. In practice, the upper limit may be shorter than the chain length because a conformational transition displacement along the chain will be damped out by various dissipative processes.

The parameters of the various models, which describe cooperativity in segmental motion, can be obtained by fitting the experimental relaxation data of polymer systems. However, these parameters are strongly model-dependent and there are several circumstances [3,4,45,46,99] where different models give different ranges of cooperativity for the same polymer system. Furthermore, the width parameters represent a collective measure of cooperativity involving chain segments of various lengths, and give no information about the relationship between cooperativity and chain structure.

Recent Brownian dynamics simulations have shown that conformational transitions in the polyethylene chain [98] are localised to about two repeat units, the distortion being negligible more that six atoms away from the position of the conformational transition. For poly(isoprene) [86] the length-scale of cooperativity is smaller than that of polyethylene, and is about one repeat unit. It appears that the range of cooperativity in a polymer chain depends on the structural details of the repeat unit.

Calculations along these lines, based on a mathematical formalism for local chain dynamics of real chains [87,88–91], are in agreement with conclusions derived from a Brownian dynamics simulation for the polyethylene chain [66,79,80,84–86,98]. Also, they confirm [87] that the occurrence of an increase in "chain stiffness" accompanies a decrease in the size of the mobile segment. Longer sequences are found to relax faster as a result of an increase in the number of degrees of freedom, and hence in the number of allowable paths to relaxation. However, environmental resistance due to friction in dilute solutions or chain-entanglement in the bulk tends to slow down the motion of the mobile segment as its size increases. Therefore, the length-scale of cooperativity in a polymer chain must be a compromise between frictional forces exerted by the medium, the number of moving atoms, and their displacement during a conformational transition. An upper bound for the size of the motional sequence has been given by Bendler and co-workers [56] in the form of a long wavelength cutoff as mentioned earlier in this section.

3.3 Time correlation functions and spectral density functions for polymer segmental motions

3.3.1 Chain segmental motion

3.3.1.1 Distribution of correlation times. As shown in Fig. 1, the experimental relaxation parameters for a polymer behave differently from those for molecules of low molecular weight. In particular, T_1 values show raised and broadened minima, low T_2 values ($T_2 < T_1$), and broadened NOE transitions. In view of these observations, which are a direct result of polymer segmental motions of high complexity, it is not surprising that polymer motion cannot be described by using a single correlation time. The first attempts to interpret quantitatively the ^{13}C relaxation parameters of a polymer system invoked a semi-empirical distribution of correlation times. The distribution is

expressed in the form of a mathematical density function, $F(s)$, such as

$$\int_{-\infty}^{+\infty} F(s)\,dt = 1 \tag{22}$$

the variable s is defined by

$$s = \ln(\tau_c/\tau) \tag{23}$$

where τ is an average correlation time defining the center of the distribution. The correlation function, $G(t)$ is written as

$$G(t) = \int_{-\infty}^{+\infty} F(s)e^{[(-t/\tau)\exp(s)]}\,ds \tag{24}$$

The form of the distribution function characterizes the model used to describe the polymer dynamics. Two symmetric (about τ) and one asymmetric distributions have been used in the past to interpret the relaxation data of polymers in solution and in the bulk. The two symmetric distributions are:

Cole–Cole distribution [48]

$$F(s) = \frac{1}{2\pi}\frac{\sin(\varepsilon\pi)}{\cosh(\varepsilon s) + \cos(\varepsilon\pi)} \tag{25}$$

Fuoss–Kirkwood distribution [49]

$$F(s) = \frac{\beta}{\pi}\frac{\cos(\beta\pi/2)\cosh(\beta s)}{\cos^2(\beta\pi/2) + \sinh^2(\beta s)} \tag{26}$$

The asymmetric distribution with tails toward longer correlation times is the $\log(\chi^2)$ distribution

$$F(s) = \frac{p}{\Gamma(p)}(ps)^{p-1}e^{(-ps)}p \tag{27}$$

introduced by Schaefer [51], considering segmental motion to be dominated by high-frequency local motions damped out by low-frequency cooperative motions. The parameters ε, β and p define the width of the distributions. ε and β lie in the range $0 < (\varepsilon, \beta) < 1$. The larger one is the width parameter, the narrower is the distribution. The upper limit of unity for ε or β, and infinity for p correspond to a single exponential correlation function. It should be noted that the parameter s in the $\log(\chi^2)$ distribution is defined as [51]

$$s = \log_b[1 + (b-1)\tau_c/\tau] \tag{28}$$

since the function adopted by Schaefer is an extension to a logarithmic scale of the χ^2 distribution.By introducing Eqs. (25)–(28) into Eq. (24) then Fourier transformation, the various spectral densities are obtained [3,43,44]. The spectral density for the $\log(\chi^2)$ model is given by [51]

$$J(\omega) = 2\int_0^{\infty} \frac{F(s)\tau[b^s - 1]\,ds}{(b-1)\{1 + \omega^2\tau^2[(b^s-1)/(b-1)]^2\}} \tag{29}$$

Eq. (29) is evaluated numerically. In fact the $\log(\chi^2)$ distribution is a three-parameter model, i.e. in addition to τ, the two parameters, p and b, are needed to specify this distribution. However, in practice only two parameters, p and τ, are fitted to the experimental data, provided that b is sufficiently large [51]. The parameter b is often fixed at 1000.

Although the distribution functions may be useful in providing a quantitative balance between fast and slow motions in a polymer chain, they do not provide any information about the nature of

these motions. Also, the $\log(\chi^2)$ distribution is valid for $p > 2\ln b$, where the distribution is normalizable. For p less than $2\ln b$, the tail of the distribution is poorly parametrized and log correlation times may be unduly weighted [100]. However, these functions may be applied in cases where either the motional mechanisms are too complex to be described by a definite model, or the heterogeneous surroundings of the chains (e.g. in amorphous or semi-crystalline polymers) lead to an inhomogeneous distribution of correlation times. For the latter situation some modifications introduced [100] in the $\log(\chi^2)$ and the Fuoss–Kirkwood distribution [101] may be more effective than the original functions at describing changes in the width of the distribution in the high and low temperature regions for the same polymer system [45,46].

Another distribution function that has been briefly applied to NMR relaxation is the log normal distribution [100]. The unsymmetrical Davidson–Cole distribution [50,102], which has been applied to dielectric relaxation, has the tails toward the short correlation times, and thus it does not seem physically reasonable for the NMR relaxation of polymers

Besides the continuous distributions, discrete distributions of correlation times may be used in the analysis of the ^{13}C relaxation data. Such models, leading to a discrete distribution of two [103] or three [104] correlation times, have proven to be of limited value [105].

3.3.1.2 Diamond-lattice models. The class of models represents a serious attempt to describe segmental motion in terms of conformational transitions. The general theory has been developed in a series of papers [71–77] by Valeur, Jarry, Geny, and Monnerie (VJGM model). According to this theory, a polymer chain is distributed randomly on a diamond- or tetrahedral-lattice subjected to three- and four-bond transitions of the crankshaft type shown in Fig. 5. The dynamics have been studied by both Monte Carlo [71,72] and analytical methods [73–75]. A major conclusion derived from this analysis is that all other types of crankshaft motions can be reduced to a succession of these two elementary processes. The TCFs for three-bond and four-bond jumps in the VJGM model are obtained by solving the appropriate diffusion equations [73–75], which for the three-bond motion describe the diffusion of orientations along the chain, whereas for the four-bond motion, in addition to the diffusion term, the diffusion equation contains a dissipative term representing the creation and destruction of orientations by four-bond transitions. These functions are given by Eqs. (30) and (31), for the three- and four-bonds motion, respectively.

$$G(t) = e^{t/\rho}\,\mathrm{erfc}[(t/\rho)^{1/2}] \tag{30}$$

$$G(t) = e^{-t/\theta}e^{t/\rho}\,\mathrm{ercf}[(t/\rho)^{1/2}] \tag{31}$$

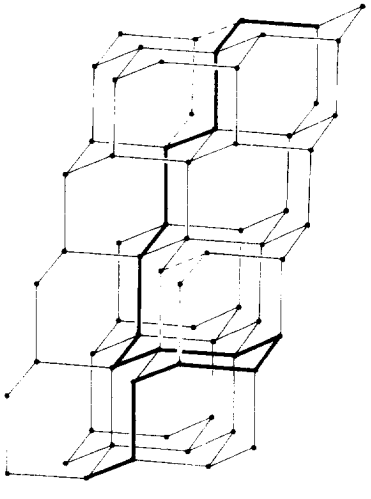

Fig. 5. Three-bond (top) and four-bond (bottom) transitions on a diamond-lattice. Transitions are shown by broken lines.

Here, ercf is the complementary error function. In general terms, the correlation time ρ describes cooperative transitions, i.e. crankshaft three- or four-bond motions, whereas the correlation time θ represents processes leading to loss of orientation, not necessarily with distortions of neighboring degrees of freedom [106]. These parameters are defined as follows: in Eq. (30) by

$$\rho = (\lambda^2 w_3)^{-1} \tag{32}$$

and in Eq. (31) by

$$\rho = [\lambda^2(3.16w_3 - 9.61w_4)]^{-1}, \qquad \theta = (4.74w_4)^{-1} \tag{33}$$

where λ is a constant which depends on the conformational probabilities, and takes the value of $\lambda = \ln 9$ for equally populated trans and gauche conformations [73]. w_3 and w_4 are the jump rates for three-bond and four-bond motions, respectively.

There are two serious approximations involved in the derivation of Eq. (30). First, the chain is assumed to be infinite, which is not true regarding the nature of segmental motion discussed in Section 3.2. This aspect is the major cause for the very slow decay of the correlation function of Eq. (30) at long times. Second, the assumption that trans and gauche orientations are equally probable is not realistic because of steric interactions. These deficiencies are remedied somewhat in Eq. (31), where the introduction of the term $\exp(-t/\theta)$ makes the correlation function decay more rapidly at long times than the function in Eq. (30). Also, it has been suggested [75] that the same term can account for deviations from strict lattice conditions and rigid tails. The spectral density functions [3,4] corresponding to Eqs. (30) and (31) had been evaluated earlier by Hunt and Powles [107] for relaxation in solids by lattice defect diffusion.

Jones and Stockmayer [78] chose different boundary conditions to solve the diffusion equation describing three-bond motion. The first condition was to relax the coupling between neighboring-bond orientations, so that a bond may rotate even though its neighbors are not in the correct orientations for the crankshaft process. The second condition was to impose a sharp cutoff on the effects of directional coupling, thus limiting the conformational coupling to a finite chain segment of length $2m - 1$, where m is the number of bonds involved in the cooperative motion. The quantity $2m - 1$ stands for the width of the distribution of correlation times. The TCF of this model, the Jones and Stockmayer (JS) model, is expressed as a discrete distribution of correlation times, i.e. [78]

$$G(t) = (1/5) \sum_{k=1}^{s} B_k e^{-t/\tau k} \tag{34}$$

with

$$s = (m + 1)/2, \qquad \tau_k = (\lambda_k w_3)^{-1} \tag{34a}$$

Analytical expressions for the weighting functions B_k and the parameter λ_k are given in Ref. [78], which also includes values of these parameters for $m = 3, 5$, and 7. The distribution of the correlation times is described by an arithmetic mean correlation time, τ_a, or by a harmonic mean correlation time, τ_h, defined [78] as $\tau_a = \langle \tau_k \rangle$ and $\tau_h = \langle \tau_k^{-1} \rangle^{-1}$, respectively. Also, τ_h is usually expressed in terms of the rate of the three-bond transitions, i.e. $\tau_h = (2w_3)^{-1}$.

An alternative solution of the diffusion equation has been attempted by Bendler and Yaris [56] (BY model) who pointed out that the JS model is quite reasonable if the number of cooperative units along the chain is rather small (3–9 bonds). For longer length-scale of cooperativity, the solution of the diffusion equation becomes unwieldy. By going over a continuum limit, a diffusion equation was set up involving an experimental diffusion constant, D. By using plane waves as eigenvectors and eigenvalues of the spatial part of the diffusion equation, the TCF for segmental motions is evaluated. However, in their method, Bendler and Yaris did not allow solutions for all wave vectors. A long wave vector cutoff, k_B (or short wavelength) was introduced to account for the smallest unit in a macromolecule that can be displaced. On the other hand, there must be a short wave vector, k_A (or long wavelength) describing motions of the polymer chain as a whole. As mentioned earlier (Section 3.2), the long wavelength cutoff will be shorter than the length of a polymer chain, since a conformational transition along the chain will damp out by frictional forces. The resulting TCF and spectral

density function of the BY model [56, 57] (or cutoff diffusion (CD) model) contains two parameters, ω_A and ω_B, that can be fitted to the experimental data, i.e.

$$G_{BY}(t) = (\tfrac{1}{10})(\tfrac{\pi}{t})^{1/2}(\omega_B^{1/2} - \omega_A^{1/2})^{-1}\{\mathrm{erfc}[(\omega_A t)^{1/2}] - \mathrm{erfc}[(\omega_B t)^{1/2}]\} \tag{35}$$

where

$$\omega_A = 2k_A^2 D/5, \qquad \omega_B = 2k_B^2 D/5 \tag{35a}$$

In a later report, Skolnick and Yaris [57] attempted to remove the arbitrary feature of the BY model associated with the long wavelength cutoff and approximate the effects of damping by including directly in the diffusion equation a phenomenological constant, the damping constant β. After considerable manipulation, the TCF obtained in this model (the Skolnick and Yaris (SY) or damped diffusion (DD) model) is given by [57, 58]

$$G_{SY} = (\tfrac{1}{10})(\tfrac{\pi}{\delta t})^{1/2}\,\mathrm{e}^{-\beta t}\,\mathrm{erfc}[(\delta t)^{1/2}] \tag{36}$$

where

$$\delta = D\omega_C^2, \qquad \omega_C^2 = k_B^2 - \beta/D \tag{36a}$$

As in the BY model, the parameter δ (or ω_C) represents a short wavelength cutoff corresponding to the smallest motional unit.

The introduction of a damping term in Eq. (36) is physically more realistic, but actually both the BY and SY models are characterized by the same physics. In this context, the parameter ω_B of the BY model and δ of the SY model should be the same, since they represent the short wavelength cutoffs. The β and ω_A parameters represent the long wavelength cutoffs of the SY and BY models, respectively. However, β must be slightly smaller than ω_A, since the cutoff is expressed as a wave vector which is reciprocally related to the wavelength.

Skolnick and Yaris [58] have generalized their damped diffusion model (Eq. (36)) to include chain–chain interactions, which occur in concentrated polymer solutions or in the amorphous state. The chain–chain interaction is modeled rather generally by using multiple scattering theory, leading to a complex diffusion equation [58]. Solution of the diffusion equation lead to a complex TCF

$$G_{CD}(t) = \mathrm{e}^{-i\gamma t} G_{SY}(t) \tag{37}$$

where the subscript CD denotes complex damping, and γ is the parameter that accounts for the exchange of orientational correlation between neighboring motional segments. $G_{SY}(t)$ is the TCF of Eq. (36). The spectral density function of the complex damping model is identical to the damped diffusion model, except the frequency is shifted by γ, i.e. [58]

$$J_{CD}(\omega) = J_{SY}(\omega - \gamma) \tag{38}$$

The explicit form of $J_{SY}(\omega)$ is given in Refs. [57] and [58].

In a later paper [108], Skolnick et al. have extended their ideas on motional segment–segment dynamic interactions to include restricted rotational diffusion motion. In contrast to previous models [25, 30] describing restricted rotational diffusion in terms of a sum over an infinite series of rational polynomials, they derived a closed form analytic expression for the TCF, which incorporates the complex damping constant. Numerical calculations show [108] that segment–segment interactions expressed by the parameter γ are more effective when $\gamma \approx \omega\,(\omega_H + \omega_C, \omega_C, \omega_H - \omega_C)$ in the slow reorientation limit. Strong interchain interactions result in a relatively large positive or negative NOE ($-3.5 < \mathrm{NOE} < 5$), and T_1 values become less than T_2 values ($T_2 \approx 2T_1$). Although this model offers a basis for understanding when interchain dynamic coupling is important in the restricted diffusion model of segmental motion, experimental relaxation parameters in the range predicted by this model have not been measured yet for synthetic polymers in solution or in the bulk. The lattice models have been used in many instances (Refs. [3, 4] and section 4 of the present article) for describing the chain local dynamics of polymer systems. However, one should keep in mind that the TCFs derived from those models are deficient for several reasons: (a) they show unrealistic derivatives at $t = 0$, (b) the first-order and second-order TCFs are unrealistically

equal, (c) they neglect the effect of chain connectivity, (d) hydrodynamic interactions are not considered.

3.3.1.3 Models derived from polymer chain dynamics simulations. In addition to analytical approaches, local polymer dynamics relevant to NMR have been investigated by utilizing numerical simulations. In principle computer modeling is very effective in tracing the shape and motions of polymer molecules individually, thus allowing evaluation of much more detailed information on the dynamic properties of the system than any experimental measurements can provide [109]. Moreover, numerical simulations may involve realistic structures and potentials leading to a much closer understanding of structure–property relationships. Attempts in this direction have been discussed previously in relation to the diamond-lattice model [71, 72, 76, 77] leading to Eqs. (30) and (31) for the TCFs of bond orientations in polyethylene and polyethers using chains randomly generated on a tetrahedral-lattice, and taking into account both excluded volume and energy differences between trans and gauche isomers.

Helfand and co-workers [80–84] have simulated polymer dynamics by solving numerically the Langevin equation of motion of a polyethylene chain moving in a viscous medium subject to α frictional force, a potential force (from bond rotations, bond stretching and bond angle bending), and a random Brownian force. Conformational transitions have been described in the high friction limit. Moreover, excluded volume effects and hydrodynamic interactions have been neglected in this treatment. As mentioned in Section 3.2, single-bond conformational transitions dominate the backbone rearrangement, although cooperative transitions may also occur. Any associated movement of the tails initially takes place by distortion of neighboring degrees of freedom. Weber and Helfand [84] have evaluated vector TCFs for unit vectors oriented at different angles relative to the polyethylene backbone. It was found that the TCFs associated with different orientations of the unit vector decay at different rates. In particular, the out-of-plane vector, i.e. the vector perpendicular to the plane of the chain segment, relaxes much faster than the bond vector along the main chain. Although the observed anisotropy in the relaxation of the bond vectors perpendicular and parallel to the main chain has been described in terms of the experimentally inaccessible conformational TCFs, it may reasonably be inferred that DD interactions oriented at different angles relative to the backbone may be associated with different TCFs. Such an anisotropy in local relaxation interactions in polymer chains has been detected by Fuson and co-workers [37, 38] as mentioned earlier.

A similar anisotropy for local relaxation of the polyethylene chain has also been detected independently by Bahar and Erman [110] and Takeuchi and Roe [111] using orientational TCFs. In addition, these studies have shown that the anisotropy of local relaxation depends on the molecular structure of the polymer repeat unit and the environment of the polymer chain. Thus, in poly(ethylene oxide), vectors along the skeletal bonds relax faster than those vectors oriented perpendicular to the main chain [110], in contrast to what has been observed for the polyethylene chain. Also, the anisotropy of local relaxation is expected to be much stronger when the influence of the surrounding chains is considered explicitly in the correlation function in terms of non-bonded interaction potentials between chain segments. Indeed, molecular dynamics simulation of local chain motions in bulk amorphous polymers has revealed [111] that the anisotropy is about two orders of magnitude greater than that observed in the Brownian dynamics simulation [84], where constraints exerted on the motion of the chain segment by the surrounding non-bonded segments are neglected.

The various conformational TCFs associated with the different orientations of the unit vectors with respect to the backbone are represented by a semi-empirical function of the form [81, 84]

$$G(t) = (1 - \alpha)\,e^{-t/\tau_0} e^{-t/\tau_1} I_0(t/\tau_1) + \alpha e^{-t/\mu} \tag{39}$$

where I_0 is a modified Bessel function of zero order, τ_0 and τ_1 are the correlation times associated with single-bond and bond-pair transitions, α and μ are constants. The contribution of the second term in Eq. (39) depends on the particular vector correlation function considered. The parameter α is very small (0.0018 at 330 K) for correlation of vectors perpendicular to the chain, and, therefore, the second term in Eq. (39) is very small relative to the first term and can be omitted. The spectral density

function for this model, the so-called Hall–Weber–Helfand (HWH) model, is given by [112]

$$J(\omega) = \mathrm{Re}\left[\frac{1}{(\alpha + \mathrm{i}\beta)^{1/2}}\right] \tag{40}$$

where

$$\alpha = \tau_0^{-2} + 2(\tau_0\tau_1)^{-1} - \omega^2, \qquad \beta = -2\omega(\tau_0^{-1} + \tau_1^{-1}) \tag{40a}$$

Two recent theoretical models developed by Bahar and co-workers [87, 88, 90, 91] and Perico and co-workers [113–116] have enriched significantly our knowledge about local chain dynamics. The most important advantage of these theories is the fact that real chain characteristics such as the molecular structure and configurational statistics are incorporated into the calculations. Information about intramolecular potentials can be included in these models provided that a detailed conformational energy map is constructed. The time-dependence of the orientational TCF can be computed, and thus its shape can be determined, for specific vectorial quantities rigidly embedded in short segments of real chains subject to conformational transitions. Mathematical details of these models and the derivation of TCFs in analytical forms can be found in the appropriate references cited. Here, the final forms of the TCFs will be given. The TCF of the first model, the so-called dynamic rotational isomeric state (DRIS) model [87, 90], appropriate for NMR relaxation is given by

$$G(t) = \sum_{i=1}^{3^N} k_i \mathrm{e}^{\lambda_i t} \tag{41}$$

here, λ_i is the relaxation rate corresponding to the motional mode i, and represents the eigenvalues of a rate transition matrix, $\boldsymbol{A}^{(N)}$, the elements of which $A_{ij}^{(N)}$, represent the rate constants for the passage between different configurations. The matrix is constructed [87, 90] according to a suitable kinetic scheme depending on the specific configurational characteristics of the polymer considered. The summation index runs over 3^N configurations available in the sequence, N being the number of the backbone bonds involved in conformational transitions. The time-independent parameter k_i depends on the molecular structure and the equilibrium statistics of the chain, and represents the a priori probability of relaxation through internal mode i with frequency λ_i

$$k_i = \sum_{j=1}^{3^N} \sum_{n=1}^{3^N} B_{ni}^{(N)} [B_{ij}^{(N)}]^{-1} P_n^{(N)}(0) [3(m_j m_n) - 1]/2 \tag{42}$$

$P_n^{(N)}(0)$ is the equilibrium probability of the initial configurations $\{\Phi\}_n$ ($n = 1, 2, 3, \ldots, 3^N$) specified by a complete set of rotational angles $(\Phi_1, \Phi_2, \ldots, \Phi_N)$ for a sequence consisting of N backbone bonds. m_i is the vectorial representation of the bond of interest when the sequence assumes the configuration $\{\Phi\}_i$ at time t, and $B_{ni}^{(N)}$ and $[B_{ij}^{(N)}]^{-1}$ are the elements of the matrix $\boldsymbol{B}^{(N)}$ and its inverse $[\boldsymbol{B}^{(N)}]^{-1}$ which are found from the similarity transformation $\boldsymbol{A} = \boldsymbol{B}\boldsymbol{\Lambda}\boldsymbol{B}^{-1}$, $\boldsymbol{\Lambda}$ being the diagonal matrix of the eigenvalues λ_i.

Recently, Perico and co-workers [113–116] have derived an orientational TCF for local dynamics by using the optimum Rouse–Zim approximation (ORZ) to the generalized Langevin diffusion equation in the full configurational space.

$$\frac{\partial R_i(t)}{\partial t} + \sigma \sum_{j=0}^{n-1} (HA)_{ij} R_j(t) = v_i^*(t) \tag{43}$$

This equation describes the time evolution of the bead coordinates, $R_i(t)$, $i = 1, 2, 3, \ldots, (n-1)$ (the polymer chain has been modeled as a collection of n friction beads of equal friction coefficient, ζ, connected by a potential of mean force $V(\{R_i\})$ and fluctuating in a theta solvent due to Brownian motion), under random forces responsible for the Gaussian random velocity, $v_i^*(t)$, the intramolecular potential, $V(\{R_i\})$, friction forces, and hydrodynamic interactions, the last being expressed by the matrix $\boldsymbol{H}$. The quantity A is a structural matrix given in terms of the inverse $\boldsymbol{U}^{-1}$ of the static bond correlation matrix. $\boldsymbol{U}$ has a central role in this theory, the so-called ORZ for local dynamics (ORZLD), since it contains all the conformational details of the polymer system. It can be calculated

either from the full conformational energy map of the chain [117] or from rotational isomeric state (RIS) models of different degrees of sophistication (RIS-ORZ hierarchy) [115, 116]. The constant σ is defined as the characteristic bond-rate constant of the model, expected to be an upper limit to the jump transition rate. This parameter takes into account temperature and solvent viscosity effects, and is roughly estimated as a function of the solvent viscosity, η_0, the length of an effective (virtual) bond vector, l, through the following equation

$$\sigma = 2k_B T/\pi\eta_0 l^3 \tag{44}$$

k_B is Boltzman's constant. However, in a quantitative comparison with experiments, σ should be allowed to vary smoothly in order to compensate for the approximations in the ORZ approach.

Decoupling Eq. (43) by transformation to normal modes, $\{\xi_a\}$, and solving under the hypothesis of a Gaussian random process, the joint Gaussian probabilities are obtained, allowing calculation of the appropriate TCF for the NMR relaxation experiments [113, 117, 118]

$$G(t) = 1 - 3\{x^2 - x^3(2/\pi)[1 - (2/\pi)\arctan x]\} \tag{45}$$

with

$$x = \frac{\{1 - [M_1^i(t)]^2\}^{1/2}}{M_1^i(t)} \tag{45a}$$

where $M_1^i(t)$ is the bond vector TCF expressed in terms of the eigenvalues, λ_a, and eigenvectors, $\boldsymbol{Q}$, of the matrix ($\boldsymbol{HA}$) in Eq. (43), i.e.

$$M_1^i(t) = \sum_{a=1}^{n-1} (Q_{i,a} - Q_{i-1,a})^2 \mu_a^{-1} e^{-\sigma\lambda_a t} \tag{46}$$

The quantity μ_a^{-1} is proportional to the mean square length of the normal modes $\{\xi_a\}$. A fitting of the experimental values of T_1 and NOE for a polymer system allows the determination of the parameter σ, and, through Eq. (44), the segment length describing the stiffness of the chain. In the case of a freely rotating chain with an effective bond length, l_0, and a valence angle, θ, the stiffness parameter, g, and the persistence length, p, can be calculated through Eqs. (47) and (48) [118]

$$g = -\cos\theta \tag{47}$$

$$p = l_0(1 - g)^{-1} \tag{48}$$

Perico [115] has shown that in the case of a Gaussian chain in the free-draining limit, Eq. (46) can be easily summed to give for the central segment

$$G(t) = e^{2\sigma t} I_0(2\sigma t) \tag{49}$$

which is relevant to the HWH TCF of Eq. (39), if the relatively less important exponential factors, $\exp(-t/\tau_0)$ and $\exp(-t/\mu)$ are ignored, and τ_1 is identified as $(2\sigma)^{-1}$. This result, which is a particular solution of the more general ORZLD model, indicates that the latter approach is far superior, giving much more information about intramolecular potential and hydrodynamic interactions in dilute and concentrated solutions. Also, the ORZLD model provides the actual form of the TCF required to interpret different relaxation experiments (dielectric, NMR, fluorescence polarization, etc.), to describe bond motions in central or end positions of the chain, and to analyze short-range stiffness for semi-flexible polymers.

Another approach, that may prove useful for stiff macromolecules, is the Helical Worm-like Chain (HW) model developed by Yamakawa and Fujii [119]. This theory is also based on the generalized diffusion equation for a polymer model built up from a collection of rigid sub-bodies and particularly devised for spin–spin dipolar vectors attached rigidly or with a rotational degree of freedom to each of the sub-bodies composing the chain. For flexible chains, outside the extreme narrowing limit, the agreement between HW theory and experiment is satisfactory for the T_1 relaxation parameter, but not for T_2 and NOE [119].

3.3.1.4 Librational models. In many instances, the two-parameter models failed to reproduce the relaxation data at the minimum of the curve of T_1 vs. temperature. Furthermore, the unimodal distribution functions were unable to predict values less than 2 for the ratio

$$R = T_1(\mathrm{CH})/T_1(\mathrm{CH}_2) \tag{50}$$

of the relaxation times of the backbone methine and methylene carbons observed for polymer systems in solution [21,120–123] and in the bulk [8,46,45,124–128]. These results indicate that there exists, inside the polymer chain, an additional motion which has not been considered previously. This additional motion must be much faster than the orientational diffusion process along the chain, and thus more local than the latter motion. Dejean de la Batie, et al. [126] have proposed a librational motion of limited amplitude for the backbone C–H vectors about their equilibrium conformation. It has been suggested [126], and verified [98] by Brownian dynamics simulation, that this additional motion occurs within dihedral potential wells, in contrast to conformational transitions which reflect motions between wells. The boundaries of the libration are defined by a cone of half-angle, θ, the axis of which coincides with the rest position of the C–H vector (Fig. 6). These conical boundaries of libration had been proposed earlier by Howarth [129] in his restricted rotation model. Following Howarth's description of bond librations, and assuming that the correlation time of the librational motion is much shorter than the correlation times describing backbone conformational transitions, the composite TCF for this model, the so-called DLM model, can be written as

$$G(t) = (1 - A)\mathrm{e}^{-t/\tau_0}\mathrm{e}^{-t/\tau_1} I_0(t/\tau_1) + A\mathrm{e}^{-t/\tau_2} \tag{51}$$

The first term in Eq. (51) is the HWH TCF mentioned earlier with correlation times τ_0 and τ_1 for isolated and cooperative transitions, respectively. The second term accounts for the contribution of the librational motion associated with correlation time, τ_2. The parameter $(1 - A)$ is given as a function of the cone half-angle θ, i.e.

$$1 - A = \left[\frac{\cos\theta - \cos^3\theta}{2(1 - \cos\theta)}\right]^2 \tag{52}$$

The Fourier transform of Eq. (51) gives the spectral density function

$$J(\omega) = \mathrm{Re}\left[\frac{1 - A}{(\alpha + \mathrm{i}\beta)^{1/2}}\right] + \frac{A\tau_2}{1 + \omega^2\tau_2^2} \tag{53}$$

with parameters α and β defined in Eq. (40a). The effect of the librational motion on the T_1 value at the minimum is to increase its value by a factor of $1/(1 - A)$ [126]. Therefore, the height of the T_1 minimum is strongly dependent on the amplitude of the librational motion. Moreover, the deviation of the relaxation ratio, R, in Eq. (50), from its theoretical value of 2 is attributed to the different conic

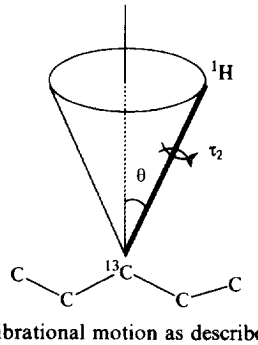

Fig. 6. Schematic representation of the librational motion as described in terms of a random anisotropic fast reorientation of the C–H vector with a characteristic correlation time τ_2, inside a cone of half-angle, θ, the axis of which is the rest position of the ^{13}C–^{1}H bond [123].

half-angles θ associated with the librational motions of the C–H vectors at the CH and CH_2 carbon sites. In vinyl polymers the presence of the substituent at the methine carbon hinders the librational motion of the methine C–H vector resulting in a smaller angle θ than that of the C–H vectors of the methylene group.

With appropriate mathematical treatment, librational motion has also been incorporated into the Cole–Cole distribution function [21] (Eq. (25)) and it may be possible to append this fast motion to other TCFs.

3.3.2 Side-group motion

The conformational energy of a polymer chain depends, among other factors, on the presence of side-groups. Steric interactions between side-groups and/or between side-groups and the main polymer chain are reflected to some extent in the backbone flexibility. Therefore, studies of the side-group mobility can provide useful information about factors controlling backbone motion and offer important conformational data on the motional freedom of the side-groups themselves. Side-groups that have been mostly considered in relaxation studies and dynamic modeling of polymers are methyl, phenyl, pyridyl, and naphthyl groups. Also, relaxation experiments have been conducted for a number of polymer systems bearing short alkyl side-chains.

In principle, it is possible to model the dynamics of side-chain groups by constructing a composite TCF analogous to Eq. (19) written as a product of the TCFs for segmental motion and side-group internal motion. An important assumption inherent in the formulation of Eq. (19) is that internal and segmental motions are mutually independent, and uncorrelated. For isotropic, segmental motion and side-group internal rotation well separated in time-scale by a factor of 100 or more, Eq. (19) represents a good approximation for the composite TCF. When segmental motion or side-group motion is anisotropic, the composite TCF cannot be factored out rigorously into a product of contributions due to segmental and internal motions. Nevertheless, Eq. (19) is retained in many applications as a first approximation to the problem. The validity of this decoupling approximation becomes apparent while modeling the dynamics of these types of polymer motions [130].

3.3.2.1 Methyl side-group motion. Methyl internal rotation has been usually described as a free diffusional stochastic process [103] or jumps among energy minima in the potential energy curve [131]. The TCF functions describing these two motional processes are combined with the appropriate TCF used to describe segmental motion. Such combinations have been established for the JS [78, 112, 132–134]. HWH [6, 112, 133], VJGM [135] and $\log(\chi^2)$ [99] models. Doddrel et al. [136] have discussed in detail the results of theoretical calculations of ^{13}C relaxation parameters in the presence of internal rotation. They consider isotropic diffusion of the backbone motion described by a single correlation time and free internal rotation, but their conclusions are valid qualitatively for other models. Qualitative conclusions for hindered methyl internal rotation that results from severe steric crowding that may exist in disubstituted polymer chains have been reached on the basis of calculated activation energies [6, 78, 112, 132–135].

3.3.2.2 Aromatic side-group motion. Jones [137] has proposed that rotation by 180° jumps is a realistic model for aromatic substituents. This stems from the fact that conformational energy calculations performed for the phenyl ring of polystyrene find [138–140] a two-fold potential with quite a high barrier. Modification of this model to include segmental motion in terms of the JS and HWH models can be found in the literature [6, 134, 141]. The free rotational diffusion model has also been used [6, 112, 132, 143, 144] to describe the internal motion of the aromatic ring, but with limited success. As expected, this model is highly unrealistic in view of the theoretical calculations. However, even the Jones two-state jump model may not be applicable in cases where strong non-bonded interactions operate between adjacent aromatic rings and/or between aromatic rings and the backbone, especially for bulky groups such as naphthyl groups. A more realistic physical description is to treat internal motion as an oscillatory motion occurring within a specific angular region, i.e. restricting the amplitude of internal rotation. Such a restricted rotation model developed by Gronski [145] and Wittebort and Szabo [25] can be combined with the JS or

HWH segmental motion TCFs to obtain a composite TCF or spectral density function [6, 141, 143, 144].

3.3.2.3 Alkyl side-chain motion. TCFs describing multiple internal rotations of an alkyl chain attached to a heavy anchor can be divided into two general classes. In the first class, the various C–H vectors of the side-chain are assumed to undergo successive independent, free diffusional motions about the C–C bonds [23, 25, 28, 29]. These models, assuming no motional restriction, i.e. an amplitude of 360°, about the C–C bonds, are able to describe successfully the dynamics of chain molecules in the fast motion regime [29, 146–148]. The second class of models [28, 28–31, 149] describe side-chain motion in terms of multiple internal rotations of restricted amplitude. Conformational constraints imposed by the environment of the alkyl chain (e.g. side-chains in synthetic polymers, proteins, phospholipids) restrict the motion about certain C–C bonds to amplitudes smaller than 360°.

Spyros and Dais [26] have carried out a detailed investigation of new composite spectral densities for describing local backbone motions of flexible chains in addition to multiple internal rotations of attached alkyl chains. The composite spectral densities describing free or restricted rotations superimposed on chain segmental motion, the latter being described by the HWH model, are given by [26]

$$J(\omega) = Q_i \times \mathrm{Re}\left[\frac{1}{(\alpha' + \mathrm{i}\beta')^{1/2}}\right] \tag{54}$$

where

$$\alpha' = \tau_{01}^{-2} + 2(\tau_{01}\tau_1)^{-1} - \omega^2, \qquad \beta' = -2\omega(\tau_{01}^{-1} + \tau_1^{-1}) \tag{54a}$$

For free internal rotations

$$\tau_{01}^{-1} = \tau_0^{-1} + b_1^2 D_1 + b_2^2 D_2 + \cdots + b_n^2 D_n \tag{55a}$$

and

$$Q_i = Q_1 = \sum_{b_1, b_2, \ldots, b_n} |d^{(2)}_{b_1 b_2}(\beta_{12})|^2 |d^{(2)}_{b_2 b_3}(\beta_{23})|^2 \cdots |d^{(2)}_{b_n 0}(\beta_{nF})|^2 \tag{55b}$$

For restricted internal rotations

$$\tau_{01}^{-1} = \tau_0^{-1} + \left(\frac{n_1\pi}{2\varphi_1}\right)^2 D_1 + \left(\frac{n_2\pi}{2\varphi_2}\right)^2 D_2 + \cdots + \left(\frac{n_n\pi}{2\varphi_n}\right)^2 D_n \tag{56a}$$

and

$$\begin{aligned} Q_i = Q_2 = \sum_{n_1, n_2, \ldots, n_n} \sum_{b_1, b_2, b_2', \ldots, b_n} & \Gamma^{b_1 b_1'}{}_{n_1}(\varphi_1) d^{(2)}_{b_1 b_2}(\beta_{12}) d^{(2)}_{b_1' b_2'}(\beta_{12}) \cos[(b_1 - b_1')a_{12}] \\ & \times \Gamma_{b_2 b_2' n_2}(\varphi_2) d^{(2)}_{b_2 b_3}(\beta_{23}) d^{(2)}_{b_2' b_3'}(\beta_{23}) \cos[(b_2 - b_2')a_{23}] \cdots \\ & \times \Gamma_{b_n b_n' n_n}(\varphi_n) d^{(2)}_{b_n 0}(\beta_{nF}) d^{(2)}_{b_n' 0}(\beta_{nF}) \cos[(b_n - b_{n'})\alpha_{nF}] \end{aligned} \tag{56b}$$

The functions $\Gamma_{b_i, b_i', n_i}(\varphi_i)$ are given explicitly in Ref. [25] as a function of the amplitude, φ_i, of the restricted internal motions. The functions, $d^{(2)}_{ij}(\beta_{ij})$, are elements of the reduced Wigner rotation matrices [24] which are functions of the angles $\beta_{N-1,N}$ formed between successive internal rotation axes. For tetrahedral arrangement of a hydrocarbon chain, these angles are all equal to 70.5°. The last angle β_{NF} is the angle between the Nth rotation axis and the last C_N–H_N bond, and is taken as 70.5°. The first summation indices, $n_1, n_2, \ldots$ in Eq. (56b) run from zero to infinity (practically, convergence is obtained for the first 5–10 terms), whereas the second summation indices, $b_1, b_2, \ldots$ run from -2 to $+2$. The angles $a_{N,N+1}$ specify the torsional angles between C_{N-2}–C_{N-1} and C_N–C_{N+1} bonds when viewed along the C_{N-1}–C_N bond axis and are all 180° for the all-trans configuration of the chain. Similarly a_{NF} is the dihedral angle between the C_{N-2}–C_{N-1} and C_N–H_N bonds viewed along the C_{N-1}–C_N bond and takes values of $\pm 60°$. The geometrical parameters of the chain used in Eqs. (55b) and (56b) are shown in Fig. 7. As one proceeds away from the polymer backbone, the torsional angle α_{ij} becomes meaningless, if internal rotations are assumed to be independent. This results in averaging of the torsional angle α_{nF}, which does not appear in the

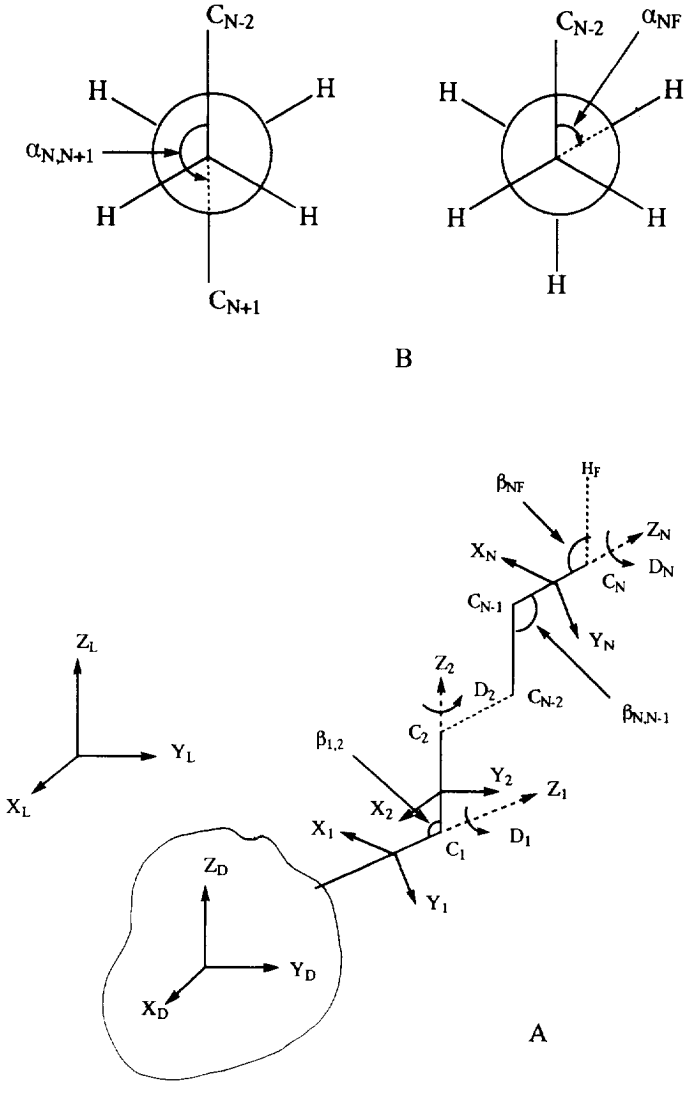

Fig. 7. (A) The definition of the coordinate systems, the Euler angles, β_{ij}, and the rotational diffusion constants, D_i, used in the diffusional models for multiple internal rotations. (B) Newman projections defining the Euler angles $\alpha_{N,N+1}$ and α_{NF} for the restricted diffusional model. Reprinted with permission from J. Chem. Phys. [25], copyright 1978, American Chemical Society.

calculations. Moreover, the angle α_{12} does not appear in Eq. (56b), since the segmental motion is considered isotropic. D_i is the diffusion constant of rotation about the ith diffusion axis (C–C bond). If one or more internal motions are free and the remaining rotations are restricted, Eq. (56b) can be modified accordingly. Analogous composite spectral density functions can be formulated adopting other models for segmental motion [26] or upon combining jump models describing side-chain motions with models of chain segmental motion. It is worthwhile mentioning at this stage the interesting theoretical work of Levy et al. [150] regarding the interpretation of the NMR relaxation behavior of side-chains by using stochastic dynamic trajectories. These authors obtained trajectories describing the motion of a heptane molecule by using the diffusive Langevin equation. Then, they mimicked a pseudo side-chain of a macromolecule by isotropically reorienting the C_1–C_2 bond, i.e.

the coordinate system centered at C_2 is assumed to be rigidly attached to the macromolecule, which is tumbling isotropically with correlation time τ_0. Finally, they calculated the exact trajectory values of T_1, T_2, and NOE parameters for all carbons along the heptane chain at two magnetic fields with $\tau_0 = 1$, 10, and 100 ns, and compared the exact values with those obtained from simplified diffusion and jump models with no correlated motions along the chain. They found that for macromolecules with short hydrocarbon side-chains moving freely in a non-viscous solvent, both models provide a satisfactory description of the NMR relaxation.

3.4 Comparison of models

In section 3.3, we presented a number of models used to describe polymer backbone motions. These models are characterized by different functional forms and some of them were derived on the basis of different physical interpretation of chain segmental motions. As an example, the BY model involves one-dimensional diffusion and is insensitive to local molecular details, whereas the HWH model describes segmental motion at a molecular level in terms of correlated and isolated transitions. Nevertheless, fitting a given set of experimental relaxation data by using various models may give essentially identical results, making the choice of a suitable model questionable. Even more speculative is the practice of interpreting the fitting parameters of a model in terms of the mechanism of segmental motions assumed by this model, which may not be consistent with the structural and conformational details of the polymer system of interest. The presence of an attached side-chain to the backbone, the introduction of a heteroatom or an aryl group in the backbone are expected to alter the conformational characteristics of the polymer chain from the idealized picture of the unperturbed polyethylene chain which is the vehicle for several Brownian dynamics simulations. However, mention should be made of a theoretical analysis of conformational transitions in branched polyethylene-like chains based on a multi-dimensional extension of Kramers' theory [151]. In general, it is found that branches somewhat reduce the transition rate relative to the linear molecule, but this effect is fairly minor. It is concluded that conformational transitions occur on the same time-scale in branched molecules as in their linear counterparts. However, these predictions have not yet been tested by performing Brownian or molecular dynamics simulations.

Several attempts have been made in the past to compare models either by using careful experiments that accurately characterize the shape of the TCF (e.g. time-resolved optical experiments), or by numerical comparison of various TCFs.

The fluorescence polarization decay of polystyrene labeled with anthracene has been used by Viovy et al. [152] to compare quantitatively a number of models including the VJGM (Eq. (31)), JS (Eq. (34)), HWH (Eq. (39) with $a = 0$), and BY (Eq. (35)) TCFs. They found that only the BY and JS, and to a lesser extent, the HWH, models appear to account for the orientational dynamics of labeled polystyrene. Also, they proposed [152] a generalization of the HWH TCF, the generalized diffusion and loss (GDL) model, which uses the same physical picture as the HWH model, but introduces a new term in the form of a Bessel function of the first order to account for the presence of the label and side-chain groups. Weber and Helfand [84] have compared the VJGM model (Eq. (30)) with the HWH model (Eq. (39)) using the former equation to replace the term $\exp(-t/\tau_1)I_0(t/\tau_1)$. These functions show a similar behavior at long times, but not at short times. Lin et al. [153] have compared the JS and HWH models by fitting numerically the HWH TCF and spectral density function to those of the JS model. Both functions in the time and frequency domain are broadly similar in shape. The fits in the frequency domain gave a ratio of correlation times, τ_1/τ_h, for cooperative transitions equal to 1.4–1.8. This value is in close agreement with experiments [112, 133, 134, 141, 143, 145] where this ratio is 1.2–1.7. Thus, it appears that the two models agree in characterizing the cooperativity of the chain motion despite the fact that they are developed from quite different starting points (the crankshaft motion in the JS model is not a common transition in the HWH model). Bahar et al. [89] have calculated the orientation TCF for polyethylene by using the DRIS model and compare this function with those involved in the JS, BY, and HWH models. The reader should recall that the latter three functions contain two parameters reflecting the diffusive propagation of orientation along the chain and the vanishing of the propagation of

orientations by various molecular mechanisms, whereas in the DRIS model the TCF is described in terms of the time-dependent probability that embodies all configurational and hydrodynamic information. From this analysis, it was concluded that the DRIS TCF may be approximated to a certain extent by all the three functions considered, although best fits are achieved with the HWH and BY TCFs. Fig. 8 illustrates graphically the best decay curves of the three models that approximate the TCF resulting from the DRIS model. In this Figure, $G_1(t)$ and $G_2(t)$ represent the first and second orientational TCFs, respectively. The former type of TCF is appropriate for optical and dielectric relaxation experiments, while the latter TCF describes ^{13}C–^{1}H and ^{1}H–^{1}H dipolar interactions. An important feature of these curves is the faster decay of $G_2(t)$ relative to that $G_1(t)$ (Figs. 8(A) and 8(B)). Nevertheless, the correlation time associated with the first and second orientational TCFs are very close to each other. This is unlike the case of isotropic motion where

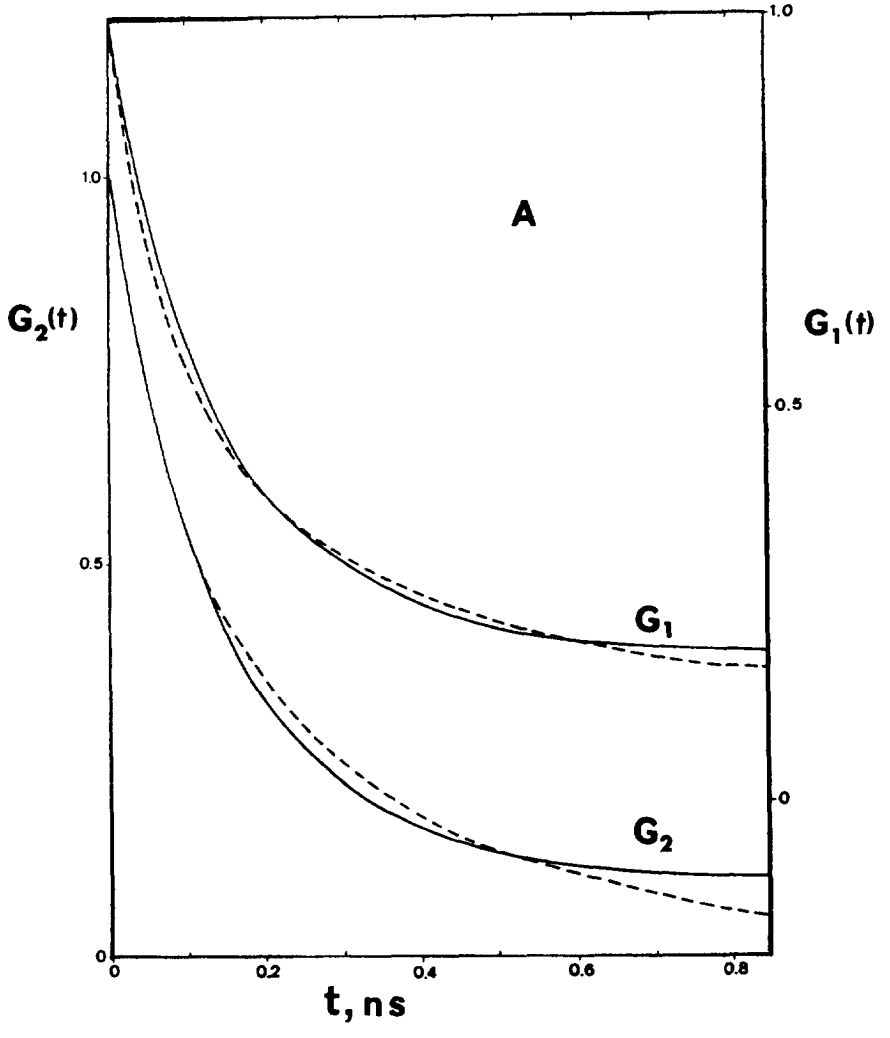

Fig. 8. Comparison of the DRIS model (solid curves) for $G_1(t)$ and $G_2(t)$ with results of: (A) the BY model; (B) JS model; (C) HWH model (dashed curves). Calculations are performed for a sequence of six bonds ($n = 6$), $T = 300$ K for a vector along the x-axis (bond-axis) (A and B), and for three directions along x, y, z axes (C) of the bond-based coordinate frame. Reprinted with permission from Macromolecules [89], copyright 1989, American Chemical Society.

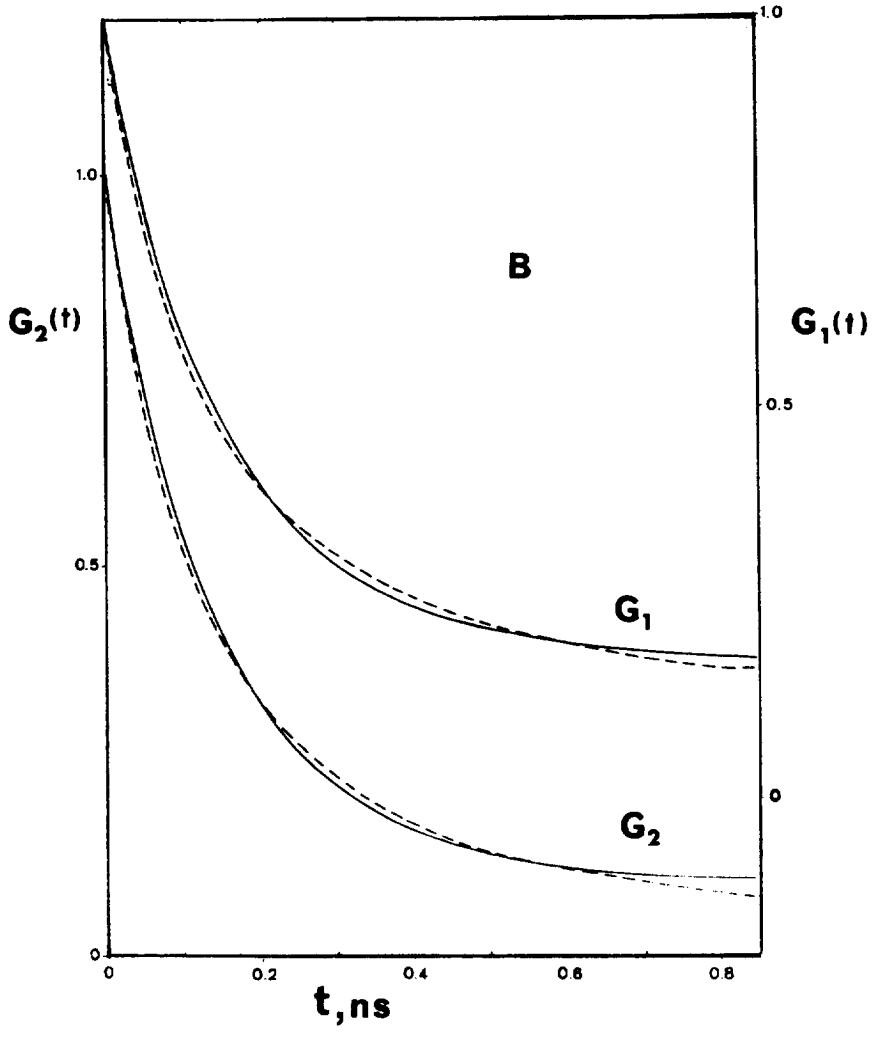

Fig. 8. (continued)

correlation times differ by a factor of three. Another significant observation is the different decay rates of $G_2(t)$ along the different directions x, y, z with respect to the bond vector (Fig. 8(C)).

In the light of the previous discussion, it is clear that experimental data can be fitted acceptably by several TCFs. At present, the limitation in accuracy and frequency range of ^{13}C NMR relaxation measurements appears to preclude a differentiation of the two-parameter models. However, a recent study by Gisser et al. [21] of the local dynamics of polyisoprene in dilute solution examined through ^{13}C NMR relaxation measurements demonstrates the superiority of the librational models over the unimodal distributions (Cole–Cole, Fuoss–Kirkwood, $\log(\chi^2)$, JS) in interpreting the relaxation data. Models that invoke motion on two well-separated time-scales, as the correlation time τ_1 (10^{-9} s) for conformational transitions and τ_2 (10^{-11}–10^{-12} s) for librational motion of the DLM model, appear to be more successful than models introducing one correlation time (Cole–Cole, Fuoss–Kirkwood, $\log(\chi^2)$, JS), or two correlation times not well separated in time scale (HWH model).

Lipari and Szabo [105] considered a model-free approach to the interpretation of NMR relaxation data for macromolecules. Both isotropic and anisotropic overall motions combined with various models for internal motion were considered. The data were analyzed in terms of two

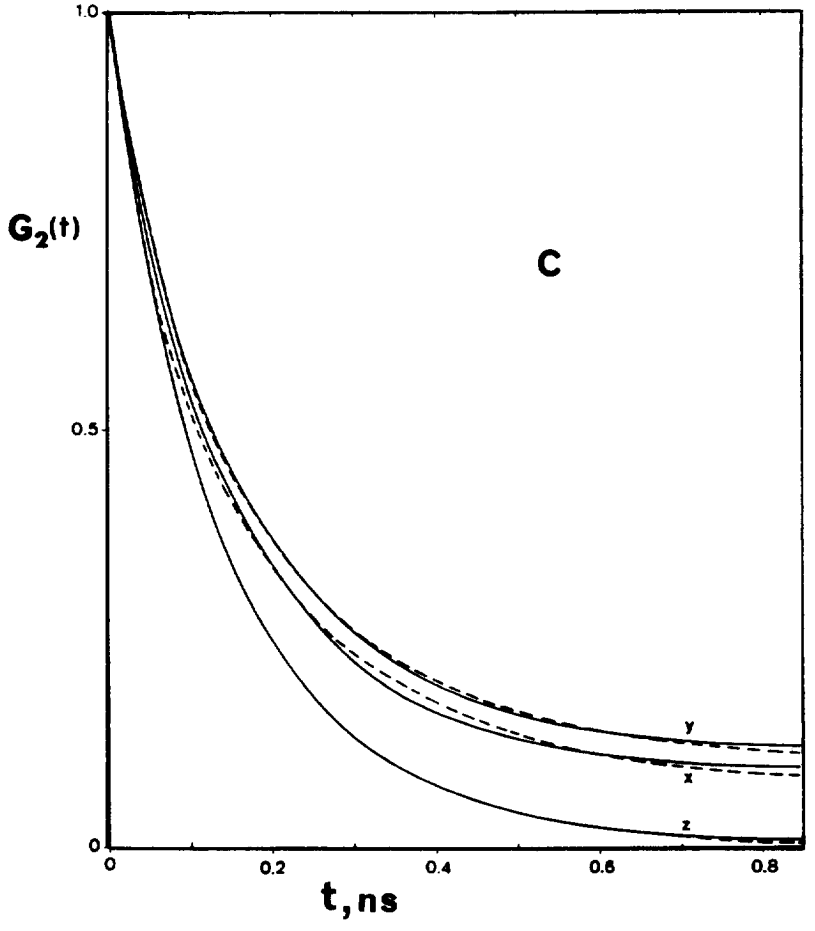

Fig. 8. (continued)

model-independent parameters, the generalized order parameter, S^2, which is a measure of the degree of spatial restriction of the motion, and the effective correlation time, τ_e, which is a measure of the rate of motion. The spectral density function for overall isotropic motion (anisotropic motion has also been considered) characterized by correlation time, τ_R, is given by [105]

$$J(\omega) = \frac{2}{5}\left[\frac{S^2\tau_R}{1+\omega^2\tau_R^2} + \frac{(1-S^2)\tau_e}{1+\omega^2\tau_e^2}\right] \tag{57}$$

Parameters S^2 and τ_e are extracted either by least-squares fitting to the experimental data, or, in favorable cases, by using simple analytical forms, and these are compared with exact values generated from a variety of motional models describing internal motion [105, 154]. Models without sufficient flexibility to reproduce the numerical values of S^2 and τ_e extracted from the experiment are eliminated. Such a model-free formalism can be very useful in characterizing the dynamics of stiff and helix-like macromolecules of biological origin [4]. However, for random-coil synthetic polymers, even though a model-free approach may describe the data, it does not optimally interpret the data in physically realistic terms. Modification of Eq. (57) to include chain segmental motion has been proposed by Perico et al. [118].

Another model-independent approach is based on the complete analysis of coupled spin-relaxation of a $^{13}CH_N$ group located in the macromolecule in terms of auto-correlation and

cross-correlation spectral densities. This method developed by Fuson et al. [39] has been described briefly in Section 2.3, and applied to several chain molecules [155, 156], including polymers [37, 38]. Although this approach is very useful in delineating experimentally existing local motional anisotropy predicted by theoretical treatments [84, 110, 111] of polymer dynamics, it does not give a self-sufficient physical picture of chain segmental motion. Moreover, this method is time-consuming, since separate experiments are needed for each non-equivalent $^{13}CH_N$ group in the molecule at the lowest possible concentration, or the data must be extrapolated to infinite dilution, in order to minimize the effects of ^1H–^1H intermolecular interactions. Furthermore, the transformation of the observed spectral densities to a molecule-fixed Cartesian coordinate system requires knowledge of the geometry of the spin system, which may not be the case for certain polymer systems [38].

4. Applications

A significant number of reports have appeared in the literature during the last 15 years, dealing with the dynamics of polymer systems in solution and in the bulk.

Relaxation data obtained as a function of temperature, magnetic field and solvent (for dilute solutions) have been analyzed in quantitative terms by using theoretical motional models. Most of the models used in these studies have been discussed in Section 3.3, and will be mentioned in this section without further details. Since the dynamics of the majority of the polymer systems has been analyzed on the basis of the same models, we feel that the classification of the various studies on an individual polymer basis is more didactic and facilitates the evaluation of the ability of models to describe local chain motions.

4.1 Chain segmental motion

(i) Poly(butadiene) (PBD). Local chain dynamics of PBD has been a frequent subject of investigation over the past 20 years. As early as 1973, Schaefer [2, 51] recognized that a distribution of correlation times was necessary to account for the PBD relaxation data. Three years later, Gronski [61] invoked specific, rapid conformational jumps along the PBD chain to interpret the relaxation data of this polymer in solution [60]. The specific local transitions along a three-bond segment of the *cis*-1,4 PBD chain are illustrated in Fig. 9. The symbol C represents a cis double bond, the symbols s^+ represent skewed conformations of the allylic bond of opposite sense (Fig. 9), and the symbols t and g (or g′) represent trans and gauche conformations of the CH_2–CH_2 bond. Specific motions are shown in Fig. 9. In the a → b type of motion, two counter-rotations occur about the C_2–C_3 and C_4–C_5 bonds ($s^+ts^- \rightarrow s^-ts^+$). As a result of this motion, the $C_5=C_6-C_7-C_8-C_9=C_{10}$

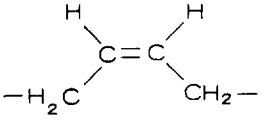

cis–1,4 PBD

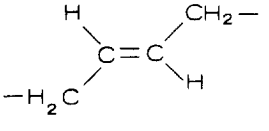

trans–1,4 PBD

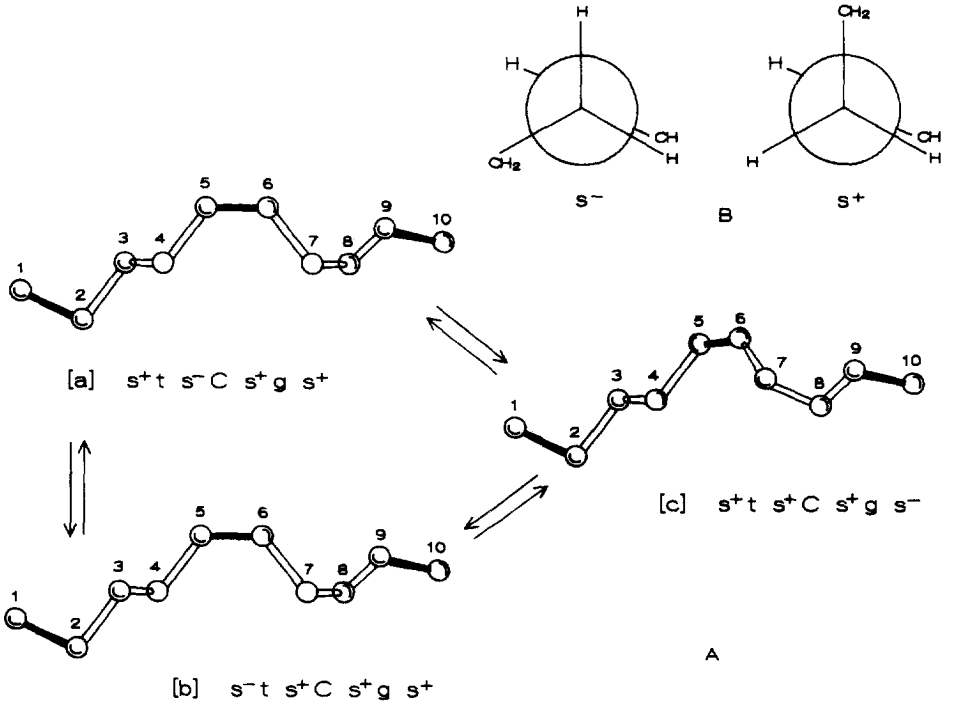

Fig. 9. (A) Specific counterrotations in *cis*-1,4 polybutadiene. Double bonds are represented by a thick line. The central unit considered for the calculation of the TCF is composed of C_4–C_5=C_6–C_7 groups. (B) Definition of the s^+ and s^- conformations of the C–C bonds adjacent to a double bond. Reprinted with permission from Macromolecules [128], copyright 1989, American Chemical Society.

part of the chain remains immobile, whereas the $C_1 = C_2 - C_3$ part is translated due to $\approx 120°$ rotation about the C_4–C_5 bond. In the case of the a → c and b → c motions the counterrotations occur in a similar way about the C_4–C_5 and C_8–C_9, and C_2–C_3 and C_8–C_9 bonds, respectively.

A recent study of Fuson and Grant [38] for *cis*-1,4 PBD in CD_2Cl_2 solution led to the same conclusion regarding the PBD backbone rearrangement. These authors used the coupled spin relaxation technique to describe the anisotropy of motion in terms of three Cartesian correlation times, τ_{yy}, τ_{zz}, τ_{xy} calculated from the $^{13}CH_2$ dipolar spectral densities extrapolated to infinite dilution. By comparing the experimental ratio τ_{zz}/τ_{yy} for PBD with the calculated correlation time, τ_1, associated with correlated pair transitions in a polyethylene chain of the HWH model, they suggested that the spin relaxation of the PBD chain is dominated by cooperative conformational transitions about the C_3–C_4 and C_9–C_{10} bonds for a segment of three monomer units, leaving the outer double bonds C_2–C_3 and C_{10}–C_{11} essentially unmoved.

Several theoretical [158–163] studies and experimental [164–168] data on *cis*- and *trans*-PBD favor the description of the segmental motion of this polymer in terms of the coupled transitions which localize the motion along the PBD chain. The tails of the chain experience very little movement as was the case with the coupled transitions observed by Helfand [66]. Moreover, in the a → b process (Fig. 9), which is more favored energetically, C–H vectors of the vinyl carbons are not oriented, whereas those of the C_4 methylene carbon are involved in a $\approx 120°$ rotation about the C_4–C_5 axis. These different reorientations of the C–H vectors of the CH and CH_2 groups result in different relaxation contributions and may explain the fact that the *R* ratio is found to be smaller than 2 [60].

However, in a recent publication, Dejean de la Batie et al. [128] invoked librational motions of the C–H vectors at the CH and CH_2 carbon sites of PBD to explain the lower value of the ratio *R* than

its theoretical maximum. By applying the DLM model to the relaxation data of a sample of PBD containing 98.8% cis-1,4 linkages in 15% (w/v) chloroform-d solution and in the amorphous state, they found very similar values of the conic half-angles for the methine ($\theta_{CH} = 26°$) and the methylene ($\theta_{CH_2} = 36°$) C–H vectors in both solution and bulk states. The similarity of the amplitudes of the librational motion in the bulk and in solution, which is also observed for other polymer systems, provides strong evidence for the very local character of this type of motion and supports the recent hypothesis that this fast process is independent of the influence of the chain environment [8, 21]. Also, Dejean de la Batie et al. [128] examined the possibility of interpreting the relaxation data of PBD by invoking the specific conformational jump model of Gronski (Fig. 9). They were able to fit the relaxation data in the bulk. However, because librational motion has been observed in most polymer systems without double bonds in the backbone chain, they concluded that the fast anisotropic process is in favor of a libration rather than a conformational jump. They reported a value of $\approx 15\ kJ\ mol^{-1}$ for the activation energy of the backbone motion.

Gisser and Ediger [169] have studied the dynamics of the cis and trans monomer units of a PBD sample containing 40% cis-1,4, 52% trans-1,4, and 8% vinyl-1,2 linkages in viscous Aroclor solutions. The relaxation data are similar within experimental uncertainty for the two concentrations of 10% and 20% (w/v) studied. This indicates again the very local character of the PBD polymer chain dynamics detected by NMR. They invoked a librational motion three decades faster than segmental motion and fitted their data by means of a bi-exponential TCF of the form

$$G(t) = (1 - f)e^{-t/\tau_{seg}} + fe^{-t/\tau_{lib}} \tag{58}$$

where f denotes the amplitude of the libration ($0 < f < 1$) with correlation time, τ_{lib} describing C–H bonds librations. The time constant τ_{seg} for segmental motion reflects transitions between conformational potential minima. These motions occur on the length-scale of 1–2 repeat units, approximately the size of a solvent molecule. Although the temperature dependence of the shape of the bi-exponential function was not examined in this study due to insufficient relaxation data, their analysis was justified from the fact that the form of Eq. (58) was found to be temperature- and solvent-independent for the structurally similar poly(isoprene) [22, 128, 169]. These authors reported a value of $\approx 11\ kJ\ mol^{-1}$ for the activation energy of segmental motion in Aroclor solutions. This value was obtained by fitting the relaxation data of the methylene carbons of the cis and trans repeat units. The cis and trans methine carbons could not be studied in Aroclor due to spectral overlap in this solvent. The amplitude of librations for the cis and trans methylene carbons are rather similar, $f = 0.66$ and 0.62, respectively.

(ii) Poly(isoprene) (PI). PI is an important commercial polymer with numerous industrial applications. Therefore it is not surprising that the dynamics of this polymer, both in solution and in the bulk, has attracted the attention of several research groups during the last decade [10, 22, 45, 46, 128, 169, 170]. Dejean de la Batie et al. [128] have investigated the dynamics of a PI sample containing 92% cis-1,4 linkages in solution and in the rubbery state. Among the various models used the DLM model was found to be the most successful in fitting the experimental data over the whole temperature range studied. Also, this model consistently describes the lower value of the relaxation time ratio, R (Eq. (50)), observed for PI in both solution and bulk states. In the latter situation, the R values for the methylene carbons vicinal to the methyl group are 1.67 at 25.15 MHz and 1.49 at 62.5 MHz. For the other methylene carbon, these ratios are 1.40 at 22.15 MHz and 1.35 at 62.5 MHz. The deviation of R from the theoretical value of 2 has been attributed to the presence of the methyl substituent and the neighboring methylene groups which inder the librational motion of the methine C–H vector relative to that of the C–H vectors of the methylene groups. This difference in local dynamics is reflected in the conic half-angles $\theta_{CH} = 20°$, $\theta_{CH2(1)} = 33°$ and $\theta_{CH2(4)} = 37°$ for the methine, and the C_1 and C_4 methylene C–H vectors. The librational motion at the methylene carbon site near the methyl group is slightly more hindered than that in the other methylene group as expected. Good fits are also obtained for the relaxation data of PI in chloroform-d and 1,1,2,2-tetrachloroethane-d_2 solutions by using the DLM model and assuming that the θ parameters have the same values in both solvents and close to the amplitude of the bulk process. Spin–lattice

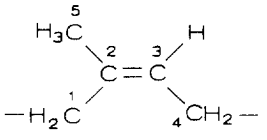

PI

relaxation in poly(isoprene) has also been analyzed in terms of specific conformational jumps as in PBD. This model fits the relaxation data of PI in the bulk, but not in solution [128].

Denault and Prud'homme [45] have studied the dynamics of PI in bulk using the ^{13}C T_1 and NOE data of the C–1 methylene carbon at two Larmor frequencies over a temperature range of 20–100°C, which is well above the glass transition temperature of the two PI samples ($T_g = -63$ and -67°C). Backbone segmental motion was studied by using the Cole–Cole, Fuoss–Kirkwood, log(χ^2), and JS distribution models. Regardless of the model used, a change of regime is observed near 60°C for the backbone motion associated with an important loss of motional cooperativity with increasing temperature. This transition is inferred from singularities in the Arrhenius plots of the average correlation times for segmental motion, and in plots of either the distribution width or the kinetic segment length for orientational correlation. In the high-temperature regime (above $\approx$ 60°C), the activation energy was found to be in the range 15–19 kJ mol^{-1} depending on the model used, whereas in the low-temperature regime (below $\approx$ 60°C) it increases to 47–65 kJ mol^{-1}. On the basis of the application of the more sensitive NOE data to dynamic modeling, the Cole–Cole, Fuoss–Kirkwood and log(χ^2) distribution functions are more successful than the JS model in describing the PI backbone motion. However, no models are able to fit the relaxation data of the methine carbon of PI using the set of simulation parameters of the models obtained from the fitting of the relaxation data of the methylene carbon. This failure must be attributed to the marked deviation of the T_1 ratio, R, from the theoretical value of 2. This ratio is fairly constant ($R = 1.61$) over the entire temperature range studied and very similar to the value reported for PI in solution [22, 128]. The inadequacy of the distribution models to describe simultaneously the methine and methylene relaxation data is a major disadvantage of this analysis and casts some doubt on the existence of a motional transition with increasing temperature.

In a second paper [46], Denault et al. reported the bulk dynamics of the PI microphase in a series of poly(styrene-b-isoprene) diblock copolymers of various molecular weights. The chain segmental motion of the PI component of these block copolymers, as well as of PI homopolymers of previous studies [45, 128], was described by using the DLM model and the log(χ^2) distribution. A model-independent change of regime was observed in the Arrhenius plots of the correlation times describing backbone segmental motion for all polymer systems. For copolymers, the transition temperature increases with decreasing molecular weight. Unlike the work of Dejean de la Batie et al. [128] they allowed the width of the DLM TCF, i.e. the ratio τ_0/τ_1 in Eq. (53), to change with temperature in order to fit the data. This introduces a large degree of flexibility into the fitting procedure. Furthermore, no attempt was made to fit the relaxation data of the methine carbon. These facts and the need to test the NMR correlation times with the Williams–Landel–Ferry [171] (WLF) equation (see below), as well as to examine the temperature dependence of the shape of the TCFs used, leaves this point open. It is worthwhile to mention the study of Dekmezian et al. [10] on the bulk dynamics of *cis*-1,4 PI using the ^{13}C T_1 and NOE data at 67.9 MHz over a temperature range between -10 and 80°C. They reported that the average correlation time for backbone motion obtained by employing the log(χ^2) model follows the empirical WLF equation in good agreement with mechanical and dielectric relaxation data.

In a recent report, Glowinowski et al. [22] have studied the local segmental dynamics of PI dissolved in ten different solvents covering a viscosity range from 0.33 to 1.54 cP. Interestingly it was found that the ratio R significantly deviates from the value of 2 in all solvents, having an average value of 1.62 which is very similar to the value reported for PI in the amorphous state [45, 46, 128].

In a subsequent paper [21], these authors have used the multi-field, variable temperature relaxation data of *cis*-1,4 PI in dilute toluene-d_8 solution to examine its local dynamics. The data were analyzed in terms of eight motional models. Only librational models that invoke motion on two well-separated time scales were successful in fitting the relaxation data of the methine and methylene carbons. The slower, conformational motions correspond to the activated torsional dynamics, whereas the faster motions are librations within potential energy wells as described by the DLM model [128]. Only the amplitude of the librational motion was changed, $\theta_{CH} = 33^\circ$ and $\theta_{CH2} = 36^\circ$, in order to fit the methine and methylene relaxation data. These values are, however, different from those obtained by Dejean de la Batie et al. [128] in chloroform-d and 1,1,2,2-tetrachloroethane-d_2 solution and in the rubbery state. This discrepancy may be real or may be an artifact of the analysis, since different r_{CH} values were used and the contribution of the CSA anisotropy to the spin relaxation of the unsaturated methine carbon was taken into consideration through Eqs. (6)–(10) by Gisser et al. [21], but not by Dejean de la Batie et al. Furthermore, spin relaxation with non-bonded protons may be more important in the bulk polymers. This type of interaction has been neglected in both studies. The activation energy for conformational transitions of PI toluene-d_8 was found to be equal to 13 ± 2 kJ mol^{-1} which is consistent with the value obtained in other solvents [22, 128, 169].

(iii) Poly(methylene oxide) (PMO). The configuration and dynamics of PMO in solution has been the subject of intensive studies. PMO adopts an all-gauche structure in the crystalline state due to the anomeric effect, i.e. the interaction of carbon–oxygen dipoles between monomers [172]. This structure largely persists in solution. Earlier studies [173, 174] have focused primarily on modeling intramolecular potentials in order to predict configurational properties. More recently, the dynamics of this chain has been of interest [76]. Simulation of the dynamics of PMO as Brownian motion on a tetrahedral-lattice predicts that the PMO helix is quite stiff in solution [76]. The primary motions are considered to be diffusion of trans defects between the helical sections and the "flip-flop"

$$-(-CH_2-O-)-$$

PMO

creation and destruction of trans defects in the helix. Recently, Fuson et al. [37] have reported on the dynamics of PMO in 1% (w/v) solution in phenol-d_6 by using the coupled-spin relaxation technique. They describe the anisotropy of the motion of PMO in terms of the Cartesian correlation times, which were found to be smaller than that in hydrocarbon chains. This observation has been attributed to the higher rigidity of the PMO chain in solution relative to the more flexible hydrocarbon chains. The conformational rigidity of PMO is expected to be enhanced in strongly hydrogen bonding solvents such as phenol, which strengthen the anomeric effect. This suggests that anisotropic correlated transitions occurring in hydrocarbon chains are not important for the PMO chain, and that rapid librational motions, consistent with the DLM model, are responsible for the spin relaxation of the PMO chain. The librational motion of the methylene group is believed to be the result of a complex torsional twisting about the helix axis of PMO, observed in an earlier solid-state NMR study [175].

(iv) Poly(ethylene oxide) (PEO). The dynamics of linear PEO has been studied by Bahar et al. [90] by using the DRIS model. The rates of transitions between isomeric states were assumed to be inversely proportional to solvent viscosity, leading to a linear dependence between viscosity and correlation times. Predictions of the DRIS theory are in satisfactory agreement with the isotropic

$$-(-CH_2-CH_2-O-)-$$

PEO

correlation times and spin–lattice relaxation times from ^{13}C and ^{1}H NMR experiments for PEO in a variety of solvents. The dependence of correlation times on temperature is displayed by the Arrhenius plot in Fig. 10. Points represent experimental ^{13}C and ^{1}H NMR, whereas the solid line is obtained theoretically by repeating the calculations through the DRIS model for the various temperatures. The calculated activation energy of about 7.5 kJ mol^{-1} for local motions of PEO is in good agreement with that determined experimentally from both ^{13}C and ^{1}H relaxation data and confirms that energies of about one barrier crossing between isomeric states activate local conformational transitions in polymeric chains in dilute solution.

An interesting ^{13}C NMR relaxation study on linear and cross-linked PEO samples has been performed by Dejean de la Batie et al. [127]. ^{13}C spin–lattice relaxation times have been measured for a number of PEO cross-linked with urethane well above the glass transition temperature at two Larmor frequencies. Table 1 summarizes the abbreviated names of the different samples and their

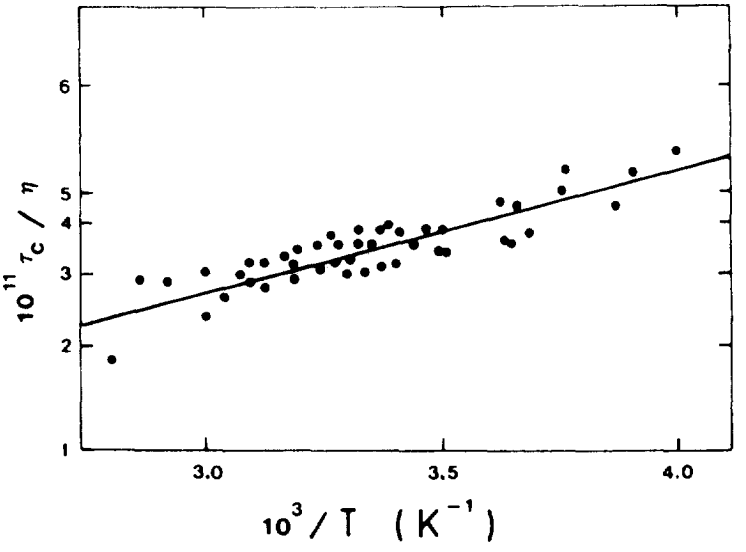

Fig. 10. Temperature-dependence of correlation times for PEO in various solvents. Points represent experimental data. The solid line is obtained by using the DRIS model. Reprinted with permission from Macromolecules [90], copyright 1989, American Chemical Society.

Table 1
Abbreviated names, characteristics, and simulation parameters of the DLM model for linear and cross-linked PEO samples[a]

Name	M_n^b	n_a^c	T_g (°C)	A^d	τ_0/τ_1	τ_1/τ_2
PEO 400	400	9	0	0.56	30	200
PEO 600	600	4	− 26	0.56	30	200
PEO 1000	1000	23	− 42	0.56	30	200
PEO 1500	1500	34	− 43	0.56	100	200
PEO linear	9200	0	− 43	0.56	200	200

[a] Adapted with permission from Macromolecules [127], copyright 1981, American Chemical Society.
[b] Number average molecular weight.
[c] Mean number of ethylene oxide units between two cross-links.
[d] Amplitude of the librational motion (Eq. (52)).

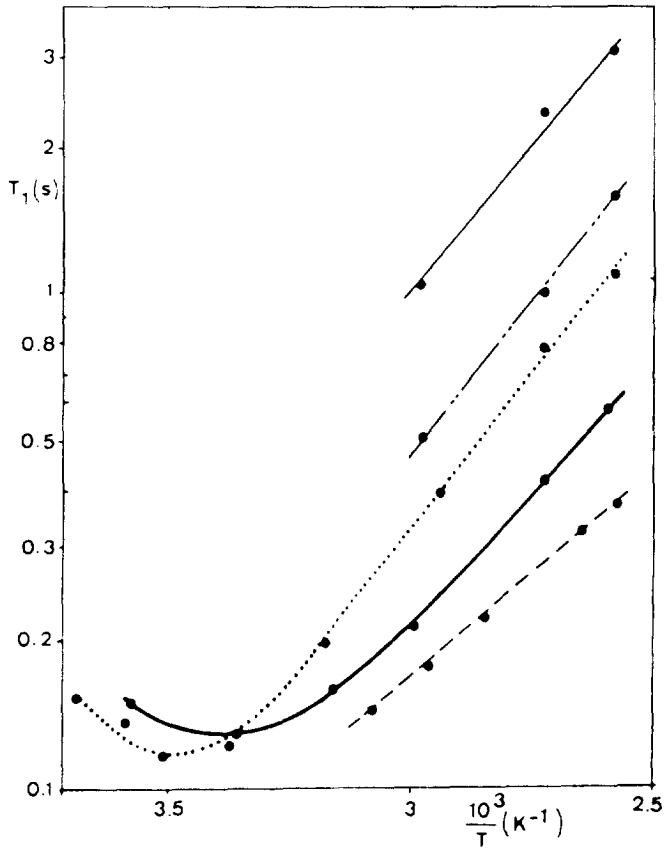

Fig. 11. 25.15 MHz carbon-13 NT_1 values in bulk PEO samples. ———, linear PEO; · · ·, PEO 1500; · · ·, PEO 1000; ——— PEO 600; - - -, PEO 400. Reprinted with permission from Macromolecules [127], copyright 1988, American Chemical Society.

physical characteristics. By focusing on the dynamics of the "mobile" methylene units of cross-linked PEO samples observed by conventional NMR experiments, they derived the following conclusions.

(1) The various cross-linked PEO samples, including linear PEO, show distinctly different T_1 values over the entire temperature range studied. These values decrease with increasing degree of cross-linking, reflecting a slowing down of segmental motion as the length of the ethylene oxide strand decreases. However, the T_1 value at the minimum of the NT_1 vs. $1/T(K^{-1})$ curve does not depend on the degree of cross-linking. These observations are shown graphically in Fig. 11.

(2) The experimental T_1 minima for all samples are much too high to be reproduced by the isotropic, the HWH or the GDL (see Section 3.4) models. However, by taking into account librational motions for the C–H vectors (DLM model), these authors were able to fit successfully the T_1 data of the PEO samples. The parameters of the DLM model used in these fits are given in Table 1. The conic half-angle is similar for all PEO samples and independent of the degree of cross-linking, as well as the τ_1/τ_2 ratio. However the τ_0/τ_1 ratio decreases when the degree of cross-linking increases. This result reflects the fact that the orientation diffusion process along the chain described by the τ_1 correlation time is interrupted when it reaches the cross-linking points. Moreover, the variations of the τ_1 values at a given temperature show that the chain mobility

increases from PEO-400 to PEO-600 and then to PEO-1000 and PEO-1500, in agreement with the fact that segmental mobility is higher in long flexible sub-chains than in shorter ones.

(3) Local motions of the methylene carbons near the urethane junction are slower than those in the middle of the PEO sub-chain due to the rigid bulky nature of the aromatic urethane cross-link. However, the motion of the central units even for PEO-1500 is slower than in linear PEO, indicating that even at a distance of about 50 bonds away from the cross-link, local dynamics are affected by constraints.

PEO samples cross-linked with cyclosiloxane have been used to study the effect of cross-linking on the PEO dynamics [176]. Flexible cyclosiloxane cross-links are used to construct membranes which have better mechanical and conductivity properties than those of the more rigid and polar aromatic urethane cross-links. In contrast to the results obtained for urethane cross-linked PEO samples, ^{13}C spin–lattice relaxation measurements above T_g and dynamic modeling performed on cyclosiloxane cross-linked PEO have shown [176] that the introduction of siloxane junctions does not alter significantly the local dynamics of PEO segments. Motion of the cross-links is only slightly slower than that of the sub-chains. Moreover, the local chain dynamics of these networks are satisfactorily described by the DLM model. The amplitude of the libration, reflecting the steric hindrance at the methylene site, was found to be the same as that of the urethane cross-linked PEO, and independent of the position of the CH_2 carbon in the PEO sub-chain This result indicates that the extent of the libration for the PEO segment does not depend on the chemical structure of the cross-link and the length of the PEO sub-chain. This is consistent with the very local nature of the librational motion affected only by the steric hindrance at the considered sites, as mentioned earlier.

(v) Poly(propylene oxide) (PPO). The bulk local dynamics of PPO has been examined by Dejean de la Batie et al. [127] by using ^{13}C T_1 data at 25.15 and 62.5 MHz at temperatures well above T_g. These authors successfully described the experimental relaxation data of PPO over the whole temperature range including the T_1 minimum by employing the DLM librational model. The conic half-angles for the C–H vectors of the methine and methylene groups are 25 and 37°, respectively. These different θ values account for the fact that the R ratio is not approximately equal to 2, and they underline the fact that the C–H vectors at the two carbon sites do not share exactly the same local dynamics. It should be noted that the θ value for the internuclear vectors of the CH_2 group of PPO is slightly smaller than the one determined for the methylene carbon of PEO, supporting the idea that θ is mainly influenced by steric hindrance.

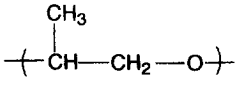

PPO

(vi) Polycarbonates (PCs) and polyformals (PFs). Aromatic polycarbonates and their structural analogs polyformals have been studied extensively by multi-nuclear magnetic relaxation in solution [6, 112, 132, 141, 144, 177, 178] and in the solid state [7]. Fig. 12 shows the structures of the repeat units of the various PC and PF macromolecules studied to date along with their abbreviated names. Polyformals are obtained from polycarbonates upon replacing the carbonate group on the latter by a formal group. These polymers have been studied in chloroform-d and 1,1,2,2-tetrachloroethane-d_2 solutions over a wide temperature range covering approximately 120°C. For BPA-PC [112] and BPA-PF [141] the concentration-dependence of the local chain motions was also examined. The results of multi-field ^1H and ^{13}C spin–lattice relaxation studies of PCs and PFs have been discussed in terms of correlation times for segmental motion, methyl, formal, and phenylene groups rotation. Backbone segmental motion has been described in all cases with the HWH model, although in some early reports [112, 132, 178] the JS model was applied as well. In most PC and PF molecules, the phenylene internal motion has been characterized as free stochastic

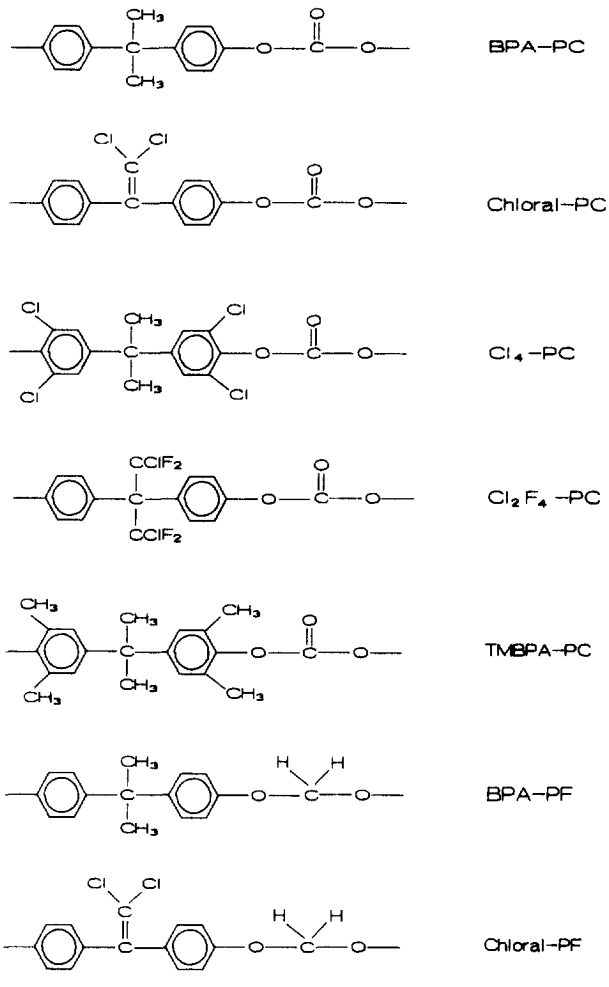

Fig. 12 Chemical structures of the repeat units of polycarbonates and polyformals.

diffusion or rotation by 180° jumps with the exception of TMBPA-PC [6] and BPA-PF [141, 177] at high concentrations. In the latter polymers, a model of restricted internal rotation [25, 145] has been adopted to interpret the relaxation data of the phenylene ring. Methyl group internal rotation has been described by the Woessner three-fold jump model, whereas the formal group rotation has been modeled as double trans–gauche rotations about the C–O axis of the polyformal backbone [141, 177].

In solution, BPA-PC has been found to be a rather mobile chain. Segmental motion is dominated by cooperative backbone motions as opposed to single backbone bond reorientations. Phenylene group rotation is rapid and rather similar to the cooperative backbone motion in time-scale, suggesting a possible coupling between these two local motions. This similarity is observed over the whole concentration range studied (5–30% (w/v)). Methyl group rotation is also facile although it occurs on a different time-scale than cooperative segmental motion or phenylene internal rotation. Also, methyl internal motion is very little affected as the concentration is raised from 5 to 30% (w/v). This difference in concentration dependence is quite plausible, since segmental motion and phenylene group rotation sweep out a larger solvent volume than methyl group rotation. Table 2 lists the

ratios of the correlation times describing local motions of the various polycarbonates over the corresponding correlation times of BPA-PC. The correlation times were obtained in $CDCl_3$ solutions by fitting the experimental data with the JS model. Although the experimental data base is somewhat limited and should be extended by additional experiments, useful comparisons can be made for the various local motions occurring in the polycarbonate chain. BPA-PC and Chloral-PC macromolecules are quite similar dynamically, with Chloral-PC displaying somewhat slower phenylene group rotation. The Cl_4 and Cl_2F_4 polycarbonates (Fig. 12) are significantly different from BPA-PC and Chloral-PC. Segmental motion is somewhat slower in these two polymers, but phenylene group rotation slows dramatically. In Cl_4, the methyl group rotation slows a little relative to BPA-PC, but in Cl_2F_4, the $CClF_2$ rotation slows a great deal.

The correlated segmental motion for TMBPA-PC appears to be slower than for the unsubstituted BPA-PC. Phenylene group rotation is described in terms of restricted rotational diffusion instead of complete anisotropic rotation. This result is in agreement with recent CNDO calculations [179] indicating that the mobility of the phenylene rings in TMBPA-PC is much more restricted than the phenylene ring motion in BPA-PC. The time scale for backbone methyl group rotation is comparable to that in BPA-PC, a fact indicative of a weaker cooperativity between this motion and the other types of local motions. Rotation of the methyl group attached to the phenylene ring is too fast to contribute significantly to relaxation except by partially averaging the dipole–dipole interactions. These motional characteristics of polycarbonates are summarized in Table 3 in the form of activation energies and prefactors calculated from the Arrhenius plots of the various correlation times.

A common dynamic property of all PCs is the phenylene group rotation, which has been correlated to the impact resistance [7, 132, 180, 181]. Indeed, BPA-PC and Chloral-PC with faster phenylene ring rotation have good impact resistance while the other three polycarbonates are brittle. Furthermore, phenylene group rotation has been associated [132] with the γ-loss peak in dynamical mechanical studies [7]. NMR studies [7, 181, 182] in the solid state and theoretical calculations [179, 180] for PCs have identified the nature of the phenylene ring motion as a combination of π-flips and restricted rotation about the C_1–C_4 symmetry axis. In the case of BPA-PC, the γ-peak is observed at -100°C and for TMBPA-PC at $+50$°C. This difference in the γ-loss peak can be correlated with the more restricted nature of the phenylene group internal rotation observed in TMBPA-PC, although the change in segmental motion in TMBPA-PC may also be relevant. Shortly after the 180° ring flipping had been identified as one of the major molecular motion in polycarbonates, Jones [183] proposed coupled carbonate bond torsion and ring flips involving cooperative movement of three consecutive rings along the backbone as the origin of the γ-loss peak (Fig. 13).

Segmental motion, phenylene, methyl and formal group rotations in polyformals, BPA-PF and Chloral-PF, have been studied as a function of temperature, concentration and magnetic field

Table 2
Correlation time ratios of the various polycarbonates relative to BPA-PC in chloroform solutions[a]

Polycarbonate	Segmental motion τ_α/τ_α(BPA-PC)[b]	Phenyl internal rotation τ_{irp}/τ_{irp}(PBA-PC)[c]	Methyl internal rotation τ_{irm}/τ_{irm}(BPA-PC)[c]
PBA-PC	1	1	1
Chloral-PC	1.0 ± 0.1	2.7 ± 0.5	
Cl_2F_4	1.6 ± 0.2	15 ± 2	20 ± 8
Cl_4	1.8 ± 0.2	17 ± 2	2.3 ± 0.6

[a] Adapted with permission from Macromolecules [132], copyright 1981, American Chemical Society.
[b] τ_α is the arithmetic mean correlation time of the JS model.
[c] τ_{irp} and τ_{irm} denote the correlation times associated with the phenyl and methyl internal rotations, respectively.

Table 3
Apparent activation energies and Arrhenius prefactors of the various types of local motion in the polycarbonates and polyformals [6, 7, 132, 141, 177]

Polymer[a]	Solvent[b,c]	Apparent activation energy ($kJ\,mol^{-1}$)					Arrhenius prefactor ($\tau_x \times 10^{14}$ s)				
		Correlated segmental τ_1	Single backbone rotation, τ_0	Phenylene rotation	Methyl rotation	Formal rotation	Correlated segmental τ_1	Single backbone rotation, τ_0	Phenylene rotation	Methyl rotation	Formal rotation
BPA-PC	TCE-d_2[d]	19	16	22	24		28	1003	6	1	
	$CDCl_3$	≈ 19		13	22						
Chloral-PC	TCE-d_2	17	18	18			94	409	40		
	$CDCl_3$	≈ 13		15							
TMBPA-PC	TCE-d_2	23	34		22.5		11	3		5	
Cl_4	$CDCl_3$	≈ 18		15	19						
Cl_2F_4	$CDCl_3$	≈ 16		13	14						
BPA-PF	TCE-d_2	23	18	21	23	23	8	163	7	1	5
Chloral-PF	TCE-d_2	24.5	17.5	21		26	5	516	19		8

[a] See Fig. 12 for structures of the repeat units and corresponding abbreviations.
[b] 10% (w/v) solutions.
[c] The studies performed in $CDCl_3$ are less accurate because they are based on a limited data set.
[d] TCE-d_2, 1, 1, 2, 2-tetrachloroethane-d_2.

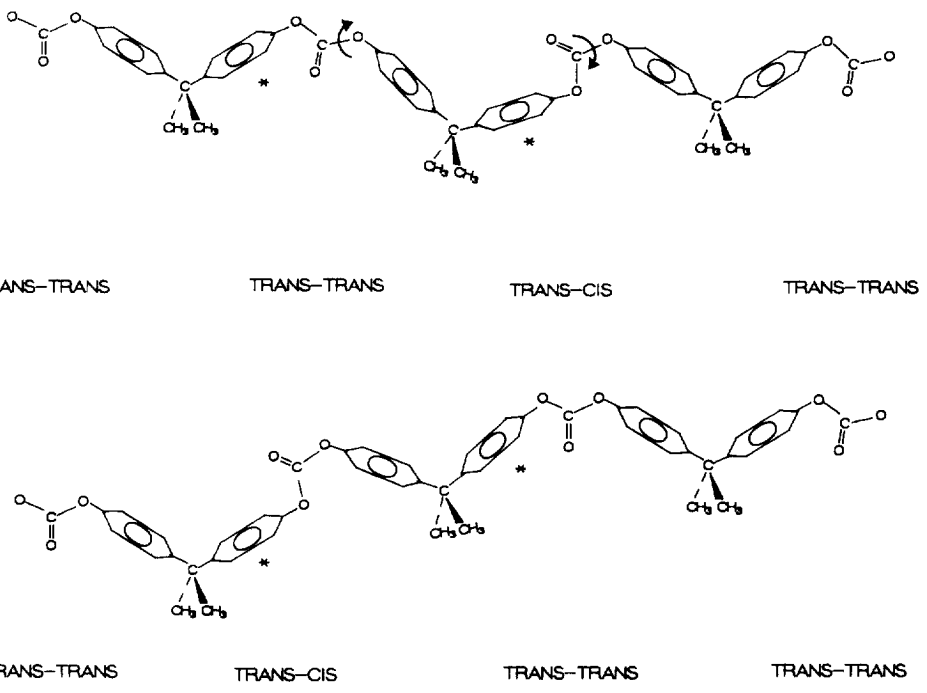

Fig. 13. BPA polycarbonate chains and the local motion corresponding to the loss maxima and relaxation minima in the glass. The carbonate CO bonds with arrows indicate points of bond rotation. The phenylene rings undergoing flips in association with the CO bond rotations are denoted by asterisks. The correlated conformational change from the top chain to the lower chain involves two neighboring carbonate groups and is produced by the CO bond rotations which interchange the trans-trans and cis-trans conformations. Conventional bond angles of 109° are used for all backbone bonds except the carbonate bonds, which are set at 120°. These choices lead to an 11° change of the C_1–C_4 axis of the phenylene groups in the BPA unit between the carbonate unit undergoing conformational change. Reprinted with permission from Macromolecules [183], copyright 1985, American Chemical Society.

[141, 144, 171]. It is interesting to compare the common motional characteristics of the polyformals to their corresponding polycarbonates, BPA-PC and Chloral-PC. Tables 3 and 4 list these comparisons in terms of correlation times and activation energies. The time-scale of segmental motion in BPA-PF is slightly faster than in Chloral-PF. However, both PFs are characterized by a slower segmental motion than the corresponding BPA-PC and Chloral-PC. Generally, the activation energies for cooperative transitions follow the order Chloral-PF $\approx$ BPA-PF > BPA-PC $\approx$ Chloral-PC. For methyl group rotation, the time-scale and activation energy are nearly the same for BPA-PF and BPA-PC (Tables 3 and 4), indicating that the methyl group rotation is a localized process and is essentially unaffected by changing from a carbonate link to a formal link. The activation energy for phenylene ring internal motion is nearly identical for polycarbonates and Chloral-PF in the same solvent. This observation is commensurate with a very localized process, as has been suggested [112, 141] previously for this internal motion. The time-scale of phenylene group rotation in BPA-PF is almost identical to BPA-PC, whereas the time-scale for this motion in Chloral-PF is a little slower by a factor of 3 relative to BPA-PC (Table 4).

The description of the dynamics of polyformals diverges from the polycarbonate pattern when the formal group is considered. The formal link provides new dynamic information relative to the polycarbonate chain, where no detailed analysis of the carbonate unit is possible, since it has no directly bonded protons. Among the various models used to interpret the relaxation data of the

Table 4
Comparison of local motions of polyformals relative to BPA-PC [112, 141, 177]

Polymer	Segmental τ_1/τ_1(BPA-PC)	Phenylene τ_{irp}/τ_{irp}(BPA-PC)	Methyl τ_{irm}/τ_{irm}(BPA-PC)	Formal τ_{irf}/τ_{irf}(BPA-PF)
BPA-PC	1.0	1.0	1.0	
BPA-PF	1.62 ± 0.26	1.00 ± 0.10	0.90 ± 0.10	1.0
Chloral-PF	1.88 ± 0.42	2.87 ± 0.39		2.73 ± 0.31

[a] The ratio is obtained by dividing the correlation time for each local motion of polyformals (Refs. [141] and [177]) by that of BPA-PC (Ref. [112]) at each temperature. Then the average value and standard deviation in this table are obtained from those ratios over the entire temperature range. For formal rotation, the rate of this motion in BPA-PF is used as a reference.

formal group, the best simulation for formal group rotation is obtained by adopting a model of double internal rotations about the C–O bonds, which does not allow these motions to contribute to phenylene relaxation. This local process involves conformational changes of the form [141, 144, 177]

$$gg' \rightarrow (tg') \rightarrow tg \tag{59a}$$

$$gg' \rightarrow (gt) \rightarrow g't \tag{59b}$$

Fig. 14 illustrates local formal group motion in a repeat unit resulting from conformational changes in Eq. (59a). It should be noted that the intermediate states tg′ or gt do not represent realistic intermediates, since they would involve a large rotation of the chain end. Rather these intermediates are used as calculational intermediates, i.e. to set up the appropriate TCF and provide a suitable mathematical pathway from gg′ to tg [141, 144, 177]. From Tables 3 and 4, it is clear that the formal motion in BPA-PF is a factor of 3 faster than in Chloral-PF, characterized by a lower activation energy in the former polyformal. The effect of concentration on local motions for both polyformals has been discussed extensively in Ref. [141].

(vii) Poly(vinyl chloride) (PVC). Radiotis et al. [123] have studied the dynamics of PVC in 1,1,2,2-tetrachloroethane-d_2 and dibutyl phthalate solvents. The latter solvent belongs to the group of phthalate diesters which are used extensively as primary plasticizers to convert the rigid PVC resin into workable and flexible compounds. By applying a number of models to the multi-field and variable temperature ^{13}C relaxation data of PVC, these authors concluded that only the DLM model can successfully describe the chain segmental motions of PVC in both solvents. Table 5 compares the ability of various models used to fit the ^{13}C relaxation parameters of the CH and CH_2 carbons of PVC at a temperature at which T_1 exhibits a minimum. As seen in this Table, it clear from the σ values (defined as the root mean squares of the relative deviations between calculated and experimental data) that the JS and HWH models are inadequate for describing the segmental motion of PVC. The high σ values arise from the fact that these models grossly underestimate the value of T_1 at the minimum. The $\log(\chi^2)$ distribution provides smaller σ values than the previous models. However, different values of the width parameter should be used in order to obtain good fits for both the CH and CH_2 groups, which is not a recommended method for fitting the data. In contrast, the DLM model gives an excellent fit ($\sigma = 0.5\%$) between experimental and calculated T_1 and NOE data for both the CH and CH_2 carbons at both fields. The most important difference

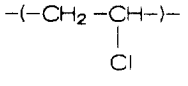

PVC

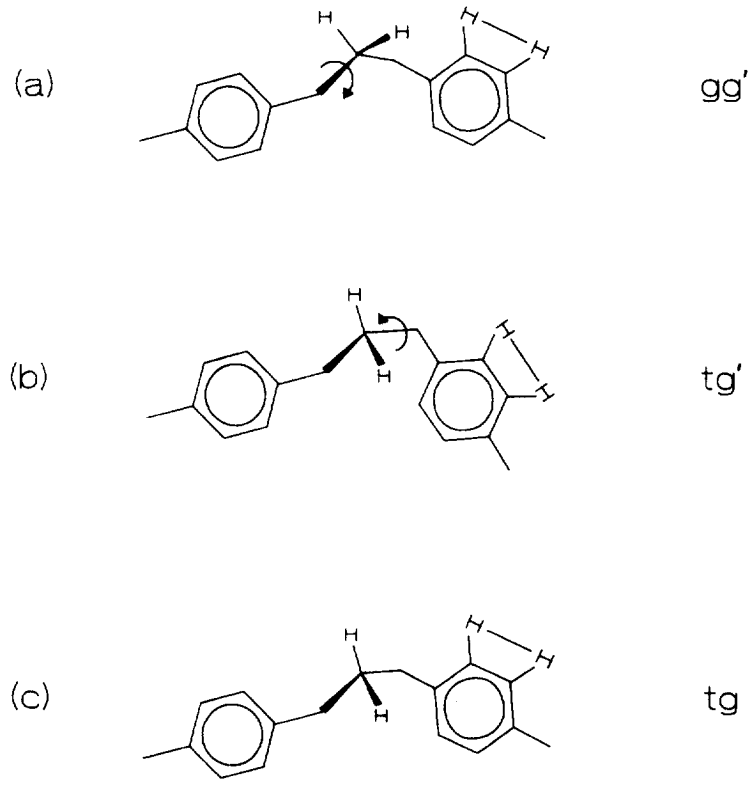

Fig. 14. Likely conformational transitions in the formal group. The motional process associated with Eq. (59a) is shown (see text). The arrows indicate the rotations of the conformational changes from (a) to (c). The overall conformational change is gg' to tg with the intermediate state tg' shown only to indicate the two conformational changes involved in the overall process. Note the $^1H-^1H$ dipole of the phenylene group is only translated and not reoriented. This is a Helfand type 2* motion thought to be a generally plausible form of segmental motion. The overall effect of this motion is two-site exchange (gg' to tg) which is a very restricted rotation far short of isotropic motion. Reprinted with permission from Polymer [141], copyright 1987, Butterworth & Co. Ltd.

found in modeling the dynamics of PVC in the two solvents using the DLM TCF was the different conic half-angles of the librational motion of the C–H vector for the methine carbon. These values were 27° and 30° in dibutyl phthalate and tetrachloroethane, respectively, indicating a greater steric hindrance to the librational motion of this vector in dibutyl phthalate. This observation has been rationalized by assuming a specific type of interaction between the carbonyl of the plasticizer and the chlorine atom of PVC, i.e. C=O ··· Cl–C.

(viii) Poly(vinyl methyl ether) (PVME). The local chain dynamics of this polymer has been studied in $CDCl_3$ solution and in the bulk by Dejean de la Batie et al. [126]. These authors, by analyzing the variable temperature ^{13}C T_1 data at 25.15 and 62.5 MHz with the DLM model, found that local motions in the PVME chain are of the same nature in both solution and in bulk. The magnitude of the librational motion is the same (33°) for both the methine and methylene C–H vectors.

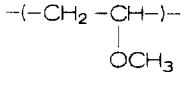

PVME

Table 5
Experimental and calculated ($\log(\chi^2)$, HWH, JS, and DLM) carbon-13 spin–lattice relaxation times (T_1, ms) and NOE values[a] of methine and methylene carbons of poly(vinyl chloride) (PVC) in DBP[b] and TCE-d_2[b] for two magnetic fields at a temperature at which T_1 exhibits a minimum [123]

Source	50.3 MHz		75.4 MHz		σ(%)
	CH	CH_2	CH	CH_2	
PVC in DBP, 61°C					
Expt.	136(1.75)	77(1.72)	202(1.54)	114(1.50)	
$\log(\chi^2)$	135(1.68)	68(1.68)	206(1.61)	103(1.61)	2.3
HWH	106(1.82)	54(1.82)	154(1.61)	79(1.61)	6.8
JS	107(1.83)	55(1.83)	154(1.62)	79(1.62)	6.7
DLM	136(1.74)	77(1.74)	202(1.55)	114(1.55)	0.4
PVC in TCE-d_2, 20°C					
Expt.	147(1.72)	81(1.71)	214(1.59)	115(1.58)	
$\log(\chi^2)$	143(1.69)	72(1.69)	218(1.63)	109(1.63)	1.7
HWH	109(1.91)	56(1.91)	156(1.71)	80(1.71)	7.6
JS	107(1.81)	55(1.81)	154(1.60)	79(1.60)	7.6
DLM	146(1.75)	80(1.75)	215(1.57)	117(1.57)	0.5

[a] Values in parentheses.
[b] DBP, dibutyl phthalate; TCE-d_2, 1,1,2,2-tetrachloroethane-d_2.

The activation energy of the backbone segmental motion is 38.5 ± 2 kJ mol^{-1} in the bulk polymer, while in solution the energy barrier for conformational transitions is equal to about one barrier crossing.

(ix) Poly(isobutylene) (PIB). PIB is an important industrial polymer, which in the form of butyl rubber, the copolymerization product of isobutylene with small amounts of isoprene, shows improved properties compared to natural rubber. PIB is quite different from nearly all other rubbery polymers, demonstrating unusually high WLF parameters [171] (see below), corresponding to a slow increase in segmental motion above the glass–rubber transition. PIB has been repeatedly studied in the past by ^1H and ^{13}C relaxation techniques. These early studies have been reviewed by Jones et al. [184] who, in addition, attempted to correlate earlier measurements on the basis of specific motional models. Local chain dynamics of PIB have been examined by Dejean de la Batie et al. [185] by using a number of models to interpret the relaxation data of PIB in 10% (w/v) chloroform solution and in the bulk at two Larmor frequencies. The HWH and GDL TCFs fail to account for the relaxation parameters at the T_1 minima in both fields. On the contrary the DLM model fits the data very well over the whole temperature range including the T_1 minima. Within the accuracy of the data analysis the same set of the DLM simulation parameters accounts for both the solution and bulk dynamics of PIB. The calculated energy for conformational transitions along the PIB chain was estimated to be 21 kJ mol^{-1} in chloroform solution and 45 kJ mol^{-1} in bulk. The abnormally high value for the activation energy in chloroform solution, which was also observed in earlier studies in carbon tetrachloride [184] and *o*, *m*-dichlorobenzene [186] solutions, has been attributed to the high barrier height involved in the rotation about the $C(CH_3)_2$–CH_2 bond.

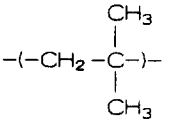

PIB

Conformational energy calculations for PIB [187, 188] and infra-red experiments for 2,2-dimethylpentane [189] suggest a high barrier crossing of about 17–21 kJ mol^{-1}.

A more recent detailed relaxation study on bulk PIB has been reported by Bandis et al. [190] These authors used three different TCFs to treat the variable temperature ^{13}C T_1 and NOE data at three magnetic fields, thus extending the data base of previous experiments [184, 185]. All the models (DLM, HWH and Kohlrausch–Williams–Watts [191], the last two combined with restricted anisotropic diffusion [145]) give a satisfactory description for the local dynamics of the backbone CH_2 carbon, yielding comparable values for the time-scale of segmental motions, apparent activation energies (34–36 kJ mol^{-1}), and distribution of correlation times. ^{13}C T_1 values were also determined in this study for PIB under pressure of CO_2 gas to investigate changes in segmental motion in the presence of the gas.

(x) Poly(R,S)-3-methyl-1-octene] (PMO) and poly[(R,S)-3,7-dimethyl-1-octene] (PDMO). PMO and PDMO are the first synthetic polymer systems whose local chain dynamics has been described by the ORZLD model of Perico [113–116]. The relaxation data of these polymers were analyzed by using the single exponential TCF, the HWH, and ORZLD TCFs [118]. Reasonable best fit parameters were found in each case. Therefore no discrimination between the three models for the backbone relaxation on the basis of the fitting results was achieved. However, neither the single exponential nor the HWH models are directly connected to the degree of chain flexibility in terms of the structural features of these two polymers as is the ORZLD model. The calculated stiffness parameter of the ORZLD model (Eq. (47)) is similar for both PMO and PDMO polymers, but PMO exhibits a slightly higher value for the persistence length, p (Eq. (48)). The small difference in the parameter p has been attributed [118] to the different structures and stereoregularities of the two polymers.

(xi) Poly(β-hydroxyalkanoate)s (PHAs). PHAs consist of a class of β-mono-alkyl-substituted poly-β-esters which are naturally occurring in a wide variety of bacteria [192]. A great deal of research has been carried out on the microbial production and characterization of PHA homopolymers and copolymers. These polymers exhibit characteristic properties such as environmental degradability, biocompatibility, optical activity, and so on. Some of these polyesters are now produced on a large scale as commercial thermoplastics and are suitable for medical and controlled drug release applications.

The local dynamics of the first member of PHAs, poly(β-hydroxybutyrate), (PHB), has been studied in chloroform-d and tetrachloroethane-d_2 solutions [120, 121, 133]. The multi-field ^{13}C T_1 and NOE data are described more successfully in both solvents by employing the DLM TCF. The excellent fit of the T_1 data of PHB in chloroform with the DLM model over the entire temperature range studied is illustrated in Fig. 15 for both the methine and methylene carbons at 75.4 and 100.5 MHz [121]. Very good fits have also been obtained for PHB data in tetrachloroethane solutions [120]. Also, Fig. 15 illustrates the less satisfactory fits of the data with the JS and HWH models. This indicates that the C–H internuclear vectors of the two carbon sites do not experience exactly the same local dynamics as the JS and HWH models predict. This is reflected in the simulated values of the conic semi-angle θ of the DLM model, which are 26° for the CH carbon, and 31° for the CH_2 carbon of PHB in chloroform. The corresponding values in tetrachloroethane are 22° and 29°, respectively. The greater θ value for the CH_2 carbon indicates less steric hindrance to the librational motion of the corresponding C–H vector relative to that in the CH carbon where the presence of an adjacent methyl group restricts the amplitude of local libration.

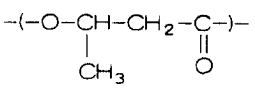

PHB

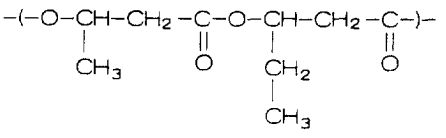

P(HB/HV)

The application of the DLM model to the relaxation data of the copolymer poly(β-hydroxybutyrate-co-β-hydroxyvalerate), [P(HB/HV)], containing 27 mol % HV, in chloroform reveals the following motional characteristics of the copolymer chain [122]: (1) the local dynamics of a comonomer unit, e.g. HB, is independent of the presence of a nearby HV unit and vice versa, (2) different local dynamics prevail not only between the various comonomers, but also within a given comonomer unit in the random copolymer chain, (3) chain segmental motion of the copolymer described by cooperative conformational transitions is similar to that observed for the PHB homopolymer in the same solvent. These characteristics are summarized in Table 6 in terms of the simulation parameters of the DLM model for the HB and HV units in the copolymer. The greater θ value for the CH carbon in the HB comonomer reflects lower steric hindrance to the librational motion of the corresponding C–H vector as compared to that for the CH carbon in the HV unit bearing the bulkier ethyl group. Also differences in local dynamics within a given sequence are reflected on the different θ_{CH} and θ_{CH_2} values for each monomer unit. Finally, the correlation

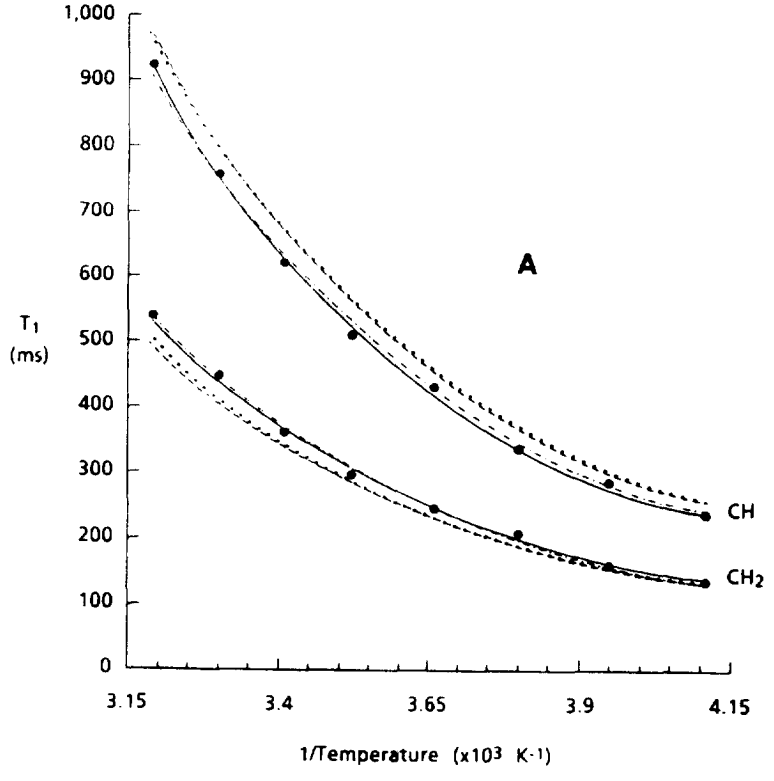

Fig. 15. Plots of ^{13}C spin–lattice relaxation time T_1 (ms) vs reciprocal temperature of PHB in $CDCl_3$ at: (A) 75.4 MHz; (B) 100.5 MHz. Full curves and data points are experimental data; - - -, HWH model; · · ·, JS model; - · -, DLM model [121].

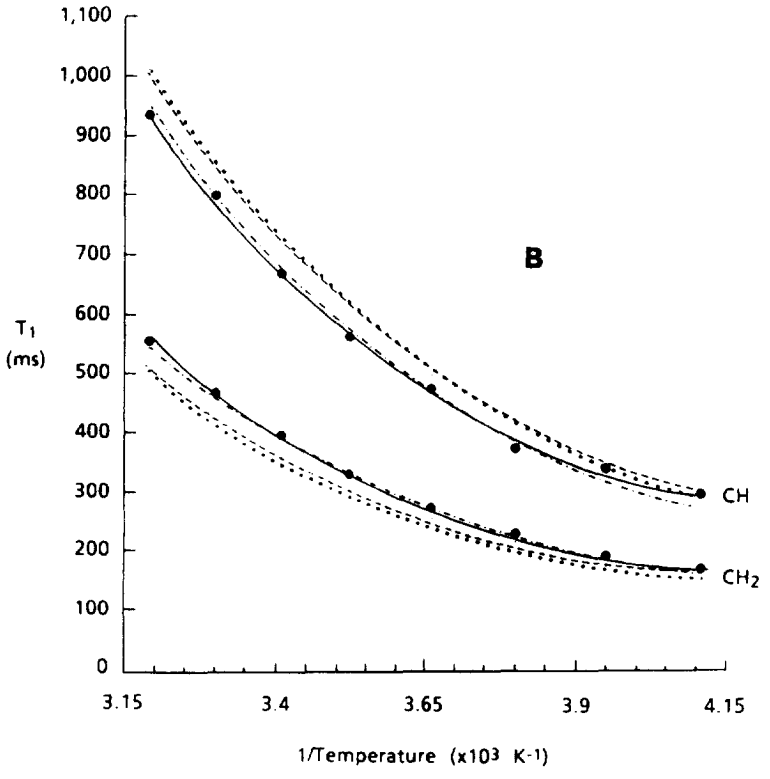

Fig. 15. (continued)

Table 6
Simulation parameters for (PHB/27% HV) copolymer and PHB homopolymer in chloroform solutions using the DLM model [121, 122]

Temp. (°C)	τ_1(HB)[a,b]	τ_1(HV)[a,c]	τ_1(PHB)[a,d]
−30	4.59	4.65	4.26
−20	2.98	2.86	3.04
−10	2.46	2.07	2.26
0	1.67	1.51	1.63
10	1.39	1.21	1.28
20	1.05	0.92	1.00
30	0.86	0.72	0.80
40	0.69	0.57	0.65
E_a(kJ mol^{-1})	17	18	17
τ_∞($\times 10^{13}$ s)	1.1	0.5	9
r	0.998	0.998	0.999

[a] 10^{-10} s.
[b] For the HB unit: $\tau_0/\tau_1 = 3$, $\tau_1/\tau_2 = 200$, $\theta_{CH} = 25°$, $\theta_{CH_2} = 31°$.
[c] For the HV unit: $\tau_0/\tau_1 = 5$, $\tau_1/\tau_2 = 200$, $\theta_{CH} = 21°$, $\theta_{CH_2} = 29°$.
[d] For PHB: $\tau_0/\tau_1 = 3$, $\tau_1/\tau_2 = 200$, $\theta_{CH} = 26°$, $\theta_{CH_2} = 31°$.

times, τ_1, associated with cooperative conformational transitions are nearly identical for both HB and HV units, leading to similar activation energies (17–18 kJ mol^{-1}) which are not very different from that (17 kJ mol^{-1}) obtained for PHB in the same solvent (Table 6).

Amor et al. [193] have carried out variable temperature ^{13}C NMR relaxation studies of PHB within native granules. They showed that the relaxation behavior of PHB in its native state is typical of an amorphous elastomer above its T_g. By employing the DLM model they were able to reproduce the ^{13}C NMR relaxation data obtained at a temperature range well above T_g. It was found that segmental motion is the dominant cause of spin relaxation, although the rate of this motion is slower than in solution. The activation energy (57 kJ mol^{-1}) for cooperative conformational transitions in the native state is larger than for PHB in solution and of the same magnitude as for other bulk elastomers. It is noteworthy that the DLM model used gives the same values for the amplitude of the librational motion as those observed for PHB in solution.

Variable temperature ^{13}C NMR T_1 and NOE data at two magnetic fields have been used to study the local dynamics of the amorphous part of a semi-crystalline sample (33% crystallinity) of poly(β-hydroxyoctanoate) (PHO) [8]. Fig. 16 shows ^{13}C spectra, obtained without line-narrowing techniques (e.g. CPMAS) of the amorphous component of semi-crystalline PHO as a function of temperature. As observed in other solid elastomers such as PBD and PI [9, 12], or PIB [194], as well as for some semi-crystalline polymers [9–12, 195–202], conventional ^{13}C NMR spectra are easily obtained at temperatures well above T_g because the motion of the molecules is so rapid that the line-broadening effects of the chemical shift anisotropy and ^{13}C–^{1}H dipolar coupling are effectively averaged out by molecular motion. The spectra of PHO (Fig. 16) confirm that there is also a large amorphous component of this polymer that is very mobile at room temperature which is 61°C above T_g(= − 36°C). The effects of temperature and crystallization, as well as the various mechanisms causing line-broadening of the different carbon resonances of PHO have been discussed in detail in Ref. [8].

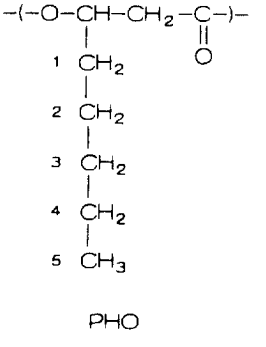

PHO

Plots of the observed T_1 values of the backbone carbons at both magnetic fields are shown in Fig. 17, and for the side-chain at one field in Fig. 18. The relaxation times clearly demonstrate the different dynamics of the backbone relative to the side-chain for this biopolyester. The T_1 values for the backbone carbons at both fields decrease with increasing temperature, reaching a minimum at $\approx$ 90°C. This demonstrates that these carbons experience motions which are within the "slow motion regime". As the temperature increases beyond the minimum, the T_1 values start increasing, indicating that motions characterized by short correlation times are contributing to the relaxation of the backbone carbons.

It is interesting to note that the plots in Fig. 17 do not reveal any discontinuity in T_1 as the melting temperature (61°C) is traversed. This indicates that the fast segmental motions reflected in the T_1 values are not influenced significantly by the formation of crystallites below the melting point of the polymer. Similar behavior has been reported [10, 12, 196–202] for other semi-crystalline polymers, where, in addition, the T_1 values are independent of the degree of crystallinity and morphology.

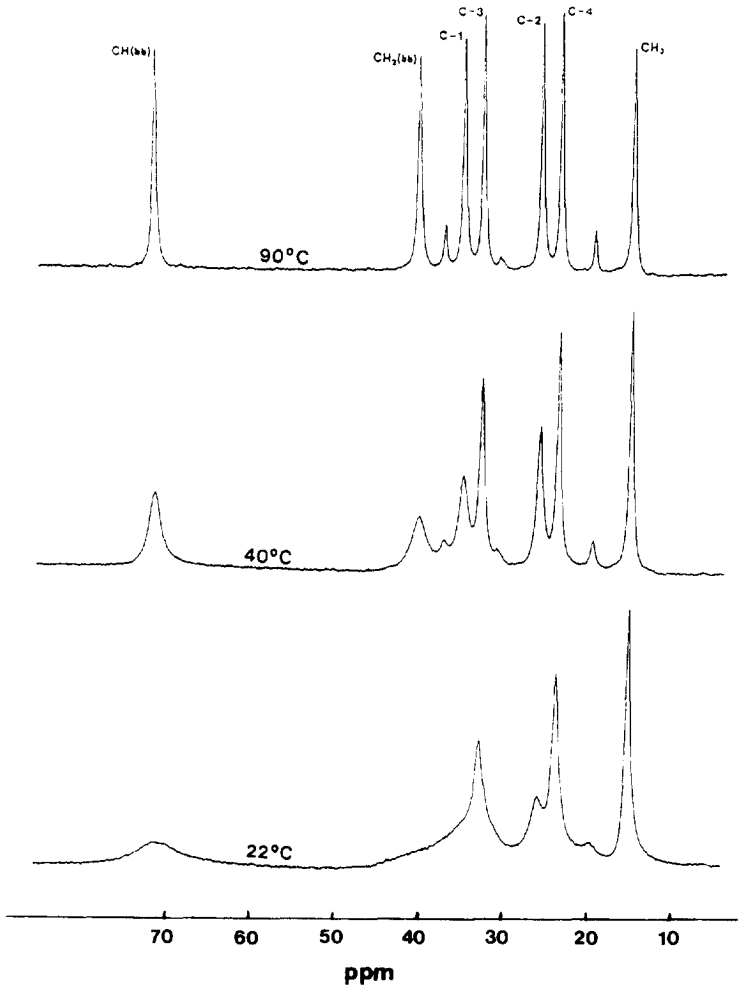

Fig. 16. ^{13}C NMR spectra of the amorphous part of the semicrystalline PHO at various temperatures. CH(bb) and CH_2(bb) denote the backbone methine and methylene carbons, and C-i (i = 1–4) and CH_3 the side chain methylene and methyl carbons [8].

The opposite behavior is observed for the relaxation times at 75.4 MHz of the side-chain carbons in Fig. 18 as compared to those of the backbone carbons (Fig. 17). Here, the T_1 values increase with increasing temperature, and therefore, fall within the "fast motion regime". A similar behavior for the T_1 values is observed at 100.5 MHz.

At a given temperature, T_1 increases monotonically with distance of the carbon from the site of attachment. This trend, which is more pronounced at high temperatures, is reminiscent of the solution behavior of hydrocarbon chains attached at one end to a heavy anchor [146]. In the present case, the polymer backbone restricts the motion of the side-chain at one end, allowing greater chain mobility as one goes toward the free end of the chain. It appears that the PHO molecule represents a case where the backbone acts as a slow moving molecular fiber with relatively fast movement, of bulky hydrocarbon side-chains acting as a diluent. It is interesting to note that the T_1 values of all ^{13}C nuclei of the side-chain (including the terminal CH_3 group) are frequency-dependent at all temperatures.

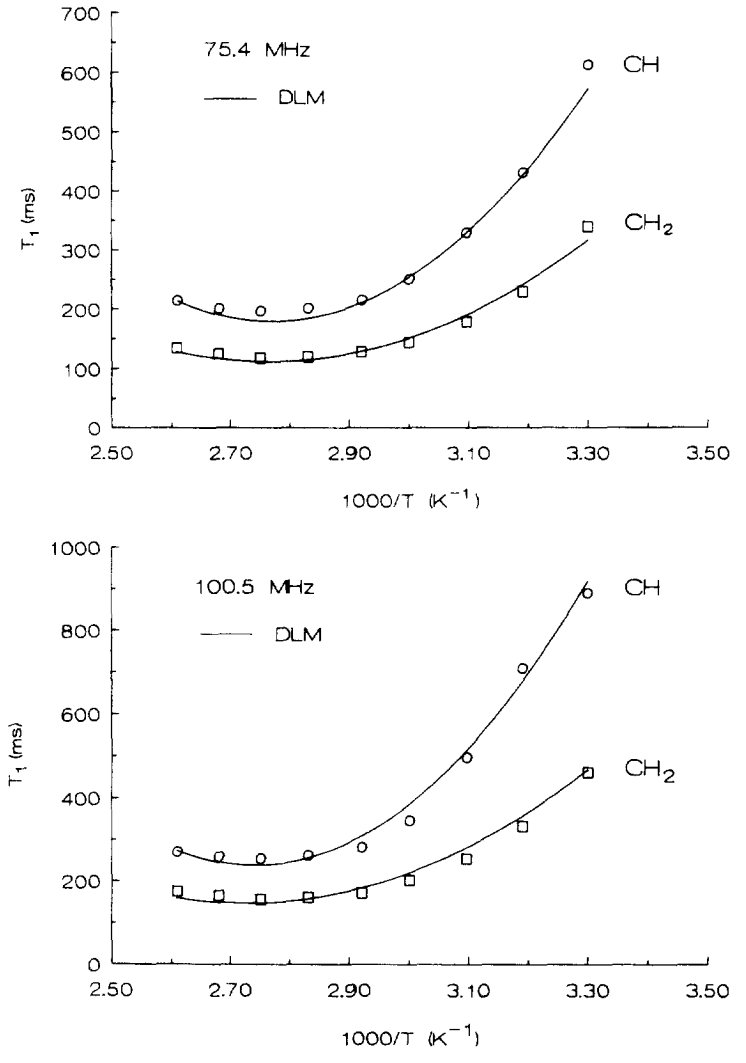

Fig. 17. Temperature dependence of the experimental and calculated T_1 values of the backbone CH(bb) and CH_2(bb) carbons of PHO at 75.4 and 100.5 MHz. Solid curves correspond to the DLM model fitting [8].

In contrast to the T_1 values, NOE is a more sensitive probe of the non-crystalline structure of a semi-crystalline polymer [9–12, 194]. From data presently available, it appears that NOE depends on the level of crystallinity and not specifically on the crystalline morphology. Moreover, it was found [9, 12, 194] that all the protonated backbone carbons of semi-crystalline polymers are characterized by similar NOE values. This is what is observed for the NOE values of the CH(bb) and CH_2(bb) carbons of PHO at both magnetic fields. The NOEs are invariant with respect to the two protonated backbone carbons within the limit of accuracy. The NOE data appear to be frequency-dependent only for the two to three highest temperatures; the NOEs at 75.4 MHz are larger by 0.1–0.2 NOE units than those at 100.5 MHz. However, at low temperatures, no appreciable field dependence is observed for the NOEs, which approach an asymptotic behavior at both fields. This behavior is shown graphically in Fig. 19, where the average NOE values for the backbone CH(bb) and CH_2(bb) carbons are plotted as a function of temperature at 75.4 MHz and 100.5 MHz, respectively.

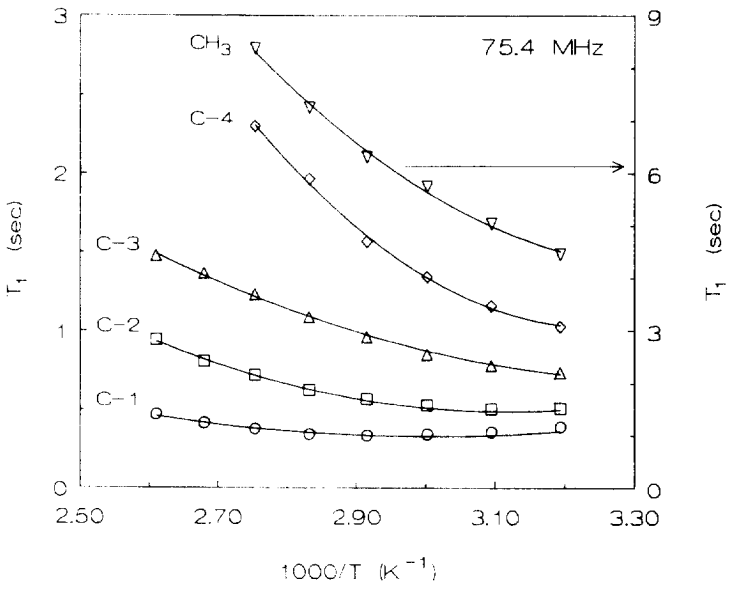

Fig. 18. Temperature dependence of the experimental and calculated T_1 values of side-chain carbons of PHO at 75.4 MHz. Solid curves correspond to the DLM plus restricted multiple internal rotations model fitting [8].

The reduced NOE values at low temperatures toward T_g is a direct result of the influence of the crystalline region on the backbone motion of PHO in the amorphous state. Evidently, the presence of crystallites favors low or near-zero frequency molecular motions reflected by this parameter. Since the NOEs for the protonated backbone carbons are similar, it is concluded that the crystalline region affects equally the motion of the CH vectors at the two backbone sites. At elevated temperatures above the melting point, PHO is completely amorphous and the NOE values cannot be affected by crystallinity. In this temperature range all restraints on chain mobility arising from the presence of crystallites must be removed. Even though chain entanglements are still present, the motional behavior of the backbone CH vectors should approach the "fast motion regime" with a concomitant increase in the NOE values.

Various models (HWH, JS, DLM, Cole–Cole, Fuoss–Kirkwood, $\log(\chi^2)$) have been used to describe the local chain dynamics of PHO in the bulk. The DLM model was found to be superior to any unimodal distribution function in fitting the relaxation data of PHO. As shown in Figs. 17 and 19 the parameters of the DLM model may be adjusted to fit the 75.4 and 100.5 MHz T_1 and NOE data for the CH(bb) and CH_2(bb) carbons. It is clear from these plots that very good agreement between experimental and calculated values is obtained from this model throughout the entire temperature range studied.

Table 7 summarizes the fitting parameters of the DLM model for the backbone carbons. The theoretical curves were computed by using temperature independent values for the parameters θ and the ratio τ_0/τ_1. The best values, $\tau_0/\tau_1 = 50$, $\theta_{CH} = 24°$, $\theta_{CH2} = 33°$, were preadjusted at the T_1 minima. The greater value for the CH_2(bb) carbon indicates less hindrance to the librational motion of the corresponding C–H vector relative to that in the CH carbon for which the presence of an adjacent hydrocarbon side-chain restricts the amplitude of the local libration. This observation is in agreement with earlier findings for poly(β-hydroxybutyrate) [120, 121, 133, 193]. (PHB) and other polymer systems.

Within experimental error, τ_1 follows an Arrhenius relationship yielding an apparent activation energy of 38 kJ mol^{-1}. This value is of the same order as the reported [193] activation energy for PHB (57 kJ mol^{-1}) in its elastomeric state within the granules.

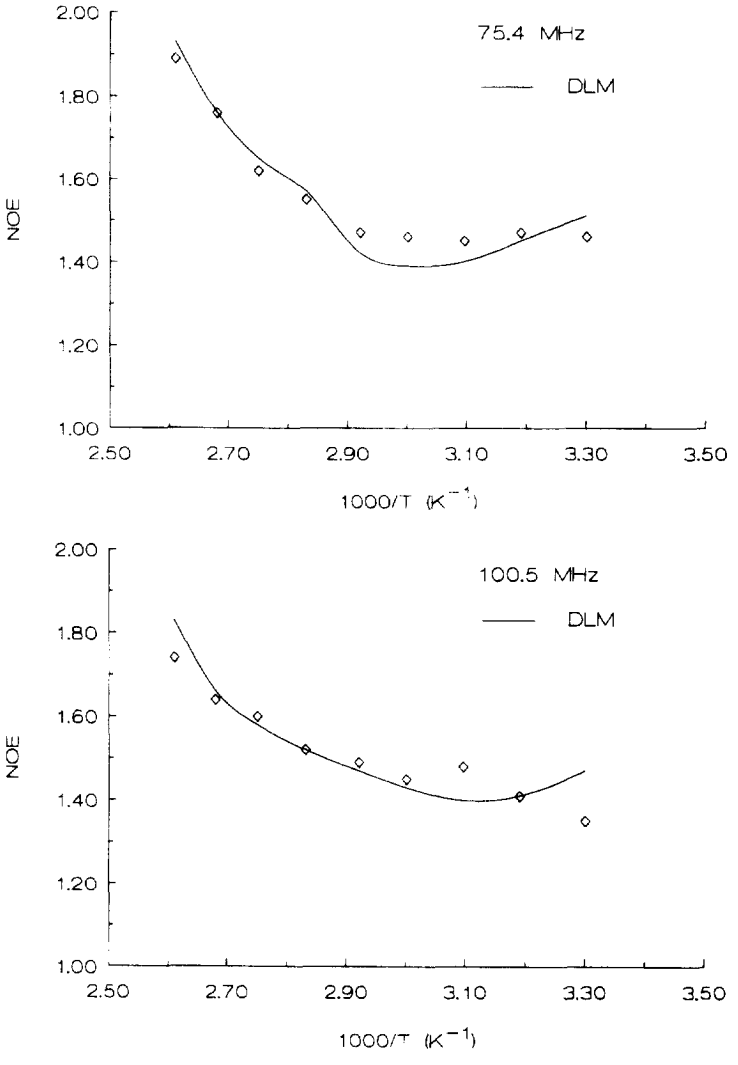

Fig. 19. Temperature dependence of the NOE values for PHO at 75.4 and 100.5 MHz. Each data point corresponds to the mean value obtained for the methine and methylene backbone groups. Individual NOE values of the latter differ by less than 0.05 NOE units. Solid curves correspond to the DLM model fitting [8].

(xii) Polyesters. Because of their commercial interest in fibers, sheets, adhesives and injection-molding resins, polyesters have been studied extensively in the past by a wide variety of techniques, including NMR. Polyesters are prepared by polycondensation reactions of the appropriate diols with the appropriate diacids of various compositions. The chemical structures of typical diols and diacids are summarized in Fig. 20. The picture that emerges for the chain mobility of these polymeric materials from various ^{1}H and ^{13}C NMR relaxation studies [106, 197, 203–207] can be described as follows.

(1) The segmental mobility of the alkyl chain segments increases with increasing distance from the diacid group. In this sense, the alkyl links behave like side-chains attached to the polymer backbone.

(2) The mobility of the alkyl chains increases overall with the length of the alkyl chain segment.

(3) The mobility of the alkyl chain depends on the type of diacid unit in the polymer, being more flexible when it is attached to azelaic acid (A) than to the more rigid terephthalic acid (T) or other phenylene-containing diacids.

Table 7
DLM simulation parameters[a] for the backbone segmental motion; rotational diffusion constants, D_i ($\times 10^9$ s^{-1}), amplitude, φ_i^0, and activation energies (kJ mol^{-1}) for restricted internal rotations about the C–C bonds of the *n*-pentyl side-chain of PHO [8]

t (°C)	τ_1[a,b]	D_1	φ_1^0	D_2	φ_2^0	D_3	φ_3^0	D_4	φ_4^0	D_5	φ_5^0
30	16.22										
40	11.44	2.9	36	5.5	40	10.0	50	10.1	53	105.2	145
50	7.52	3.5	48	8.9	41	10.9	60	12.9	58	113.9	143
60	4.33	5.1	62	9.4	40	15.3	80	17.0	62	132.4	147
70	3.19	6.3	67	13.0	43	18.7	92	17.7	67	145.2	131
80	1.72	8.6	68	15.3	46	23.7	98	24.1	70	222.7	119
90	1.39	9.6	75	18.1	47	26.5	100	30.0	74	280.3	105
100	1.11	12.1	76	22.9	49	28.5	105				
110	0.74	13.5	85	26.4	52	39.7	111				
E_a	38	23		21		19		20		19	
r	0.997	0.995		0.991		0.990		0.992		0.954	

[a] $\tau_0/\tau_1 = 50$, $\tau_2 = 50$ ps, $\theta_{CH} = 24°$ and $\theta_{CH_2} = 33°$.
[b] In nanoseconds.

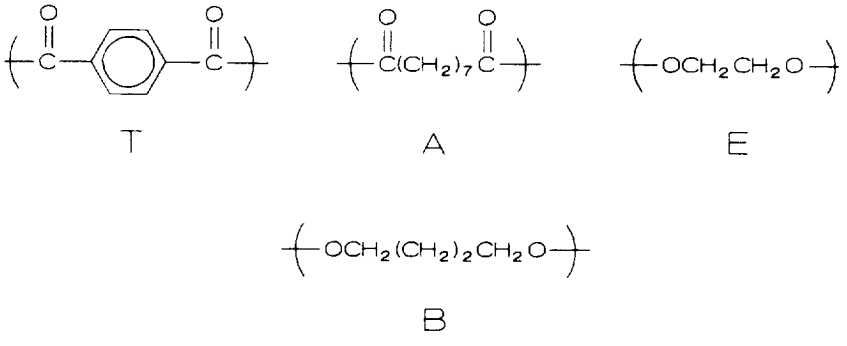

Fig. 20. Chemical structures of typical diols and diacids from which polyesters are formed: terephthalic acid (T), azelaic acid (A), ethylene glycol (E), butanediol (B).

(4) The mobility of the phenylene-containing diacids is independent of the length of the separating alkyl chain.

(5) The mobility of the hydrocarbon chains varies significantly with the type and composition, as well as with the sequence distribution of the diols and diacids in co-polyesters.

Fig. 21 illustrates the variation of the T_1 values of the ethylene glycol methylene carbons as a function of the azelaic acid composition and the triad structure of a four-component system containing a constant 70:30 ratio of ethylene glycol (E) to butanediol (B) and various proportions of terephthalic acid (T) and azelaic acid (A) [206]. The T_1 values decrease with increasing terephthalic acid content as expected. Moreover, the T_1 values vary considerably from one type of E-centered triad to another, being the highest for the A-E-A triad and the lowest for the T-E-T triad. Triads A-E-T (or T-E-A) have intermediate T_1 values. This observation indicates that internal rotation in the T-E-T triad is more hindered than in the A-E-A triad. Similar plots have been obtained for the T_1 values of the methylene carbons of butanediol and those of azelaic acid as a function of composition. These data have been discussed in Ref. [206]. The nature of the segmental motion occurring in homo- and co-polyesters has been discussed [106, 196, 203] in terms of the type of motions as classified by Helfand [66].

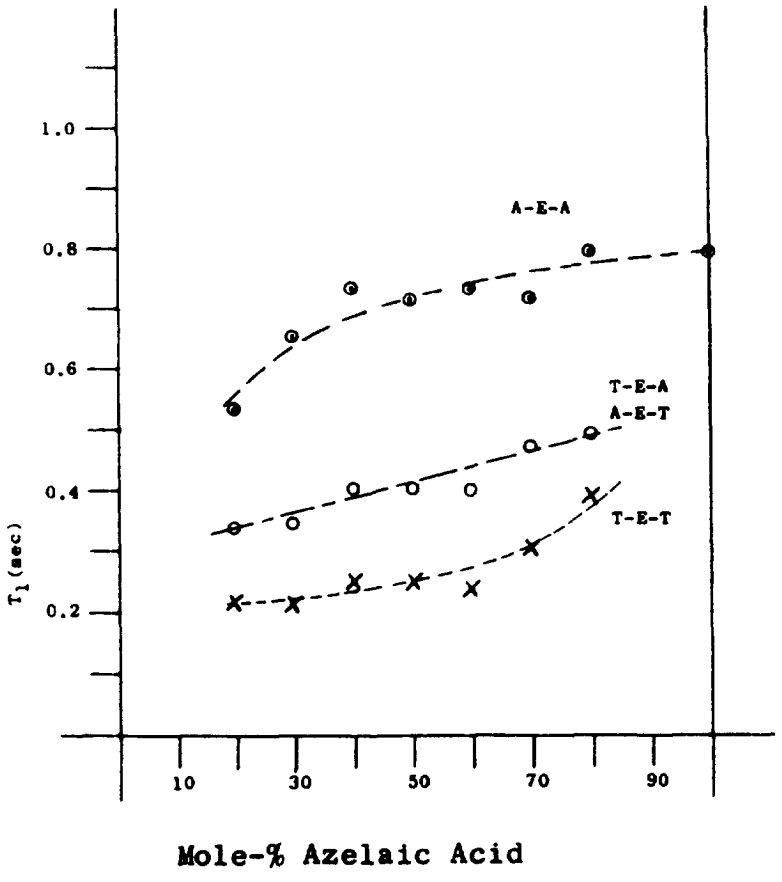

Fig. 21. Effect of monomer sequence on T_1 values of the ethylene glycol carbons. Reprinted with permission from Polym. Preprints. [206], copyright 1979, American Chemical Society.

(xiii) Poly(olefin sulfone)s. The local dynamics of this class of polymer in solution was a matter of controversy for several years [3]. Although there is a large body of experimental data in the literature, the apparent conflict between the molecular-weight-dependent maximum loss frequency in dielectric relaxation measurements and the molecular-weight-independent NMR relaxation data needs further clarification. Recent dielectric relaxation experiments [208] at high frequencies for a number of poly(olefin sulfone)s in benzene and dioxane revealed a high-frequency loss process. This process, not observed in previous dielectric relaxation measurements at low frequencies, has been attributed to a local process independent of chain length, in agreement with the NMR relaxation results. Also, this process has been attributed tentatively to local segmental rearrangements developed by Helfand and co-workers following an earlier suggestion by Cais and Bovey [62]. Although this hypothesis may be suitable for describing local dynamics in the more flexible poly(but-2-ene sulfone), it appears to be less promising for the more rigid poly(but-1-ene sulfone). The former sulfone has C–C bonds in a predominantly trans conformation, sufficiently separating, in space, the neighboring sulfone groups from each other. Thus, backbone motions in poly(but-2-ene sulfone) are not electrostatically constrained as in poly(but-1-ene sulfone), a fact which permits gauche C–C bonds, leading to a close packing of a sulfone dipole behind its neighbor [209, 210]. We believe that a possible process characterizing poly(olefin sulfones) local dynamics not included in these studies may be high-frequency local librations of the backbone C–H vectors. This suggestion is supported by the fact that the ratio, R, for the ^{13}C T_1 values of the backbone methine and

methylene carbons of several poly(olefin sulfones) in various solvents is less than its theoretical value of 2 [208].

(xiv) Poly(alkyl acrylate)s (PAAs) and poly(alkyl methacrylates) (PAMAs). The backbone motion of the first members of these series, poly(methyl acrylate) and poly(methyl methacrylate), has been thoroughly studied in the past by employing ^{1}H and ^{13}C NMR relaxation measurements and theoretical calculations [3, 4]. PAMAs with larger side-chains have been studied recently by Spyros and Dais [26] by using ^{13}C T_1 and NOE data at two magnetic fields for poly(butyl methacrylate) (PBMA) and poly(hexyl methacrylate) (PHMA) in 50% toluene solutions published earlier by Levy et al. [27]. In the original publication, the backbone relaxation data were analyzed on the basis of the $\log(\chi^2)$ distribution. However, the DLM function was found to be more appropriate for describing backbone segmental motion in these polymer systems [26]. The rate of the librational motion is about 100 times faster than segmental motion, whereas the conic half-angle is very similar for both polymers, as expected from their similar structure. Studies of the backbone motions of bulk poly(ethyl acrylate) and poly(butyl acrylate) by solid-state ^{13}C NMR relaxation and molecular dynamics calculations showed that librational motion is an important motional component of the dynamics of backbone CH and CH_2 carbons [211]. Finally, it is worth mentioning that local chain dynamics of poly(isopropyl acrylate) [212], poly(sodium acrylate) [213] and poly(methacrylic acid) [214] in solution has been described quantitatively by conducting ^{2}H NMR relaxation studies.

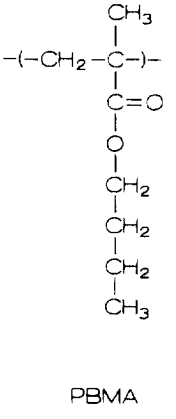

PBMA

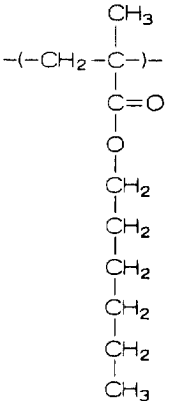

PHMA

(xv) Poly(1-naphthylalkyl acrylate)s (PNAAs). Synthetic PNAA polymers have been used in the past to study photophysical processes that appear to mimic similar effects in plant photosynthesis and to have practical consequences in the photodegradation and/or photostabilization of commercial polymers. A detailed interpretation of the photophysical behavior of these systems requires, among other factors, knowledge of their stereochemical composition and chain dynamics. Spyros and co-workers [143, 215, 216] have carried out a detailed study on chain structure and chain dynamics of a series of PNAAs, namely poly(1-naphthyl acrylate) (PNA), poly(1-naphthylmethyl acrylate) (PNMA), and poly(2-(1-naphthyl)ethyl acrylate) (PNEA), in 10% (w/v) solutions in 1,1,2,2-tetrachloroethane -d_2. In these polymers the side-chain naphthyl group is located progressively further from the main chain. The measured ^{13}C T_1, T_2, and NOE data as a function of temperature and magnetic field have been analyzed by using several motional models describing backbone motion. The JS and HWH models are unable to fit simultaneously all the experimental data not only at the T_1 minima, but also over the entire temperature range studied. In contrast, the DLM model gives an excellent fit for the data sets of the three polymer systems. Table 8 summarizes the simulation parameters of the DLM model for the three polymers. A salient feature of these figures is that the correlation times, τ_1, for backbone cooperative transitions are very similar for

Table 8
Simulation parameters of the DLM model used to describe backbone segmental motions of PNA, PNMA, and PNEA in 1,1,2,2-tetrachloroethane-d_2 solution

Temp. (°C)	τ_1(ns)		
	PNA	PNMA	PNEA
20	12.14	5.14	5.40
40	6.63	3.06	3.18
60	3.49	2.02	1.88
80	2.18	1.18	1.27
100	1.41	0.77	0.92
120	1.03	0.46	0.60
τ_0/τ_1	3	5	7
τ_1/τ_2	30	50	70
θ^0_{CH}	22.9	18.9	19.2
E_a (kJ mol^{-1})	24	23	21
τ_∞ (10^{-12} s)	0.6	0.5	1.1
r	0.999	0.996	0.999

PNMA and PNEA and shorter than the corresponding correlation time of PNA by a factor of 2. This indicates a faster backbone rearrangement for the former polymers, and hence an increasing chain flexibility relative to the PNA main-chain. However, the activation energies for the backbone motion in the three polymers, obtained from the Arrhenius plot of the corresponding τ_1 values, are not very different within experimental error. The ratio τ_0/τ_1 appears to increase from PNA to PNEA (Table 8) indicating that single conformational transitions associated with damping play a lesser role on going from PNA to PNEA polymer.

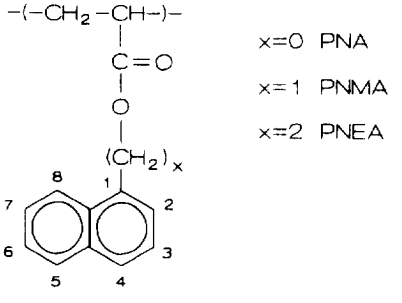

Another interesting observation is that the τ_1/τ_2 ratio increases progressively from PNA to PNEA (Table 8), reflecting an increasing rate of the librational motion of the backbone C–H vector from PNA to PNEA. This result is in agreement with the observed best fit half-angle, θ, of the librational motion, which decreases from 23° for PNA to 19° for PNMA and PNEA (Table 8). A smaller half-angle corresponds to a shorter correlation time for the librational motion [123]. The half-angle of the cone, θ, for the C–H vector at the backbone methylene carbon site of PNA is greater than that calculated for the C–H vector of the backbone methine group of the same polymer (29° vs. 23°). Although the relaxation data for the methylene carbon are not determined with the same accuracy as those of the methine carbon, and calculations were performed by using data obtained at one field only, this result supports the conclusion observed in other polymers mentioned in this article, i.e. a smaller θ value for the CH group indicates a greater steric hindrance to the librational motion of

the C–H vector relative to that in the CH_2 group. The methine carbon has a directly attached side-chain which, because of its size, physically restricts the amplitude of the local libration.

(xvi) Other polymer systems. A number of studies have appeared in the literature dealing with the dynamics of several homo- and co-polymers in solution. Although local chain motions have been described in a qualitative or semi-quantitative manner, useful information has been gathered to understand the specific motions in these polymer systems. Chapoy et al. [217] studied the relaxation behavior of six polyethers containing 1,4- or 1,2-cyclohexylene rings in the polymer backbone. The rings appear to behave more as rigid units and are opposed by relatively low barriers to internal rotation, thus being rather more mobile than the hexose rings in polysaccharides.

Spin–lattice ^{13}C and ^{1}H relaxation studies [218] on poly(vinylidene chloride) in hexamethylphosphoramide-d_{18} over a temperature range of 11–89°C and concentrations of 15 and 25% (w/v) showed that the time-scales of the backbone motions are quite similar to those of poly(vinylidene fluoride) and poly(isobutylene) when the influence of the solvent viscosity is taken into account.

^{13}C T_1 and NOE values were measured at 25 MHz and 40°C for dioxane-d_8 solutions of poly(1-vinylnaphthalene) (P1VN) and poly(2-vinylnaphthalene) (P2VN) [219]. The backbone motions were characterized by a distribution of correlation times. The average correlation times obtained from the $\log(\chi^2)$ distribution function by fitting the data of the methine carbons of both polymers indicate that the segmental motion of P1VN is slower than that of P2VN and polystyrene. This order of the relative mobilities of the polymer chains has been explained on the basis of the energy contour maps for P1VN, P2VN, and polystyrene.

Two recent relaxation studies [220, 221] have appeared in the literature dealing with the chain dynamics in poly(amido amine) dendrimers. These macromolecules represent an intriguing new approach to control molecular organization on the colloidal scale unattainable in vesicles or micelles. These compounds are built from an ammonia core via repetitive addition of methyl acrylate and ethylenediamine. End groups are either hydroxyl or amine, the former derived from 2-aminoethanol substituted for ethylenediamine in the final amidation step. Fig. 22 illustrates the structure of a dendritic macromolecule of the third generation. Expansion of the system can be further obtained upon repetition of the growth cycle. Through such a reaction sequence, a highly

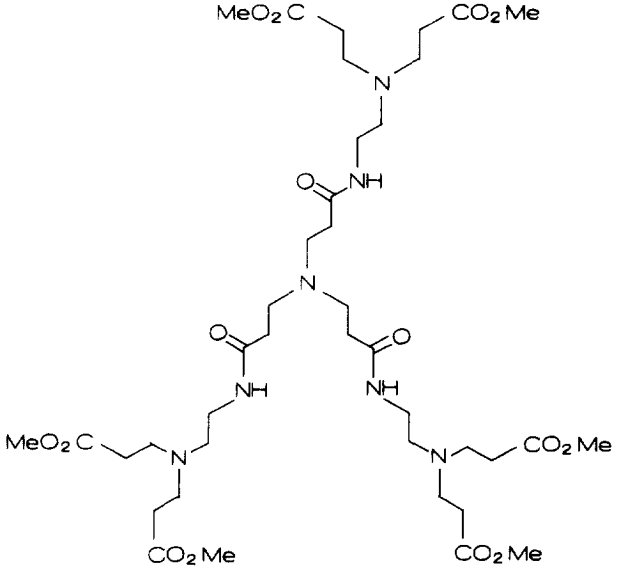

Fig. 22. Poly(amido amine) dendrimers of the third generation. Reprinted with permission from Macromolecules [220], copyright 1992, American Chemical Society.

symmetrical branched condensation polymer can be prepared leading to a construction in which the number of branch points doubles with each successive cycle. The dynamic properties of these systems have been examined with the aid of ^{13}C NMR relaxation measurements in dimethyl sulfoxide-d_6 and D_2O at two magnetic fields. These experiments showed [220] that the chain dynamics are insensitive to any steric crowding that may occur at the molecular surface, but instead support a slowing down of internal chain motions as molecular size increases. Further ^{2}H relaxation measurements [221] in polymers selectively labeled at the chain termini were consistent with results of the ^{13}C relaxation measurements and supported earlier suggestions that the terminal groups in dendrimers of this kind are folding back within the interior of the macromolecule.

^{13}C and ^{15}N dipolar rates of poly(vinylamine) and poly(iminoethylene) were measured as a function of pH in methanesulfonic acid and D_2O solutions [222]. The comparison of ^{15}N and ^{13}C relaxation times of the CH, CH_2 and NH_3^+ substituents in these two polymers allowed a determination of the relative mobility of these groups at various pH values.

A few qualitative ^{13}C relaxation studies have been reported [223–227] in the literature on various copolymers, whereas Monnerie et al. [228] have reviewed the use of the ^{13}C NMR technique to study local motions of liquid crystalline polymers with mesogenic units either in the main-chain, or in the side-chains. Finally, ^{13}C NMR relaxation measurements have been carried out in a few instances [135, 229–234] to examine the influence of the stereochemistry and regioregularity on chain segmental mobility.

4.2 Side-chain motion

The relaxation behavior of carbon nuclei located in side-chains attached to the polymer backbone depends on three general types of motion: (1) the overall rotational diffusion, (2) segmental motion, and (3) internal motion(s) relative to the backbone monomer units. Each of these motions is considered as an independent source of motional modulation of the dipole–dipole interactions, so that the composite TCF can be written as a product of the TCFs associated with each motion. As mentioned in Section 3.1, for sufficiently high molecular weight polymers, the overall rotational diffusion is much slower than the chain local motions. In this case, the overall motion is a negligible contributor to the relaxation of the side-chain carbons, and can be safely ignored when modeling the dynamics of the side-chain.

The presence of a side-chain may influence the dynamics of the polymer backbone, depending on its size and length when long hydrocarbon side-chains are considered. Conversely, backbone segmental motion may affect side-chain motion depending on the molecular structure and stereochemistry. The simple case of internal rotation of a methyl group about its symmetry axis has been frequently studied, as well as the internal motion of aromatic side-groups. However, a major concern of recent NMR relaxation studies is the quantitative description of motions occurring in long hydrocarbon chains attached to the polymer backbone. This interest arises from the fact that hydrocarbon side-chains are an important constituent of many important systems with unusual properties, such as micelles, vesicles, phospholipids, biological membranes, and liquid crystalline polymers.

(i) Methyl groups. Table 9 contains details of quantitative relaxation studies for the methyl internal rotation in various polymers. Analyses of the methyl group motion, in almost all cases, have been performed on the basis of the Woessner's model for rotation by 120° jumps in a symmetrical three-fold potential. The methyl group internal motion in polycarbonates and polyformals has been already discussed in Section 4.1. It should be added that in an earlier publication, Jones and Bisceglia [178] suggested the possibility of coupling between the methyl and the backbone motions in BPA-PC because these two types of motion are characterized by very similar correlation times and activation energies. However, subsequent relaxation measurements [112] for the same polymer as a function of concentration demonstrated that the two motions are uncoupled. In fact, segmental motion decreased with increasing concentration, while methyl internal rotation is very little affected. Similar conclusions have been derived for the methyl internal rotation in BPA-PF [141].

Table 9
Relaxation studies of methyl internal rotation using the three-state jump model

Polymer[a]	Solvent[a]	Nucleus	Frequency (MHz)	Parameters	Conc. (% (w/v))	E_a[b]	Ref.
BPA-PC	TCE-d_2	^{13}C	22.6, 62.9	T_1	10	23	[112]
		^{1}H	90, 250	T_1	20	24	
					30	26	
	$CDCl_3$	^{13}C	22.6	T_1	10	22	[178]
		^{1}H	20, 90	T_1			
BPA-PF	TCE-d_2	^{13}C	22.6, 62.9	T_1	5	23	[177]
		^{1}H	90, 250	T_1			
TMBA-PC	TCE-d_2	^{13}C	22.6, 62.9	T_1	10	23	[6]
		^{1}H	90, 250	T_1			
Cl_2F_4	$CDCl_3$	^{19}F	28.2, 84.6	T_1	10	14	[132]
Cl_4	$CDCl_3$	^{13}C	22.6	T_1	10	19	[132]
		^{1}H	30, 90	T_1			
PIB[c]	CCl_4	^{13}C	25	T_1, NOE	25	18	[184]
PHB	TCE-d_2	^{13}C	50.3, 75.4	T_1, NOE	6	12–14	[133]
	$CDCl_3$	^{13}C	75.4, 100	T_1, NOE	6	11–13	[122]
PDMPO[d]	$CDCl_3$	^{1}H	30	T_1	5–20		[134]
PMPhPO[d]	$CDCl_3$	^{1}H	30	T_1	5–20		[235]
PI[d]	bulk	^{13}C	20.1, 100.6	T_1, NOE			[45]
i-P2HEM	DMSO-d_6	^{13}C	75.5	T_1, NOE	10	19[e](20[d])	[233]
	CD_3OD	^{13}C	75.5	T_1, NOE	10	17[e](20[d])	
s-P2HEM	DMSO-d_6	^{13}C	75.5	T_1, NOE	10	31[e](31[d])	[233]
	CD_3OD	^{13}C	75.5	T_1, NOE	10	31[e](34[d])	

[a] PIB, poly(isobutylene); PHB, poly(β-hydroxybutyrate); PDMPO, poly(2, 6-dimethyl-1,4-phenylene oxide); PMPhPO, poly(2-methyl-6-phenyl-1,4-phenylene oxide); PI, poly(isoprene); i- and s-P2HEM, isotactic and syndiotactic poly(2-hydroxyethyl methacrylate); TCE-d_2, 1,1,2,2-tetrachloroethane-d_2.
[b] In kJ mol^{-1}.
[c] Free stochastic diffusion model.
[d] Fast methyl rotation (see text).
[e] Calculated according to $\log(\chi^2)$ model including methyl internal rotation.
[f] Calculated according to diamond-lattice model including methyl internal rotation.

Methyl internal rotation in the PHB polymer has been studied in two solvents [122, 133]. Despite the large difference in solvent viscosity, the methyl internal motion is characterized by the same activation energy and prefactors in both solvents. This indicates the very local character of this motion. A similar behavior is observed for the methyl internal motion in BPA-PC (Table 8). When correlation times for methyl internal rotation in PHB and polycarbonates or polyformals are compared for the same temperature and solvent, this motion is faster by a factor 3–5 in the former polymer than in the latter. This fact combined with the lower activation energy in PHB than in PCs and PFs suggests a more facile methyl group internal rotation in PHB. This result may be attributed to the greater steric hindrance experienced by the methyl groups in the more complex polycarbonate backbone.

In poly(2,6-dimethyl-1,4-phenylene oxide) (PDMPO) and poly(2-methyl-6-phenyl-1,4-phenylene oxide) (PMPhPO), the rotation of the methyl groups attached to the phenylene moieties was considered [134, 235] to be much faster than segmental motion and phenyl internal rotation. It

appears that this rapid motion serves only to partially average the dipole–dipole interactions within the methyl group, but makes no contribution to relaxation of these polymers. The correlation times associated with methyl internal rotations in these polymers was estimated to be less than 10 ps.

Early reports [3] dealing with the relaxation behavior of poly(isobutylene) in dilute solution concluded that methyl and backbone motions are coupled to some degree. In a later study, Jones et al. [184] showed that on going from dilute solution (5% (w/v) in CCl_4) to bulk PIB, methyl rotation, modeled as a stochastic diffusion process, slows down by a factor of only 1.5, while backbone motion is retarded by a factor of 190. This is direct proof of the local character of methyl rotation in PIB. The calculated activation energy of methyl internal rotation from the relaxation data of a 25% (w/v) PIB solution in CCl_4 is 18 kJ mol^{-1}.

Denault and Prud'homme [45] studied the methyl group rotation in bulk poly(isoprene). The correlation time was found equal to 0.1 ps over the entire temperature range studied, when the JS model was used to describe backbone segmental motion, and 0.3 ps when the log(χ^2) distribution is employed. This is an unusually short value compared with 0.33 ns for the corresponding correlation time reported for bulk PIB [184]. The authors have attributed the short correlation time in PI to the coplanarity of the vinyl backbone group, which lowers the barrier to methyl rotation with respect to saturated backbone structures.

Stereoregularity of synthetic polymers seems to affect the rate of methyl internal rotation. Methyl carbons are characterized by longer ^{13}C T_1 values in meso stereosequences than in syndiotactic sequences [3, 230–233]. For instance, the methyl group of isotactic poly(2-hydroxyethyl methacrylate) (P2HEMA) shows a greater freedom for internal rotation than that of the syndiotactic polymer [233]. The activation energy for methyl internal motion of the isotactic P2HEMA is substantially lower than the corresponding activation energy obtained for the syndiotactic polymer. Since the apparent activation energies of the backbone motion of the isotactic P2HEMA ($\approx$ 20 kJ mol^{-1} in DMSO-d_6 and CD_3OD solvents) are comparable to those of the methyl internal rotation (Table 9), it was concluded [233] that these two motions are coupled. However, one should be very cautious regarding this interpretation, since the data set used in this analysis is limited to one magnetic field. Also, questionable is the fact that the backbone motion of the isotactic P2HEMA is characterized by the same apparent activation energy in two solvents with very different viscosities.

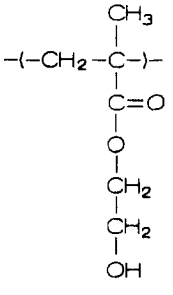

P2HEM

Methyl internal rotation has been investigated for a series of copolymers formed between α-methyl styrene and α,ω-alkyl dihalides of various chain lengths (number of CH_2 units, $n = 0$–10) [234]. The activation energies for the methyl group rotations show a gradual decrease with increasing value of n, reflecting an increased ease of internal motion with increased separation of the styrene moieties. The correlation times for the methyl internal rotation used in the Arrhenius plots were calculated by employing the Woessner formalism.

(ii) Aromatic groups. Phenyl group motion in polystyrene and other structurally similar polymers has been studied extensively by NMR relaxation, since the phenyl group is the simplest aromatic unit that can be attached to the polymer backbone. It is generally agreed now that phenyl group rotation in polystyrene (PS) takes place at a rate similar to or greater than, that of the backbone motion [3, 4]. The nature of phenyl internal rotation is far from free, and can be well described by 180° jumps in a two-fold symmetric potential [137]. Gronski [145] has used a model of restricted rotation in a square-well potential to show that small amplitude restricted motion in the range $40° < \varphi < 60°$ with correlation times of 10^{-9} s can explain the slightly higher T_1 values of the *o*- and *m*-carbons of the phenyl ring relative to that of the *p*-carbon at 63°C in THF.

Laupretre et al. [135] have used ^{13}C T_1 and NOE data at 25.15 MHz to study phenyl rotation in head-to-head (H-H) polystyrene. Analysis of the data with the two-state model [137] showed that phenyl group rotation is much slower in H-H than in head-to-tail (H-T) polystyrene. This observation appears to be reasonable, since in a H-H sequence two phenyl groups are brought closer in space than in the H-T sequence. The H-H structure leads to an increase of steric interactions between neighboring phenyl groups and slows down the rate of phenyl rotation. It would be of interest to carry out additional relaxation measurements at several fields for the H-H polystyrene and to examine the possibility that models for restricted motion can describe the data.

Phenyl internal rotation has been examined in a series of styrene–alkane and α-methyl styrene–alkane copolymers as a function of the length of the alkyl chain [234]. The lower members of both series exhibit a rotational isomeric process with activation energy of about 30–40 kJ mol^{-1}, similar to that reported for poylstyrene homopolymer [142]. Increase in the alkane chain length leads to a decrease in the activation energy for internal rotation. In these polymer systems the similar trends of the activation energies for the methyl group motion (discussed previously) and phenyl group motion with increasing alkane chain length may indicate cooperatively between these two motions. However, a detailed analysis of the individual motions was not performed in this study.

Ghesquiere and Chachaty [34] have studied the dynamic behavior of the pyridyl group in poly(4-vinylpyridine) (P4VP) quaternized by *n*-alkyl bromides of different chain length ($n = 2, 4, 6, 8$, and 10) in methanol solutions by using ^{13}C and ^{1}H relaxation data at 25 MHz, and subsidiary T_1 and NOE measurements at 62.5 MHz. The dynamics of the pyridyl ring was described as random jumps between sites separated by an arbitrary angle ψ. This model [33, 34, 236] has been used in a previous study [237] to interpret the relaxation data of P4VP and P4VPD$^+$. The jump angle, ψ, was found to vary in the range $38° < \psi < 62°$ for all the quaternized polymers over the whole temperature range of 0–100°C. This angle for P4VP ranges between 54° and 74° [34, 237]. It was concluded that the pyridyl internal motion about the C_α–C_4 bond is slightly more restricted in the quaternized form, but unaffected by the degree of quaternization and the chain length of the alkyl bromides. The activation energy of the jump was found equal to ≈ 8 kJ mol^{-1} for all polymers.

Naphthyl internal rotation has been studied [143, 216] in a series of poly(1-naphthylalkyl acrylates) in 1,1,2,2-tetrachloroethane-d_2 using ^{13}C T_1, T_2 and NOE data at three Larmor frequencies over the temperature range 20–120°C. The relaxation times of the C_2, C_3, C_6, and C_7 carbons of the naphthyl moiety on the one hand, and those of the C_4, C_5, and C_8 on the other hand (see chemical structure for numbering system) are very similar for PNA at 20 and 40°C, and for PNMA at 20°C. At higher temperatures, however, the relaxation parameters of the former group of carbons become higher than those of the latter group. For PNEA, the relaxation times of the former group of carbons are higher than those of carbons of the latter group at all temperatures. Moreover, the relaxation parameters in each group are similar within 5–10%, so that an average value of the relaxation parameters has been considered in this analysis.

Several conclusions can be made from these observations. First, the rate of the naphthyl internal motion about the O–C_1 bond for PNA and the CH_2–C_1 bond for PNMA is slow at low temperature and becomes comparable to, or faster than, the rate of the chain segmental motion at higher temperatures. Second, the rate of internal motion of the naphthyl group in PNEA is comparable to, or higher than, the rate of the backbone segmental motion at all temperatures, a fact which is attributed to the additional side-chain flexibility introduced by the presence of a second methylene group. Third, the fast internal motions about the O–C_1 and CH_2–C_1 bonds affect in

a different way the relaxation of the two groups of the aromatic carbons of the naphthyl group, mentioned previously, as a consequence of the different orientations of their C–H internuclear vectors relative to the $O-C_1$ and CH_2-C_1 axes. A C–H vector parallel to $O-C_1$ and CH_2-C_1 axes will be little affected by internal rotation about these axes, whereas internuclear vectors making an angle of about 60° with these axes are expected to be influenced by internal rotation [238].

It should be noted that additional flexibility within the ester group is expected to affect the rate of the side-chain motion. The effectiveness of these additional modes of reorientation is reflected in the relaxation times of the C_4, C_5, and C_8 carbons of PNA at higher temperatures which are longer than those of the CH backbone carbon. Normally, motions within the ester group are not amenable to an effective analysis without sufficient experimental data. Nevertheless, an effective rate of motion of this group has been simulated on the basis of the relaxation data of the para carbon of the PNA naphthyl group, whose relaxation is modulated only by this type of motion in the side-chain [216].

For PNA and PNMA, naphthyl group motion can be described neither as a free rotation, nor as 180° jumps. Therefore, a restricted rotation model [26] was used in this study [216]. This model was able to reproduce, in an excellent manner, the large experimental data set for the three polymers. Fig. 23 illustrates such a fit of the average relaxation parameters for the C_2, C_3, C_6 and C_7 carbons of the naphthyl group for the PNA polymer. Table 10 summarizes the calculated rotational diffusion constants for naphthyl internal rotation, D_{Np}, in the three polymers. As can be seen from this Table the D_{Np} values increase with increasing temperature. At each temperature naphthyl rotation is faster and less restricted in PNMA than in PNA. The amplitudes of restricted rotation, $2\varphi_{Np}$, range between 60 and 100° for PNA and 80 and 140° for PNMA over the temperature range studied. Both these observations support the conclusion that naphthyl rotation is easier in PNMA than in PNA, which can be attributed to the presence of the methylene group in the side-chain for the latter polymer. This means that steric interactions between naphthyl groups and/or between naphthyl groups and the polymer backbone diminish as the naphthyl groups are located further from the main-chain, leading to an easier naphthyl internal motion. However, high activation energies of

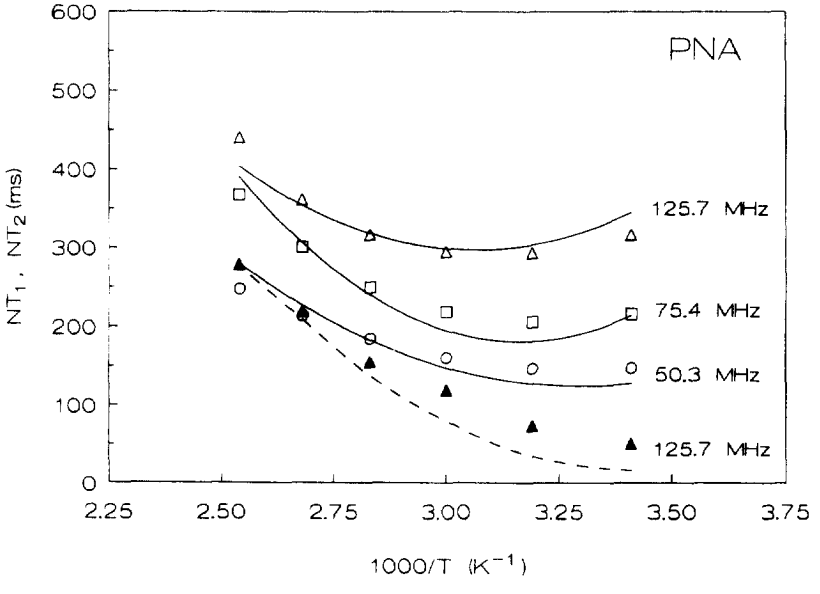

Fig. 23. Experimental average spin–lattice relaxation times (NT_1, open symbols), and spin–spin relaxation times (NT_2, solid symbols) for the C_2, C_3, C_6, and C_7 carbons of the naphthyl group of PNA in 1,1,2,2-tetrachloroethane-d_2 solution as a function of temperature and radiofrequency. Solid and dashed lines represent the best fit values calculated by using the restricted multiple internal rotations model [216].

Table 10
Simulation parameters of the restricted multiple internal rotation model used to describe side-chain (methylene and naphthyl groups) motions of PNA, PNMA, and PNEA in 1,1,2,2-tetrachloroethane-d_2 [216]

Temp. (°C)	PNA		PNMA				PNEA					
	D_{Np}[a,b]	φ_{Np}[c,d]	D_1[a,b]	φ_1[c,d]	D_{Np}	φ_{Np}	D_1	φ_1	D_2[a,b]	φ_2[c,d]	D_{Np}	φ_{Np}
20			5.66	53	0.19	43	5.66	57	1.83	40		
40	0.20	33	7.28	55	0.48	38	7.72	63	2.46	47	0.14	133
60	0.45	36	9.78	52	1.27	56	11.38	69	3.27	56	0.15	129
80	1.00	43	12.20	62	2.33	62	16.69	77	4.43	62	0.21	129
100	1.63	50	16.22	75	3.25	69	18.27	88	6.22	66	0.33	130
120	2.78	51	21.60	75	5.52	70	22.33	128	6.63	69	0.38	137
E_a ($kJ\,mol^{-1}$)	34		13		32		14		13		15	
D_∞ (10^{12} s)	88		0.98		114		1.67		0.38		0.033	
r	0.998		0.995		0.994		0.992		0.994		0.968	

[a] $D_i \times 10^9\ s^{-1}$.
[b] D_{Np}, D_1, and D_2 are the rotational diffusion constants describing restricted internal rotations for the side-chain naphthyl and methylene groups, respectively.
[c] In degrees.
[d] φ_{Np}, φ_1, and φ_2 represent the amplitudes of the restricted rotation of the side-chain naphthyl and methylene groups, respectively.

naphthyl group rotation were calculated for both polymers, ≈ 33 kJ mol^{-1} (Table 10). A slightly different picture emerged for the dynamics of the naphthyl in PNEA. Table 10 shows that the angular amplitude of the naphthyl motion is nearly constant at 260–280° over the whole temperature range studied. Moreover, naphthyl rotation is found to be slower in PNEA than in the other two polymers with a smaller activation energy of 15 kJ mol^{-1}. In summary, it is concluded that the progressive removal of the naphthyl group from the polymer backbone by the introduction of methylene groups in the side-chain relieves steric interactions leading to easier naphthyl internal rotation. A thorough discussion of the photophysical behavior of these polymer systems in relation to the their local dynamics and stereochemistry can be found in Ref. [216].

Naphthyl internal motion in PNMA has also been studied in two other solvents, $CDCl_3$ and pentachloroethane, using ^{13}C T_1, T_2 and NOE data at two Larmor frequencies [239] in an attempt to examine solvent effects on the local chain motions of this type of polymer. Results of this study will be discussed in a subsequent section.

(iii) Longer aliphatic groups. In 1978 Levy et al. [27] carried out a detailed investigation of backbone and side-chain motions in poly(butyl methacrylate) (PBMA) and poly(hexyl methacrylate) (PHMA) in 50% (w/v) solutions in toluene using ^{13}C T_1 and NOE measurements at two magnetic fields. The T_1 and NOE values of all the side-chain carbons, including the terminal methyl carbon, are frequency-dependent. The authors developed a composite spectral density function by combining the spectral density of the $\log(\chi^2)$ distribution model for the backbone motion and that of successive free multiple internal rotations in order to fit the relaxation data of the side-chain carbons. Although they did not succeed in fitting the relaxation data, they claimed in qualitative terms that the presence of a distribution of correlation times for the backbone motion is necessary to account for the frequency-dependent T_1 and NOE values of the side-chain carbons of PBMA and PHMA. Nevertheless, this conclusion proved to be unrealistic, as recently shown by Spyros and Dais [26], mainly due to the fact that the composite spectral density function used by Levy et al. [27] was apparently in error. Spyros and Dais [26] derived the correct form of $J(\omega)$, and showed that a distribution of correlation times for backbone motion does not necessarily affect the relaxation parameters of the side-chain carbons as suggested earlier [27]. It was found that the frequency-dependent T_1 and NOE values can be predicted only if the dynamics of the side-chain was described in terms of multiple internal rotations of limited amplitude. They re-examined the data of PBMA and PHMA, and found that the frequency-dependent relaxation parameters can be well reproduced by using a model combining the HWH TCF and that of the restricted multiple internal rotations in the side chain [26] (Eqs. (54), (56a), and (56b)). The use of a $\log(\chi^2)$ distribution of correlation times for the backbone motion gives the same good quality of the fit. This indicates that the side-chain relaxation is mainly affected by internal motions and is relatively insensitive to the model used to describe backbone motion. Wittebort et al. [149] came to the same conclusion by studying the dynamics of the side-chain of poly-L-lysine.

The restricted rotation model has been applied to describe the mobility of the *n*-pentyl side-chain of bulk PHO [8]. The measured ^{13}C T_1 and NOE data for all the *n*-pentyl chain carbons show a strong frequency dependence. Therefore, analysis of the relaxation data by using free internal diffusion about the C–C bonds was unsuccessful as expected. In contrast, the model of restricted rotations reproduces all the experimental data for all the side-chain carbons. The diffusion constants, D_i, and the amplitude of the restricted rotation increase progressively toward the free end of the side-chain in accordance with theory. Activation energies for the restricted C–C rotations are rather similar along the side-chain (Table 7).

Side-chain motion has been examined for PNMA and PNEA polymers [216]. In PNMA a single methylene group connects the carboxyl group with the naphthyl moiety, whereas in PNEA two methylene groups serve this purpose. The diffusion constants, D_1, for rotation about the O–CH_2 bond in PNMA and PNEA were found to be very similar and they increase with increasing temperature (Table 10). The diffusion constant, D_2, for rotation about the CH_2–CH_2 bond in PNEA is 3–4 times smaller than D_1 for the same polymer, indicating a slower motion about the CH_2–CH_2 bond than about the O–CH_2 bond. However, the calculated activation energies for rotations about

these bonds are the same (13 kJ mol^{-1}) for both rotations. A plausible explanation of this observation is based on the fact that the bulky naphthyl moiety, which anchors the other end of the side-chain, hinders the internal motion of the adjacent methylene group. This effect is also reflected in the smaller angular amplitude, $2\varphi_2$, for restricted rotation about the CH_2–CH_2 bond in PNEA relative to $2\varphi_1$ for restricted rotation about the O–C_t bond.

Local segmental motions, including side-chain methylene motions, of PNMA have been investigated in $CDCl_3$ and pentachloroethane solutions [239]. Side-chain methylene motions are of restricted amplitude in both solvents and have similar activation energies to those observed in tetrachloroethane. Thus, it can be concluded that the main reason for the methylene groups undergoing restricted internal rotation is the non-bonded steric interactions and not solvent viscosity effects. Solvent effects on PNMA dynamics will be discussed in detail in Section 4.3.

Other authors have used jump models to study the mobility of hydrocarbon side-chains attached to polymer backbones [34, 240, 241].

Ghesquiere and Chachaty [34] studied the mobility of the side-chain of poly(4-vinylpyridine) quaternized by *n*-alkyl bromides of various chain lengths. In particular, the frequency-dependent relaxation data of the side-chain carbons of poly(4-vinyl-*N*-*n*-butyl pyridinium bromide) have been analyzed by using a model describing the *n*-butyl side-chain motion in terms of jumps between three sites corresponding to the t, g, and g′ conformers, with t conformer non-equivalent to g and g′ [33, 236]. The data were consistently reproduced with $W(g \rightarrow g') < W(t \rightarrow g(\text{or } g')) < 0.5W(g(\text{or } g') \rightarrow t)$, W being the rate governing conformational jumps. This analysis for longer side-chains was prohibited due to the enormous computational time required for these calculations. For the *n*-octyl side-chain, free rotational diffusion about the first six C–C bonds can successfully reproduce the T_1 data at 25 MHz, but not the data at 63 MHz [34].

The previous jump model has been used to interpret the ^1H and ^{13}C relaxation data of the side-chain of poly(L-glutamic acid) [240] (PLGA) and poly(N^5-(3-hydroxypropyl)-L-glutamine) [241] (PHPG) in aqueous solutions. Internal rotations about the side-chain C_α–C_β and C_β–C_γ

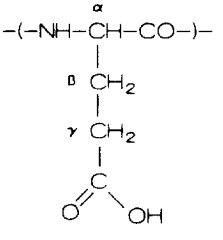

PLGA

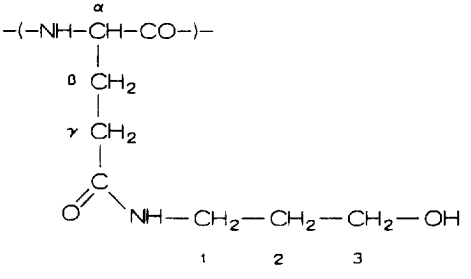

PHPG

bonds in PHPG were described by the jump model, whereas this model is applicable only for the first C_α–C_β bond rotation in PLGA. The second rotation about the C_β–C_γ bond shows a larger degree of freedom consistent with an overall isotropic motion. Also, larger reorientational freedom about the C_β–C_γ bond of PLGA in its α-helical form was detected by Hahn et al. [242] analyzing their ^{13}C T_1 and T_2 data at 67.9 MHz by the jump model. Furthermore, the internal motion of the C_β methylene group of the helical PLGA was described by a jump model between two allowed rotameric states. Steric considerations indicated that the occupation of a third rotameric position, as in the original jump model, is forbidden [242].

The data concerning the hydroxypropyl segment of PHPG are consistent with a free rotational diffusion about the N–C_1 bond. The two other methylene groups of this segment undergo random jumps among three nearly equivalent states [241]. The larger reorientational freedom about C_1–C_2 and C_2–C_3 compared with that about the C_α–C_β and C_β–C_γ bonds observed for PHPG indicates that the amide group in the side-chain effectively decouples the motion of the glutamyl and hydroxypropyl segments.

The "free model" approach developed by Lipari and Szabo [105] has been used by several authors [118, 243, 244] to analyze the relaxation data of side-chain carbons. Lipari and Szabo [105, 154] themselves have applied this method to the relaxation data of several synthetic and biological macromolecules published earlier in the literature. They claim that their approach yields virtually the same information for the side-chain internal motions as that obtained by using more complex models. On the basis of their generalized order parameter, S^2, obtained by fitting the experimental data to Eq. (57), they were able to eliminate models that did not reproduce the S^2 values.

4.3 Solvent effects on polymer local dynamics

As noted earlier in this article, studies of local chain dynamics in dilute solutions provide the opportunity to understand local motions for isolated chains, avoiding complications introduced by interchain interactions in more concentrated solutions or in the bulk. However, the solvent is expected to influence local chain dynamics in dilute solution and this will be reflected in the measured relaxation parameters. Understanding solvent effects is important in order to explore the relationship between polymer chemical structure, intramolecular barriers, and chain dynamics. In most cases, the solvent has been considered as a structureless, viscous continuum and its effect on polymer dynamics has been described in terms of two properties: solvent viscosity and solvent power.

4.3.1 Solvent viscosity

Rates of conformational transitions in viscous media can be treated by the approach introduced by Kramers [96], who studied the effects of solvent frictional forces on the rates of chemical reactions by modeling the reactive motion as the passage of a solute particle over a potential barrier. In this theory, which is based on the ordinary Langevin equation, the solvent is treated as a random frictional force opposing the passage across the barrier. Correlations in space and time of the solvent forces acting on the solute particle are neglected.

Kramers' theory with hydrodynamic friction has been tested extensively in the past decade in many photochemical isomerization reactions in solution, in an attempt to rationalize the viscosity dependence of the observed rate constants [245–247]. Also, Helfand has applied this theory to the case of conformational transitions of polymers [66]. Making the assumption that the correlation time for conformational transitions is inversely proportional to the rate constant for isomerization, the temperature and viscosity dependence of the correlation time is predicted by Kramer's theory to be [22, 96]

$$\tau_c = A\eta e^{(E^*/RT)} \tag{60}$$

The prefactor A is a viscosity-independent constant, E^* is the barrier height defined for conformational transitions, and η is the solvent viscosity. Eq. (60) predicts a linear dependence of $\log \tau$ on $\log \eta$ at a given temperature with slope equal to one.

The temperature dependence of the solvent viscosity is often described by an Arrhenius form

$$\eta = \eta_0 e^{(E_\eta/RT)} \tag{61}$$

then, Eq. (60) becomes

$$\tau_c = A' e^{[(E^* + E_\eta)/RT]} \tag{62}$$

where A' is a constant. The sum of the barrier height for conformational transitions and the activation energy of the viscous flow equals the experimental (apparent) activation energy obtained from a plot of $\ln \tau_c$ vs. $1/T$, i.e.

$$E_a = E^* + E_\eta \tag{63}$$

Any deviation from linearity in the plot of $\log \tau_c$ vs. $\log \eta$, which may be observed at high viscosities, indicates that the Kramers' expressions (60) and (63) are insufficient to describe the experimental relaxation rates. The failure of Kramers' theory has been attributed [245–248] to the breakdown of its major hypothesis that solvent–polymer collisions are uncorrelated in space and time, at the high friction limit. When the motion near the top of the barrier takes place on a very short time-scale (picoseconds or sub-picoseconds), collisions may be significantly correlated, and the time-scales for polymer and solvent motion are not cleanly separated. As a result of the curvature observed in the $\log \tau_c$ vs. $\log \eta$ plot, the experimental correlation times at high viscosities are consistently lower than those predicted by Kramers' theory. Glowinowski et al. [22] suggested the following empirical equation to describe viscosity effects on local segmental dynamics of polyisoprene in dilute solutions

$$\tau_c = A' \eta^\alpha e^{(E^*/RT)} \tag{64}$$

This equation has been used by Fleming and co-workers [245, 246] to describe the power law relationship observed between the isomerization rate constant and viscosity. The exponent α takes values in the range $1 > \alpha > 0.1$. For $\alpha = 1$, Eqs. (60) and (64) become identical. Also, Eq. (63) in the high friction limit becomes

$$E_a = E^* + \alpha E_\eta \tag{65}$$

Fig. 24(A) shows a plot of $\log \tau_1/\eta^{1.0}$ vs. $1/T$ for the PNMA polymer in three solvents. The τ_1 values are obtained by fitting the relaxation data of the backbone carbons by employing the DLM model [239] (see Section 4.1). The fact that a universal curve is obtained in all solvents supports the validity of Kramers' theory in describing the present experimental data without invoking frequency-dependent friction [22, 245–248]. This implies that the observed activation energy is equal to the sum of the internal barrier and the viscosity activation energy (Eq. (63)), and that the barrier height, E^*, is independent of viscosity. This value obtained from the best fit slope through the points of the plot in Fig. 24(A), is 11.3 kJ mol^{-1}. This value is comparable to the barrier (10–12 kJ mol^{-1}) separating the trans and gauche states, indicating that the nature of conformational transitions occurring in the PNMA chain can be described by the type 2* motion according to Helfand's terminology [66].

An analogous plot to that in Fig. 24(A) for the correlation time $\tau_{np}(=1/6D_{np})$ of naphthyl internal rotation is shown [239] in Fig. 24(B). The fact that a universal curve is obtained when τ_{np} is scaled by $\eta^{1.0}$ indicates that the data indeed follow Eq. (60), reflecting Kramers' theory. The best fit slope of the straight line ($r = 0.96$) of Fig. 24(B) yields an activation energy, $E^*_{np} = 21$ kJ mol^{-1}. This barrier to naphthyl internal rotation about the CH_2–C_1 bond is within the range of 20–25 kJ mol^{-1} obtained in several photochemical isomerization reactions in solution [245–247]. However, Kramers' theory appears to fail for the internal motion of the side-chain methylene group [239]. The data in Fig. 24(C), i.e. correlation times for CH_2 in a format suggested by Eq. (64), conform with a universal curve when the correlation time is scaled by $\eta^{0.55}$. The best fit slope obtained through the points yields $E^* = 5.5$ kJ mol^{-1} for the internal motion of the side-chain CH_2 group. This value is consistent with the theoretical value of ≈ 5 kJ mol^{-1} calculated for the barrier of the O–CH_2 bond of poly(alkyl methacrylate)s and poly(methyl acrylate) [249, 250].

One might be tempted to explain this result on the basis of the small size of the CH_2 moiety, and the theory [248] that allows frequency-dependent solvent friction. Indeed, the exponent α depends on the moment of inertia, the size of the isomerizing unit, and the curvature of the potential energy surface at the top of the barrier [22, 245–247]. Smaller size of the rotating unit, a smaller moment of inertia, and a high barrier all lead to an exponent, α, smaller than unity. Nevertheless, the present estimated barrier E^* ($= 5.5\ kJ\ mol^{-1}$) for the methylene restricted internal rotation is only twice as large as that corresponding to kT ($2.5\ kJ\ mol^{-1}$ at $T = 298\ K$). In this case, the breakdown of Kramers' theory cannot be attributed to details of solvent–solute coupling, but to the fact that inertial effects may predominate over the internal rotation of the side-chain methylene carbon [251].

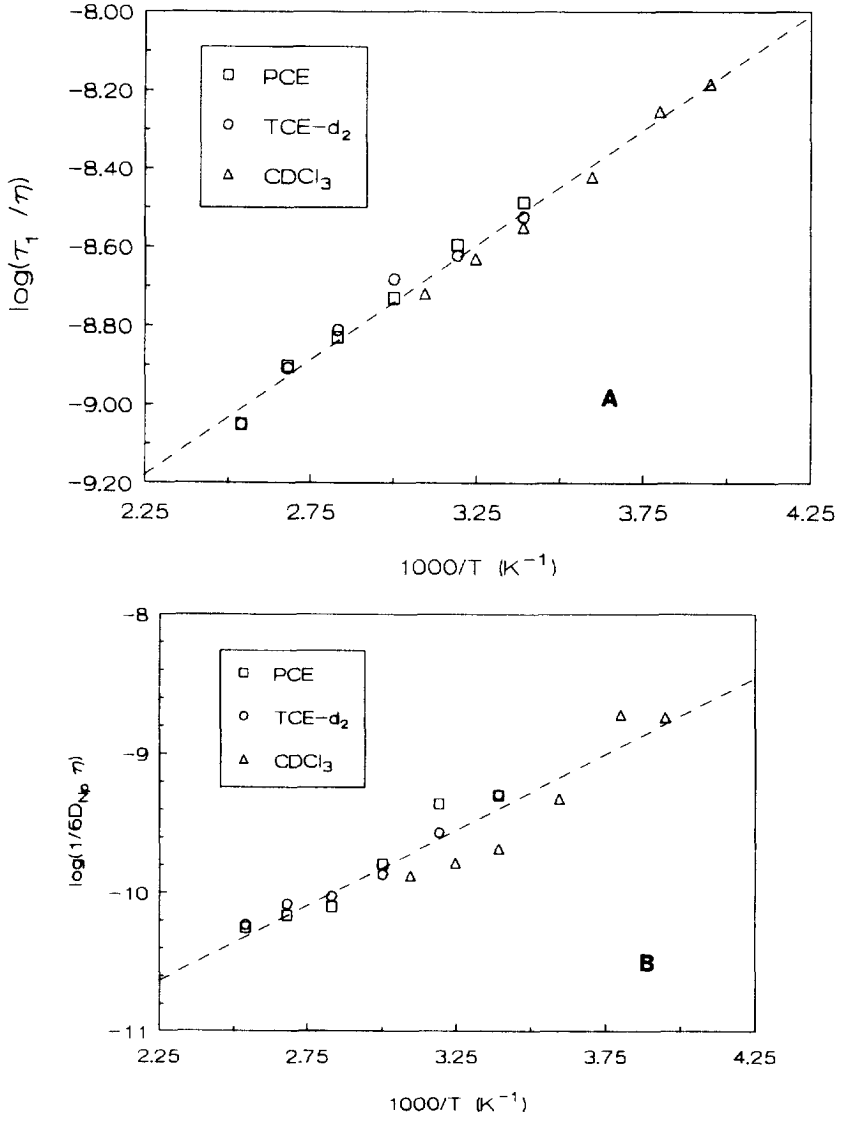

Fig. 24. Temperature dependence of: (A) the reduced correlation time (τ_1/η) for chain segmental motion; (B) ($\tau_{np}/\eta = 1/6D_{np}\eta$) for naphthyl internal rotation; (C) ($\tau/\eta^{0.55} = 1/6D_1\eta^{0.55}$) for the side-chain methylene internal rotation of PNMA [239].

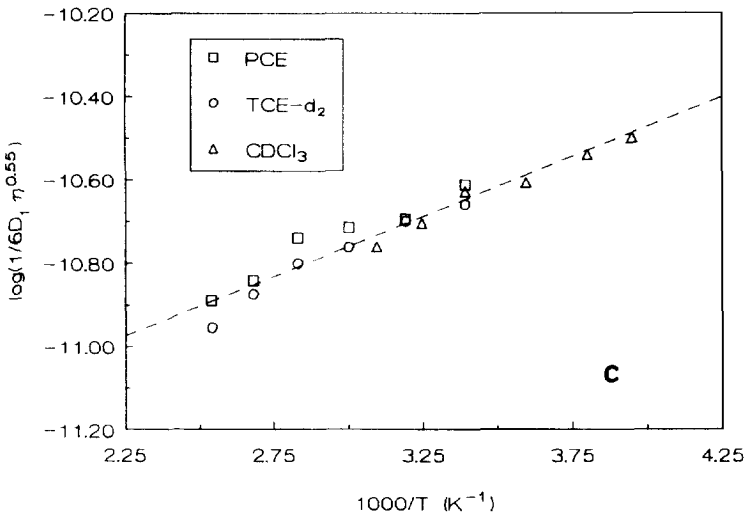

Fig. 24. (continued)

Several other studies examined the viscosity dependence of local chain motions in solution by using various experimental techniques. Liu and Anderson [252] have measured ^1H T_1 for PEO at a single temperature in a series of hydrogenated solvents covering a viscosity range of ≈ 7 cP. They concluded that chain segmental motion is predominantly influenced by the local viscosity, which in turn is related to the solvent viscosity. Lang et al. [253] have reached a similar conclusion for PEO on the basis of their ^{13}C T_1 data in a series of 12 solvents. They tried to analyze their data by using the Magee theory [254], which assumes a non-linear relationship between the correlation time of the solute and the macroscopic solvent viscosity. Glowinowski et al. [22] plotted the data of Liu and Anderson according to the format suggested by Eq. (64) leading to a straight line with $\alpha = 0.69$. The same authors [22] studied the viscosity-dependence of PI chain segmental motion by employing ^{13}C NMR relaxation measurements in ten solvents covering a factor of 70 in viscosity. Contrary to predictions of Kramers' theory, it was found that correlation times, τ_c, extracted from T_1 data follow a non-linear dependence on solvent viscosity ($\tau_c \propto \eta^{0.41}$). The potential barrier height for local conformational transitions, E^*, extracted from these measurements is 13 ± 2 kJ mol^{-1}. An apparent power law dependence, $\tau_c \propto \eta^{\alpha}$, has also been observed in optical experiments on anthracene-labeled PI in nine solvents [255]. However, the dynamics measured by optical experiments scales as $\eta^{0.75}$ as opposed to the $\eta^{0.41}$ dependence observed in NMR experiments. Also, the activation energy obtained in the optical experiments is somewhat lower, $E^* = 11$ kJ mol^{-1} than that (13 kJ mol^{-1}) obtained in NMR. These differences have been discussed in terms of the Grote and Hynes theory [248] of frequency-dependent friction and the presence of the anthracene label in the optical experiments.

Viscosity-dependence of polystyrene dynamics has been studied only by optical methods on anthracene-labeled polystyrene [256, 257]. in a variety of solvents. Waldow et al. [257] found that the correlation time is proportional to $\eta^{0.90}$ at constant temperature, in a reasonable agreement with the $\eta^{1.00}$ prediction of the Kramers' equation. This behavior has been attributed to the large size of the phenyl side groups, and the size of the label itself.

From these examples, it can be concluded that Kramers' theory, in the high friction limit, is likely to be valid in cases where the polymer dynamics occur in a sufficiently long length-scale and sufficiently slow time-scale. In this limit, the detailed structure and dynamics of solvent molecules are not important factors, and the Brownian motion description of polymer dynamics becomes rigorously correct [96]. This is what was really observed for the slow segmental motion of polystyrene and poly(1-naphthylmethyl acrylate) bearing sizeable side-chain groups. However, for rapid local

chain motions with time-scales and/or length-scales comparable to those of the solvent molecule, deviation from a linear-dependence of τ_c on viscosity occurs. The latter behavior is usually observed for polymers that do not contain bulky side-groups (perhaps, an exception to this pattern is PMMA [258] which has been discussed in Ref. [257]).

An important consequence of these results is that potential energy barriers to chain conformational transitions calculated by means of Eq. (63) may be seriously in error, when the functional form of the τ_c dependence with solvent viscosity is represented by Eq. (60), but not by Eq. (64). This in turn may lead to erroneous conclusions about the mechanism of the chain segmental motion. It is expected that none of the above conclusions about the role of solvent viscosity in chain segmental motion is appropriate for polymer/solvent systems, where specific solute/solvent interactions, or hydrogen bonding are important [22, 59].

4.3.2 Solvent thermodynamic quality

Another solvent parameter that is known to play a small role in determining the time-scale and activation energy for local conformational transitions is the solvent thermodynamic quality. Optical [59, 257, 259] and NMR [22, 123] studies have generally found that, after considering the solvent viscosity, dynamics in solvents of low thermodynamic quality (poor solvents) are slower by a factor of less than two than dynamics in solvents of high thermodynamic power (good solvents). Also, the activation energy for conformational transitions is higher for poor solvents than for good solvents. This effect is considered to be steric in nature, and it is attributed to the higher local segment concentration in poor solvents due to chain contraction in these solvents, leading to smaller overall chain dimensions [59, 257, 259]. Thus, the presence of nearby segments may interfere with a conformational transition that would otherwise be possible [259]. Solvent thermodynamic quality was invoked to explain differences in the time-scales and activation energies observed for the segmental motions of PVC in 1,1,2,2-tetrachloroethane-d_2 and dibutyl phthalate solvents [123], whereas this solvent plays a minor role in the local chain dynamics of PNMA [239]. For PVC, however, further studies in other non-polar solvents are required to obtain a more accurate picture of solvent effects on the dynamics of this polymer, and to calculate the barrier height of chain segmental motions, following the general equation (64).

4.4 Frequency–temperature superposition

Recently Guillermo et al. [260] showed that the spin–lattice relaxation rates and the NOE factors measured by NMR obey a homogeneity property, with respect to the reduced variable ω_0/ν_r, where ω_0 is the Larmor frequency and ν_r is a relaxation frequency of segmental motions. This procedure assumes that all relaxation frequencies that may be involved in segmental motions are proportional to a single basic relaxation frequency ν_r. Thus, the successful superposition of T_1 data measured at different Larmor frequencies proves that all the time constants that enter into an explicit expression for the TCF of the system under study have the temperature dependence of a characteristic time constant $\tau_c(T) = 1/\nu_r$. These authors showed [260] that the principle of frequency–temperature superposition can be successfully applied to ^1H and ^{13}C T_1 and NOE data of molten PBD at various Larmor frequencies. A single master curve was obtained by plotting ω_0/T_1 vs. $\log[\omega_0\tau_c(T)]$, where $\tau_c(T)$ is the correlation time for segmental motion of PBD.

Other authors [8, 21, 239] have applied this principle to their multi-field data in somewhat different format, i.e. plotting T_1/ω_0 vs. $\log[\omega_0\tau_c(T)]$. These plots have the familiar shape of a simple T_1 vs. $1/T$ graph. The successful superposition of T_1 data in plots of this type proves that the TCF used to study local dynamics has a shape independent of temperature, and indicates that the calculated temperature-dependence of $\tau_c(T)$ is correct. Gisser et al. [21] successfully applied the frequency–temperature superposition principle to the ^{13}C T_1 data of PI in toluene at three Larmor frequencies. Dais and co-workers [8, 26, 216] have successfully applied this principle to analyze the ^{13}C T_1 data of poly(butyl methacrylate), poly(hexyl methacrylate), poly(β-hydroxyoctanoate), poly(1-naphthyl acrylate) and poly[2-(1-naphthyl)ethyl acrylate]. The same authors [239] have

applied the frequency–temperature superposition principle to the ^{13}C T_1 data of the backbone methine carbon of poly(1-naphthylmethyl acrylate) in three different solvents. T_1 data obtained at two Larmor frequencies, and over a wide temperature range could be superimposed on a universal relaxation curve, as illustrated in Fig. 25. This was possible because the DLM τ_1 correlation times were linearly dependent on viscosity following Kramers' theory, so that frequency–temperature and solvent-viscosity superposition was achieved in this plot.

4.5 Williams–Landel–Ferry (WLF) behavior of bulk polymers

An important question regarding the motions responsible for the chain segmental dynamics of amorphous or semi-crystalline polymers detected by NMR relaxation above the glass transition temperature (T_g) is whether these motions are related to the elementary processes involved in the glass–rubber transition, or other secondary transitions. A way to approach this question is to compare the observed temperature-dependence of the NMR correlation time, $\tau_c(T)$, with the expectation derived from the temperature–correlation time relationship of the glass–rubber transition for the polymer under study. The glass–rubber transition processes in polymers obey the well-known WLF equation [171]

$$\log \frac{\tau_c(T)}{\tau_c(T_{ref})} = \frac{C_1^g(T - T_{ref})}{C_2^g(T - T_{ref})} \tag{66}$$

This equation gives the ratio of the correlation time at a temperature T to that at an arbitrary reference temperature T_{ref}, which is usually identified with T_g. Alternative definitions of the reference temperature for the NMR and optical experiments are given in Ref. [125]. C_1^g and C_2^g are coefficients characteristic of a given polymer. These coefficients were initially thought to be universal constants, but they have subsequently been found to vary among different polymers in the range 11–17 for C_1^g and 40–70 for C_2^g [261]. Poly(isobutylene) is a noticeable exception with abnormally high value of C_2^g (= 104) [262]. C_1^g and C_2^g can be obtained from NMR or optical data by plotting

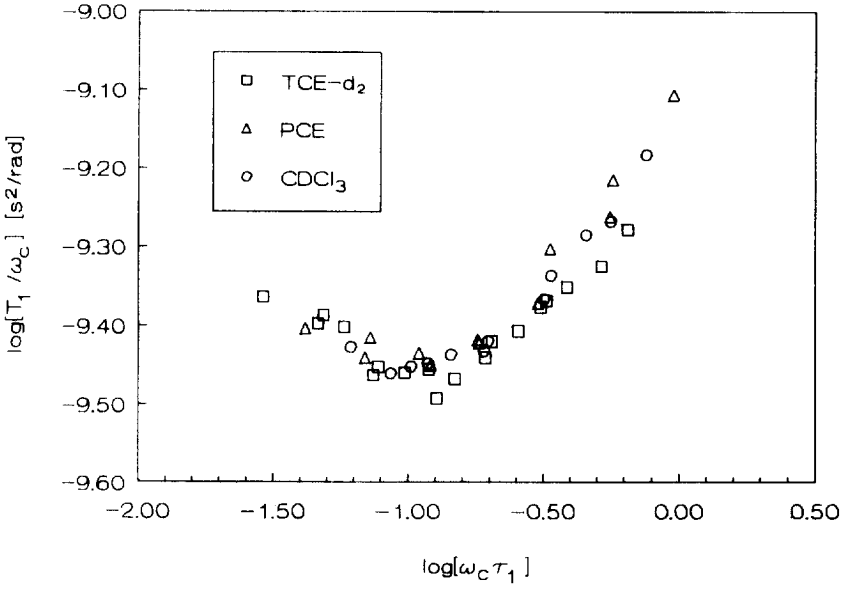

Fig. 25. Frequency-temperature superposition of ^{13}C NMR NT_1 values for the backbone methine carbon of PNMA in pentachloroethane (PCE), TCE-d_2, and $CDCl_3$ solutions. τ_1 values are the correlation times obtained from the analysis of the relaxation data by using the DLM model [239].

the quantity $(T - T_g)$ against $(T - T_g)/\log \tau_c(T)$. A typical plot is shown in Fig. 26 for five amorphous polymers [10]. The correlation times, $\tau(T)$ used in this plot, were obtained by analyzing the ^{13}C relaxation data of these polymers with the $\log(\chi^2)$ distribution function [10]. The appropriate coefficients are obtained from the slopes and intercepts of the straight lines in Fig. 26. An alternative way of obtaining C_1^g and C_2^g constants is to use a slightly modified version of the WLF equation involving the Vogel temperature [125, 261] $T_\infty = T_g - C_2^g$, i.e.

$$\log \frac{\tau_c(T)}{\tau_c(T_g)} = C_1^g + \frac{C_1^g C_2^g}{(T - T_\infty)} \tag{67}$$

Table 11 lists the C_1^g and C_2^g values for several amorphous polymers determined from NMR [10, 193] or optical [125] experiments using Eqs. (66) or (67). Also, Table 11 summarizes values of these coefficients obtained from dynamic mechanical or dielectric relaxation measurements [262, 263] as well the T_g values [10, 125, 193] for each polymer. The coefficients C_1^g and C_2^g extracted from the linear plots are in good agreement with the respective values predicted from dynamic mechanical and dielectric relaxation. This implies that the segmental motion of the amorphous polymers sensed by NMR and optical experiments belong to processes involved in the glass–rubber transition phenomenon. Furthermore, the abnormally high value of C_2^g for PIB is confirmed by NMR, although agreement between the NMR value and that of dynamic mechanical relaxation is not achieved.

Also, Table 11 summarizes the C_1^g and C_2^g coefficients for several semi-crystalline polymers obtained from NMR relaxation studies [8, 10]. The C_1^g values are found to be in the same range as those of the completely amorphous polymers, whereas lower values are calculated for the C_2^g coefficients. Unfortunately, no dynamic mechanical or dielectric relaxation data are available in the literature for these semi-crystalline polymers to make appropriate comparisons.

Laupretre et al. [125] have compared the WLF behavior of several amorphous polymers and copolymers using their NMR and excimer fluorescence data. Both techniques agreed that the segmental motions detected well above the glass transition temperature are responsible for processes occurring at T_g, although plots obtained through Eq. (67) using the NMR and optical data are not identical. This behavior is illustrated in Fig. 27, where the NMR correlation times, τ_1 (obtained from

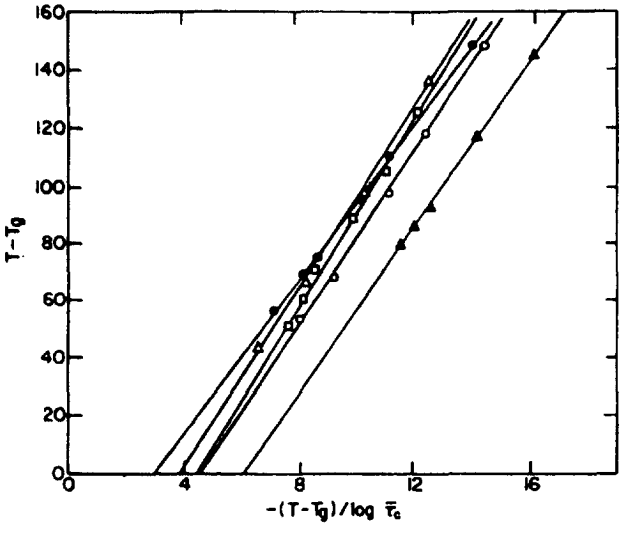

Fig. 26. WLF behavior of typical amorphous polymers: ●, ethylene–butene copolymer (26 mol% butene); ▲, polyisobutylene; ■, atactic polypropylene; ○, *cis*-polyisoprene; △, *cis*-polybutadiene. Reprinted with permission from J. Polym. Sci. Polym. Phys. Ed. [10], copyright 1985, John Wiley & Sons Inc.

Table 11
WLF parameters of amorphous and semi-crystalline polymers

Polymer	T_g(K)[b]	Literature[a]		^{13}C NMR[b]	
		C_1^g	C_2^g	C_1^g	C_2^g
Amorphous polymers					
Ethylene–propylene (63 mol% propylene)	226	13.1	40.7	15.4	67.7
cis-Poly(isoprene)	203	16.8	53.6	15.0	68.7
Poly(isobutylene)	203	16.6	104.4	14.1	91.5
Atactic poly(propylene)	253			15.2	60.7
Ethylene–butene (26 mol% butene)	193			13.5	40.6
Poly(vinyl acetate)	305	15.6	46.8	15.1	62.0
Poly(isopropyl acrylate)	262			12.2	53.6
cis-Poly(butadiene)	171	11.3	60	15.1	54.3
Poly(β-hydroxybutyrate)	230			12	51
Poly(propylene oxide)	200	16.2	24	428[c]	
Semi-crystalline polymers					
Linear poly(ethylene)	173			12.5	34.3
Poly(ethylene oxide)	206			12.5	26.3
Poly(trimethylene oxide)	209			11.8	14.7
trans-Poly(isoprene)	215			12.5	26.3
Poly(β-hydroxyoctanoate)	− 36			10.8	26.3
Poly(vinyl methyl ether)	243	11.5	58.6		

[a] From mechanical or dielectric relaxation [261].
[b] From Refs. [8], [10], [125] and [193].
[c] The product $C_1^g C_2^g$ is given.

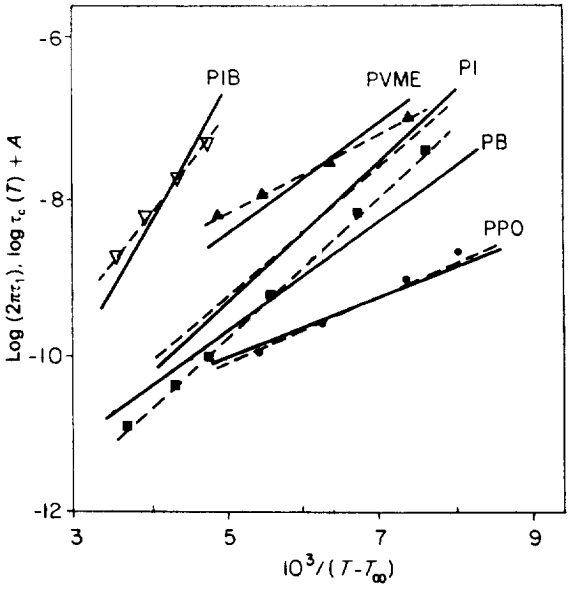

Fig. 27. Dependences of the correlation times, ——, τ_c obtained from optical experiments, and - - -, τ_1 obtained from ^{13}C NMR T_1 experiments as a function of $10^3/(T - T_\infty)$ according to Eq. (67). Reprinted with permission from Polymer [125], copyright 1993, Butterworth–Heinemann Ltd.

the DLM model), and the correlation time, τ_c, from the optical experiments are plotted as a function of $(T - T_\infty)$. The agreement between the two sets of data is very good for PPO and PI, but not so good for the other polymers. This discrepancy has been attributed to the fact that NMR measurements were carried out in a frequency domain where both glass transition and secondary relaxation phenomena merge [125].

The glass transition temperature is frequently used to compare various properties of polymeric materials, such as viscoelasticity, rheology, chain relaxation, etc. Therefore, it would be interesting to examine whether different polymers, which are characterized by nearly the same T_g, have the same segmental dynamics. From Fig. 27, it is apparent that a very large difference (more than 2 decades) exists in the correlation times for segmental motion of the various polymers, whereas their corresponding T_g values span a range of about 40°C (Table 11). For instance, PI and PIB have essentially identical T_g, but segmental motion is much faster in PI than in PIB. Nevertheless, this physical picture may be misleading, as pointed out by Monnerie and coworkers [124, 125] and chain segmental dynamics may not be so different among the various polymer systems sharing similar T_g values. These authors, defining a reference state in which all the polymer systems are in equivalent states concerning their local dynamics, showed [125] that, in this common reference state, the monomer friction coefficient of the various polymers was identical, leading to similar values of their correlation times for segmental motions. Such a conclusion is very important for it means that properties of polymers related to segmental motion have to be rescaled in terms of the friction coefficient instead of T_g or T_∞.

5. Conclusions and general remarks

The numerous NMR relaxation experiments and theoretical developments reported in this article show that the investigation of the complicated problems involving local dynamics of synthetic polymers has progressed significantly in the past 15 years. It appears that conformational transitions of the backbone bonds and librational motions of the backbone C–H vectors occurring on different time-scales are important motional contributors to the relaxation behavior of many polymer systems in solution and in the bulk. Librational processes of limited amplitudes (15–30°) are considered to be very localized, independent of the influence of the chain surroundings, as evidenced by the similarity of their amplitudes in the bulk and in dilute solutions for the same polymer system. As a result, the TCF of the DLM model, involving these two types of motion, is more successful in describing the backbone dynamics of synthetic polymers than unimodal distribution functions.

Also, progress has been made in the quantitative description of the dynamics of long hydrocarbon side-chains, which, as mentioned earlier, are important constituents of many synthetic and biological macromolecules. Models which invoke multiple internal rotations about successive C–C bonds of restricted amplitude appear to be the best choice to interpret quantitatively the frequency-dependent relaxation data of the side-chain carbons.

However, neither the unimodal distribution functions, nor bimodal TCFs for local chain dynamics can predict the actual shape of the experimental TCF, and bring us closer to understanding the relationship between local dynamics and molecular structure. In many circumstances, several dynamic models characterized by different functional forms and different physics regarding the interpretation of chain segmental motion give identical results, while fitting a given set of experimental relaxation data, thus making the choice of a particular model difficult. Further progress requires the development of analytical theories and/or computer dynamics simulations for realistic structures and potentials, which can make the structure–property relationship in polymeric materials more quantitative. Promising approaches in this direction are the DRIS and ORZLD approximations, which allow calculations of both the shape of the TCF and the absolute time-scale of its decay. In addition, important information has been gained about the length-scale of chain segmental motion, the influence of chain connectivity and other motional aspects through Brownian dynamics computer simulations.

On the experimental side, the most effective approach, using the NMR technique, is measurement of the relaxation parameters over as wide a frequency range as possible, particularly in the region $\omega_0\tau_c > 1$, and the accurate measurement of T_2 using newly developed techniques [263, 264]. Needless to say, combination of the NMR technique with other techniques such as time-resolved optical spectroscopy, dielectric relaxation, and others would be a significant advantage, as it would allow dynamics on various length-scales to be systematically investigated.

Acknowledgments

This work would not have been possible without the fruitful collaborations of Drs. A.S. Perlin and R.H. Marchessault (McGill University, Department of Chemistry, Montreal, Quebec, Canada) and Dr. F. Heatley (University of Manchester, Department of Chemistry, Manchester, U.K.) in whose laboratories many of the experimental data were obtained. Also, the authors are indebted to Dr. A. Perico who read the manuscript and made useful comments. Financial support from the Research Committee of the University of Crete, the British Council, and NATO (Grant CRG 910406) is gratefully acknowledged.

References

[1] R.T. Bailey, A.M. North and R.A. Pethrick, Molecular Motions in High Polymers, Clarendon Press, Oxford, 1981.
[2] J. Schaefer, Top. Carbon-13 NMR Spectrosc., 1 (1974) 150.
[3] F. Heatley, Progr. NMR Spectrosc., 13 (1979) 47.
[4] F. Heatley, Annu. Rep. NMR Spectrosc., 17 (1986) 179.
[5] J.J. Connoly and A.A. Jones, Macromolecules, 18 (1985) 906.
[6] A.K. Roy and A.A. Jones, J. Polym. Sci. Polym. Phys. Ed., 23 (1985) 1793.
[7] A.A. Jones, in R.A. Komoroski (Ed.), Polymer Motion in the Solid State, VCH Publishers, New York, 1986, Chapter 7.
[8] A. Spyros, P. Dais and R.H. Marchessault, J. Polym. Sci. Polym. Phys. Ed., 33 (1995) 367.
[9] R.A. Komoroski, J. Maxfield and L. Mandelkern, Macromolecules, 10 (1977) 545.
[10] A. Dekmezian, D.E. Axelson, J.J. Dechter, B. Borah and L. Mandelkern, J. Polym. Sci. Polym. Phys. Ed., 23 (1985) 367.
[11] R.A. Komoroski, in R.A. Komoroski (Ed.), Carbon-13 NMR of Solid Amorphous Polymers Above T_g, VCH Publishers Inc., Florida, 1986, Chapter 40.
[12] D.E. Axelson, in R.A. Komoroski (Ed.), Carbon-13 Solid State NMR of Semicrystalline Polymers, VCH Publishers, New York, 1986, Chapter 5.
[13] A. Abragam, The Principles of Nuclear Magnetism, Oxford University Press, London, 1961.
[14] C.P. Slichter, Principles in Nuclear Magnetism, Harper and Row, New York, 1961.
[15] N. Bloembergen, Nuclear Magnetic Relaxation, W.A. Benjamin, New York, 1961.
[16] I. Solomon, Phys. Rev., 99 (1955) 559.
[17] W.T. Huntress, Jr., Adv. Magn. Reson., 4 (1970) 1.
[18] J.R. Lyerla, Jr., and G.C. Levy, Top. Carbon-13 NMR Spectrosc., 1 (1974) 79.
[19] A.G. Redfield, Adv. Magn. Reson., 1 (1965) 1.
[20] J.D. Gutnell and J.A. Glasel, J. Am. Chem. Soc., 99 (1977) 42.
[21] D.J. Gisser, S. Glowinowski and M.D. Ediger, Macromolecules, 24 (1991) 4270.
[22] S. Glowinowski, D.J. Gisser and M.D. Ediger, Macromolecules, 23 (1990) 3520.
[23] D. Wallach, J. Chem. Phys., 47 (1967) 5258.
[24] M.E. Rose, Elementary Theory of Angular Momentum, Wiley, New York, 1957.
[25] R.J. Wittebort and A. Szabo, J. Chem. Phys., 69 (1978) 1722.
[26] A. Spyros and P. Dais, J. Polym. Sci. Polym. Phys. Ed., 33 (1995) 353.
[27] G.C. Levy, D.E. Axelson, R. Schwartz and J. Hochmann, J. Am. Chem. Soc., 100 (1978) 410.
[28] Y.K. Levine, N.J.M. Birdsall, A.G. Lee, J.C. Metcalfe, P. Partington and G.C.K. Roberts, J. Chem. Phys., 60 (1974) 2890

[29] R.E. London and J. Avitabile, J. Chem. Phys., 65 (1976) 2443.
[30] R.E. London and J. Avitabile, J. Am. Chem. Soc., 100 (1978) 7159.
[31] R.E. London and J. Avitabile, J. Am. Chem. Soc., 99 (1977) 7765.
[32] J.W. Keepers and T.L. James, J. Am. Chem. Soc., 104 (1982) 929.
[33] A. Tsutsumi and C. Chachaty, Macromolecules, 12 (1979) 129.
[34] D. Ghesquiere and C. Chachaty, Macromolecules, 12 (1979) 775.
[35] L.G. Werbelow and D.M. Grant, Adv. Magn. Reson., 9 (1977) 189.
[36] R.L. Vold and R.R. Vold, Progr. NMR Spectrosc., 12 (1978) 79.
[37] M.M. Fuson, D.J. Anderson, F. Liu and D.M. Grant, Macromolecules, 24 (1991) 2594.
[38] M.M. Fuson and D.M. Grant, Macromolecules, 21 (1988) 944.
[39] M.M. Fuson, M.S. Brown, D.M. Grant and G.T. Evans, J. Am. Chem. Soc., 107 (1985) 6695.
[40] P. Dais and A.S. Perlin, Adv. Carbohydr. Chem. Biochem., 45 (1987) 125.
[41] R. Freeman, S. Wittekock and R.R. Ernst, J. Chem. Phys., 52 (1970) 1529.
[42] K. Akasaka, J. Magn. Reson., 45 (1981) 337.
[43] F. Heatley and M.K. Cox, Polymer, 18 (1977) 225.
[44] F. Heatley, A. Begum and M.K. Cox, Polymer, 18 (1977) 637.
[45] J. Denault and J. Prud'Homme, Macromolecules, 22 (1989) 1307.
[46] J. Denault, B. Morese-Seguela, R. Seguela and J. Prud'homme, Macromolecules, 23 (1990) 4658.
[47] R. Kimmich, G. Schnor and M. Kopf, Progr. NMR. Spectrosc., 20 (1988) 385.
[48] K.S. Cole and R.H. Cole, J. Chem. Phys., 9 (1941) 341.
[49] R.M. Fuoss and J.G. Kirkwood, J. Am. Chem. Soc., 63 (1941) 385.
[50] T.M. Connor, Trans. Faraday Soc., 60 (1964) 1574.
[51] J. Schaefer, Macromolecules, 6 (1973) 882.
[52] R. Ullman, J. Chem. Phys., 43 (1965) 3161.
[53] D.A. McInnes and A.M. North, Polymer, 18 (1977) 505.
[54] D.A. McInnes and D. Pugh, Chem. Phys. Lett., 34 (1975) 139.
[55] L. Monnerie and F. Laupretre, in R. Daudel (Ed.), Structure and Dynamics of Molecular Systems, D. Reidel, Dordrecht, 1986.
[56] J.T. Bendler and R. Yaris, Macromolecules, 11 (1978) 650; F. Heatley and J.T. Bendler, Polymer, 20 (1979) 1578.
[57] J. Skolnick and R. Yaris, Macromolecules, 15 (1982) 1041; 16 (1983) 491.
[58] J. Skolnick and R. Yaris, Macromolecules, 16 (1983) 266, 492.
[59] M.D. Ediger, Annu. Rev. Chem., 42 (1991) 225.
[60] W. Gronski and N. Murayama, Makromol. Chem., 177 (1976) 3017.
[61] W. Gronski Makromol. Chem., 178 (1977) 2949.
[62] R.E. Cais and F.A. Bovey, Macromolecules, 10 (1977) 757.
[63] W.H. Stockmayer, A.A. Jones and T.L. Treadwell, Macromolecules, 10 (1977) 762.
[64] A.H. Fawcett, F. Heatley, K.J. Ivin, C.D. Stewart and P. Watt, Macromolecules, 10 (1977) 765.
[65] K. Iwata, J. Chem. Phys., 58 (1973) 4184.
[66] E. Helfand, J. Chem. Phys., 54 (1971) 4651.
[67] R.H. Boyd and S.M. Breitling, Macromolecules, 7 (1974) 855.
[68] D.A. Jones and D. Pugh, Polymer, 19 (1978) 474.
[69] P.H. Verdier, J. Chem. Phys., 45 (1966) 2118.
[70] W.H. Stockmayer, W. Gobushi, Y. Chikahisa and D.L. Carpender, Discuss. Faraday Soc., 49 (1970) 182.
[71] L. Monnerie and F. Geny, J. Chim. Phys., 66 (1969) 1691, 1698.
[72] F. Geny and L. Monnerie, J. Chim. Phys., 66 (1969) 1798, 1872.
[73] B. Valeur, J.-P. Jarry, F. Geny and L. Monnerie, J. Polym. Sci. Polym. Phys. Ed., 13 (1975) 667.
[74] B. Valeur, L. Monnerie and J.-P. Jarry, J. Polym. Sci. Polym. Phys. Ed., 13 (1975) 675.
[75] B. Valeur, J.-P. Yarry, F. Geny and L. Monnerie, J. Polym. Sci. Polym. Phys. Ed., 13 (1975) 2251.
[76] F. Geny and L. Monnerie, J. Polym. Sci. Polym. Phys. Ed., 17 (1979) 131, 147.
[77] F. Geny and L. Monnerie, Macromolecules, 10 (1977) 1003.
[78] A.A. Jones and W.H. Stockmayer, J. Polym. Sci. Polym. Phys. Ed., 15 (1977) 847.
[79] E. Helfand, J. Chem. Phys., 69 (1978) 1010.
[80] E. Helfand, Z.R. Wasserman and T.A. Weber, Macromolecules, 13 (1980) 526.
[81] C.K. Hall and E. Helfand, J. Chem. Phys., 77 (1982) 3275.
[82] J. Skolnick and E. Helfand, J. Chem. Phys., 72 (1980) 5489.
[83] E. Helfand and J. Skolnick, J. Chem. Phys., 77 (1982) 5714.
[84] T.A. Weber and E. Helfand, J. Chem. Phys., 87 (1983) 2881.

[85] E. Helfand, Z.R. Wasserman and T.A. Weber, J. Chem. Phys., 70 (1979) 2016.
[86] D.B. Adolf and M.D. Ediger, Macromolecules, 24 (1991) 5834.
[87] I. Bahar and B. Erman, Macromolecules, 20 (1987) 1368.
[88] I. Bahar and B. Erman, Macromolecules, 20 (1987) 2310.
[89] I. Bahar, B. Erman and L. Monnerie, Macromolecules, 22 (1989) 431.
[90] I. Bahar, B. Erman and L. Monnerie, Macromolecules, 22 (1989) 2396.
[91] I. Bahar, B. Erman and L. Monnerie, Macromolecules, 23 (1990) 1174.
[92] F. Schatzki, Polym. Preprints, 6 (1965) 646.
[93] H. Morawetz, Science, 203 (1979) 405.
[94] T.P. Liao and H. Morawetz, Macromolecules, 13 (1980) 1228.
[95] H. Morawetz, Pure Appl. Chem., 52 (1980) 277.
[96] H.A. Kramers, Physica, 7 (1940) 284.
[97] I. Zuniga, I. Bahar, R. Dodge and W.L. Mattice, J. Chem. Phys., 95 (1991) 5348.
[98] D.B. Adolf and M.D. Ediger, Macromolecules, 25 (1992) 1074.
[99] F. Heatley and A. Begum, Polymer, 17 (1976) 399.
[100] R.D. O'Connor and F.D. Blum, Macromolecules, 27 (1994) 1654.
[101] H. Schneider, J. Polym. Sci. Polym. Phys. Ed., 29 (1991) 1171.
[102] D.W. Davidson and R.H. Cole, J. Chem. Phys., 18 (1950) 417; 19 (1951) 1484.
[103] D.E. Woessner, J. Chem. Phys., 37 (1962) 647.
[104] R. King and O. Jardetzky, Chem. Phys. Lett., 55 (1978) 15; R. King, R. Haas, M. Gassner, R.K. Nanda, W.W. Conover and O. Jardetzky, Biophys. J., 6 (1978) 103.
[105] G. Lipari and A. Szabo, J. Am. Chem. Soc., 104 (1982) 4546.
[106] P. Tekely, F. Laupretre and L. Monnerie, Macromolecules, 16 (1983) 415.
[107] B.I. Hunt and J.G. Powles, Proc. Phys. Soc., 88 (1966) 513.
[108] J. Skolnick, D. Perchal and R. Yaris, J. Magn. Reson., 57 (1984) 204.
[109] See for instance, R.J. Roe (Ed.), Computer Simulation of Polymers, Prentice Hall, Englewood Cliffs, NJ, 1991.
[110] I. Bahar and B. Erman, J. Chem. Phys., 88 (1988) 1228.
[111] H. Takeuchi and R.J. Roe, J. Chem. Phys., 94 (1991) 7446.
[112] J.J. Connolly, E. Gordon and A.A. Jones, Macromolecules, 17 (1984) 722.
[113] A. Perico, Acc. Chem. Res., 22 (1989) 336.
[114] A. Perico and M. Guenza, J. Chem. Phys., 83 (1985) 3103; 84 (1986) 510.
[115] A. Perico, J. Chem. Phys., 88 (1988) 3996.
[116] A. Perico, F. Ganazzoli and G. Allegra, J. Chem. Phys., 87 (1987) 3677.
[117] A Perico, Biopolymers, 28 (1989) 1527.
[118] A. Perico, A. Altomare, D. Catalano, M. Colombani and C.A. Veracini, Macromolecules, 23 (1990) 4912.
[119] H. Yamakawa and M. Fujii, J. Chem. Phys., 81 (1987) 997.
[120] P. Dais, M.E. Nedea and R.H. Marchessault, Macromolecules, 23 (1990) 3387.
[121] P. Dais, M.E. Nedea and R.H. Marchessault, Polymer, 33 (1992) 4288.
[122] M.E. Nedea, R.H. Marchessault and P. Dais, Polymer, 33 (1992) 1831.
[123] T. Radiotis, G.R. Brown and P. Dais, Macromolecules, 26 (1993) 1445.
[124] L. Monnerie, J. Non-Crystalline Solids, 131–133 (1991) 755.
[125] F. Laupretre, L. Bokobza and L. Monnerie, Polymer, 34 (1993) 468.
[126] R. Dejean de la Batie, F. Laupretre and L. Monnerie, Macromolecules, 21 (1988) 2045.
[127] R. Dejean de la Batie, F. Laupretre and L. Monnerie, Macromolecules, 21 (1988) 2052.
[128] R. Dejean de la Batie, F. Laupretre and L. Monnerie, Macromolecules, 22 (1989) 122.
[129] O.W. Howarth, J. Chem. Soc. Faraday Trans., 2, 75 (1979) 863.
[130] P. Dais, Carbohydr. Res., 160 (1987) 73.
[131] D.E. Woessner and B.S. Snowden, Adv. Mol. Relaxation Processes, 3 (1972) 181.
[132] J.F. O'Gara, S.G. Desjardins and A.A. Jones, Macromolecules, 14 (1981) 64.
[133] P. Dais, M.E. Nedea and R.H. Marchessault, Macromolecules, 22 (1989) 4208
[134] A.A. Jones and R.P. Lubianez, Macromolecules, 11 (1978) 126.
[135] F. Laupretre, L. Monnerie and O. Vogl, Eur. Polym. J., 14 (1978) 981.
[136] D. Doddrell, V. Glushko and A. Allerhand, J. Chem. Phys., 56 (1972) 3683.
[137] A.A. Jones, J. Polym. Sci. Polym. Phys. Ed., 15 (1977) 863.
[138] C. Hagele and L. Beck, Macromolecules, 10 (1977) 213.
[139] Y. Tanabe, J. Polym. Sci. Polym. Phys. Ed., 23 (1985) 601.
[140] A. Tonelli, Macromolecules, 6 (1973) 682.

[141] C.C. Hung, J.H. Shibata, A.A. Jones and P.T. Inglefield, Polymer, 28 (1987) 1062.
[142] Y. Inoue and T. Konno, Polym. J., 8 (1976) 457.
[143] A. Spyros and P. Dais, Macromolecules, 25 (1992) 1062.
[144] M.F. Tarpey, Y.Y. Lin, A.A. Jones and P.T. Inglefield, ACS Symp. Ser. 247, American Chemical Society, Washington, DC, 1984, p. 67.
[145] W. Gronski, Makromol. Chem., 180 (1979) 1119.
[146] D. Pissas, P. Dais and E. Mikros, Magn. Reson, Chem., 32 (1994) 263.
[147] A.G. Lee, N.J.M. Birdsall, J.C. Metcalfe, G.B. Warren and G.C.K. Roberts, Proc. R. Soc. London Ser. B, 193 (1976) 253.
[148] W.-S. Kuo, O.J. Jakobus, G.B. Savitsky and A.L. Beyerlein, J. Chem. Phys., 70 (1979) 1193.
[149] R.J. Witterbort, A. Szabo and F.R.N. Curd, J. Am. Chem. Soc., 102 (1980) 5723.
[150] R.M. Levy, M. Karplus and P.G. Wolynes, J. Am. Chem. Soc., 103 (1981) 5998.
[151] J. Skolnick and W.L. Mattice, Macromolecules, 14 (1981) 292.
[152] J.L. Viovy, L. Monnerie and J.C. Brochon, Macromolecules, 16 (1983) 1845.
[153] Y.Y. Lin, A.A. Jones and W.H. Stockmayer, J. Polym. Sci. Polym. Phys. Ed., 22 (1984) 2195.
[154] G. Lipari and A. Szabo, J. Am. Chem. Soc., 104 (1982) 4559.
[155] M.M. Fuson and J.H. Prestegard, J. Magn. Reson., 41 (1980) 179; J. Am. Chem. Soc., 105 (1983) 168.
[156] M.M. Fuson and J.H. Prestegard, Biochemistry, 22 (1983) 1311.
[157] M.S. Brown, D.M. Grant, W.J. Horton, C.L. Mayne and G.T. Evans, J. Am. Chem. Soc., 107 (1985) 6698.
[158] R. Dodge and W.L. Mattice, Macromolecules, 24 (1991) 2709.
[159] P. Corradini, R. Napolitano, V. Petraccolone, B. Pirozzi and A. Tuzi, Eur. Polym. J., 17 (1981) 1217.
[160] C. de Rosa, R. Napolitano and B. Pirrozi, Polymer, 26 (1985) 2039.
[161] Y. Zhan and W.L. Mattice, Macromolecules, 25 (1992) 1554.
[162] J.E. Mark, J. Am. Chem. Soc., 88 (1966) 4354.
[163] Y. Abe and P.J. Flory, Macromolecules, 4 (1971) 219.
[164] A.D. English and C.R. Dybowski, Macromolecules, 17 (1984) 446.
[165] J. Viovy and L. Monnerie, Adv. Polym. Sci., 67 (1985) 99.
[166] F.C. Schilling, F.A. Bovey, A. Tonelli, S. Tseng and A.E. Woodward, Macromolecules, 17 (1984) 728.
[167] T. Kanaya, K. Kaji and K. Inoue, Macromolecules, 24 (1991) 1826.
[168] F.C. Schilling, M.A. Gomez, A.E. Tonelli, F.A. Bovey and A.E. Woodward, Macromolecules, 20 (1987) 2957.
[169] D.J. Gisser and M.D. Ediger, Macromolecules, 25 (1992) 1284.
[170] I. Bahar, B. Erman, F. Kremer and E.W. Fischer, Macromolecules, 25 (1992) 816.
[171] M.L. Williams, R.F. Landel and J.D. Ferry, J. Am. Chem. Soc., 77 (1955) 3701.
[172] R.U. Lemieux, in P. de Mayo (Ed.), Molecular Rearrangements, Part 2, Interscience, New York, 1964; R.U. Lemieux, Pure Appl. Chem., 25 (1971) 527.
[173] J.E. Mark, Acc. Chem. Res., 12 (1979) 49.
[174] J. Miyasaka, Y. Kinai and Y. Imamura, Makromol. Chem., 182 (1981) 2533.
[175] A.P.M. Kentgens, E. de Boer and W.S. Veeman, J. Chem. Phys., 87 (1989) 6859.
[176] L. Lestel, P. Guegan, S. Boileau, H. Cherabane and F. Laupretre, Macromolecules, 25 (1992) 6024.
[177] C.-C. Hung, J.H. Shibata, M.F. Tarpey, A.A. Jones, J.A. Porco and P.T. Inglefield, Anal. Chim. Acta, 189 (1986) 167.
[178] A.A. Jones and M. Bisceglia, Macromolecules, 6 (1979) 1136.
[179] Y.S. Sung, C.L. Chen and A.C. Su, Macromolecules, 24 (1991) 6123.
[180] Y.S. Sung, C.L. Chen and A.C. Su, Macromolecules, 23 (1990) 1941.
[181] A.A. Jones, J.F. O'Gara, P.T. Inglefield, J.T. Bendler, A.F. Yee and K.L. Ngai, Macromolecules, 16 (1983) 658.
[182] J.F. O'Gara, C.-C. Hung, A.A. Jones and P.T. Inglefield, Macromolecules, 18 (1985) 1117.
[183] A.A. Jones, Macromolecules, 18 (1985) 902.
[184] A.A. Jones, R.P. Lunianez, M.A. Hanson and S.L. Shostak, J. Polym. Sci. Polym. Phys. Ed., 16 (1978) 1685.
[185] R. Dejean de la Batie, F. Laupretre and L. Monnerie, Macromolecules, 22 (1989) 2617.
[186] Y. Inoue, A. Nishioka and R. Chujo, J. Polym. Sci. Polym. Phys. Ed., 11 (1973) 2237.
[187] R.H. Boyd and S.M. Breitling, Macromolecules, 5 (1972) 1.
[188] C. Donghwan, N.A. Neuburger and W.L. Mattice, Macromolecules, 25 (1992) 322.
[189] M.V. Volkenstein, Configurational Statistics of Polymeric Chains, Interscience, New York, 1963.
[190] A. Bandis, W.-Y. Wen, E.B. Jones, P. Kaskan, Y. Zhu, A.A. Jones, P.T. Inglefield and J.T. Bendler, J. Polym. Sci. Polym. Phys. Ed., 32 (1994) 1707.
[191] G. Williams and D.C. Watts, Trans. Faraday Soc., 66 (1970) 80.

[192] R.H. Findlay and D.C. White, Appl. Environ. Microbiol., 45 (1983) 71.
[193] S.R. Amor, I. Rayment and J.K.M. Sanders, Macromolecules, 24 (1991) 4583.
[194] R.A. Komoroski, J. Maxfield, F. Sakagushi and L. Madelkern, Macromolecules, 10 (1977) 550.
[195] R.A. Komoroski and L. Mandelkern, J. Polym. Sci. Symp. Ser., 34 (1976) 201.
[196] L.W. Jelinski, J.J. Dumais and A.K. Engel, Macromolecules, 16 (1983) 403.
[197] L.W. Jelinski, J.J. Dumais, P.I. Watnik, A.K. Engel and M.D. Sefcik, Macromolecules, 16 (1983) 409.
[198] J.J. Dechter, D.E. Axelson, A. Dekmezian, M. Glotin and L. Mandelkern, J. Polym. Sci. Polym. Phys. Ed., 20 (1982) 641.
[199] J.J. Dechter, R.A. Komoroski, D.E. Axelson and L. Mandelkern, J. Polym. Sci. Polym. Phys. Ed., 19 (1981) 631.
[200] D.E. Axelson and L. Mandelkern, J. Polym. Sci. Polym. Phys. Ed., 16 (1978) 1135.
[201] L. Mandelkern, Pure Appl. Chem., 54 (1981) 611.
[202] F.G. Morin and R.H. Marchessault, Macromolecules, 25 (1992) 576.
[203] P.M. Henrichs, J.M. Hewitt, G.A. Russel, M.A. Sandhu and M.R. Grashof, Macromolecules, 14 (1981) 1770.
[204] R.H. Komoroski, J. Polym. Sci. Polym. Phys. Ed., 17 (1979) 45.
[205] M.D. Sefcik, J. Schaefer, E.O. Stejskal and R.A. McKay, Macromolecules, 13 (1980) 1132.
[206] J.M. Hewitt, G.A. Russel, P.M. Henrichs and M.A. Sandhu, Polym. Preprints, 20 (1979) 413.
[207] F.A. Bovey and L.W. Jelinski, J. Phys. Chem., 89 (1985) 571.
[208] S. Mashimo, P. Winsor IV, R.H. Cole, K. Matsuo and W.H. Stockmayer, Macromolecules, 19 (1986) 682.
[209] A.H. Fawcett, S. Fee and L. Waring, Polymer, 24 (1983) 1571.
[210] S.A. Chambers and A.H. Fawcett, Macromolecules, 18 (1985) 1710.
[211] H. Kiruchi, H. Tokumitsu and K. Seki, Macromolecules, 26 (1993) 7326.
[212] F.D. Bluhm, B. Duraikaj and A.S. Padmanabhan, Macromolecules, 17 (1984) 2837.
[213] C.J.M. van Rijn, J. de Bleijser and J.C. Leyte, Macromolecules, 20 (1987) 1248.
[214] C.W.R. Mulder and J.C. Leyte, J. Phys. Chem., 89 (1985) 1007.
[215] A. Spyros, P. Dais and F. Heatley, Makromol. Chem., 195 (1994) 3271.
[216] A. Spyros, P. Dais and F. Heatley, Macromolecules, 27 (1994) 5845.
[217] L.L. Chapoy, K. Matsuo and W.H. Stockmayer, Macromolecules, 18 (1985) 188.
[218] K. Matsuo and W.H. Stockmayer, Macromolecules, 14 (1981) 544.
[219] K. Seki and Y. Imamura, Bull. Chem. Soc. Jpn., 56 (1983) 3167.
[220] A.D. Meltzer, D.A. Tirrel, A.A. Jones, P.T. Inglefield, D.M. Hedstrand and D.A. Tomalia, Macromolecules, 25 (1992) 4541.
[221] A.D. Meltzer, D.A. Tirrel, A.A. Jones and P.T. Inglefield, Macromolecules, 25 (1992) 4549.
[222] P.L. Rinaldi, C. Yu and F.C. Levy, Macromolecules, 14 (1981) 551.
[223] M. Mauzac, J.P. Vairon and F. Laupretre, Polymer, 20 (1979) 443.
[224] A.V. Cunliffe and R.A. Pethrick, Polymer, 21 (1980) 1025.
[225] F. Candau, F. Heatley, C. Price and R.B. Stubbersfield, Eur. Polym. J., 20 (1984) 685.
[226] W.T. Ford and T. Balakrishnan, Macromolecules, 14 (1981) 284.
[227] T. Asakura, K. Suzuki, K. Horie and S. Mita, Makromol. Chem., 182 (1981) 2289.
[228] L. Monnerie, F. Laupretre and C. Noel, Liquid Crystals, 3 (1988) 1013.
[229] T. Asakura and Y. Doi, Macromolecules, 16 (1983) 786.
[230] T. Asakura and Y. Doi, Macromolecules, 14 (1981) 72.
[231] H. Angad-Gaur and D.J. Sikkena, Makromol. Chem., 181 (1980) 2385.
[232] K. Hatada, T. Kitayama, N. Matsuo and H. Yuki, Polym. J., 15 (1983) 719.
[233] S.H. Oh, R. Rydo and M. Jhon, J. Polym. Sci. Polym. Chem. Ed., 27 (1983) 1383.
[234] Y. Inoue and Y. Kawamura, Polymer, 23 (1982) 1997.
[235] R.P. Lubianez, A.A. Jones and M. Bisceglia, Macromolecules, 12 (1979) 1141.
[236] A. Tsutsumi, Mol. Phys., 37 (1979) 111.
[237] D. Ghesquiere, B. Ban and C. Chachaty, Macromolecules, 10 (1977) 743.
[238] P. Dais, Magn. Reson. Chem., 25 (1987) 141.
[239] A. Spyros, P. Dais and F. Heatley, Macromolecules, 27 (1994) 6207.
[240] A. Tsutsumi, B. Perly, A. Forchioni and C. Chachaty, Macromolecules, 11 (1978) 977.
[241] B. Perly, C. chachaty and A. Tsutsumi, J. Am. Chem. Soc., 102 (1980) 1521.
[242] U. Hahn, H. Hanssum and H. Ruterjans, Biopolymers, 24 (1985) 1147.
[243] M. Paci, Polym. Commun., 26 (1985) 116.
[244] T. Tsuchikawa, M. Yamaguchi, T. Hiraoki and A. Tsutsumi, Polym. J., 22 (1990) 951.
[245] S.P. Velsko, D.H. Waldeck and G.R. Fleming, J. Chem. Phys., 78 (1983) 249.

[246] S.H. Courtney and G.R. Fleming, J. Chem. Phys., 83 (1985) 215.
[247] B. Bagchi and D.W. Oxtoby, J. Chem. Phys., 78 (1983) 2735.
[248] R.F. Grote and J.T. Hynes, J. Chem. Phys., 73 (1980) 2715.
[249] J.M.G. Cowie and R. Ferguson, Polymer, 28 (1987) 503.
[250] J. Heijboer, J.M.A. Baas, B. van de Graaf and M.A. Hoefnagel, Polymer, 28 (1987) 509.
[251] J.A. Montgomery, Jr., D. Chandler and B.J. Berne, J. Chem. Phys., 70 (1979) 4056.
[252] K.J. Liu and J.E. Anderson, Macromolecules, 3 (1970) 163.
[253] M.C. Lang, F. Laupretre, C. Noel and L. Monnerie, J. Chem. Soc. Faraday Trans. 2, 75 (1979) 349.
[254] M.D. Magee, J. Chem. Soc. Faraday Trans. 2, 70 (1974) 929.
[255] D.B. Adolf, M.D. Ediger, T. Kitano and K. Ito, Macromolecules, 25 (1992) 867.
[256] B. Valeur and L. Monnerie, J. Polym. Sci. Polym. Phys. Ed., 14 (1976) 11.
[257] D.A. Waldow, M.D. Ediger, Y. Yamaguchi, Y. Matsuchita and I. Noda, Macromolecules, 24 (1991) 3147.
[258] T. Sasaki, M. Yamamoto and Y. Nishijima, Macromolecules, 21 (1988) 610.
[259] D.A. Waldow, B.S. Johnson, P.D. Hyde, M.D. Ediger, I. Kitano and K. Ito, Macromolecules, 22 (1989) 1345.
[260] A. Guillermo, R. Dupeyre and J.P. Cohen-Addad, Macromolecules, 23 (1990) 1291.
[261] H. Vogel, Phys. Z., 22 (1921) 645.
[262] J.D. Ferry, Viscoelastic Properties of Polymers, Wiley, New York, 1981, Chapter 11.
[263] A. Bain, W.P.Y. Ho and J.S. Martin, J. Magn. Reson., 43 (1981) 328.
[264] A. Bain and G.J. Duns, J. Magn. Reson. Ser. A, 56 (1994) 109.